EXPERIMENTAL DETERMINATION OF THE STRESS SINGULARITY EXPONENT IN CRACKED BODIES USING PHOTOELASTICITY

by

Wilson Randolph Lloyd

Thesis submitted to the Faculty of the
Virginia Polytechnic Institute and State University
in partial fulfillment of the requirements for the degree of

MASTER OF SCIENCE

in

Engineering Mechanics

APPROVED:

C. W. Smith, Chairman

D. Post

R. Czarnek

September, 1986

Blacksburg, Virginia

EXPERIMENTAL DETERMINATION OF THE STRESS SINGULARITY EXPONENT IN CRACKED BODIES USING PHOTOELASTICITY

by

Wilson Randolph Lloyd

Committee Chairman: C. W. Smith
Engineering Mechanics

(ABSTRACT)

An experimental program is developed to investigate the three dimensional nature of the stress field surrounding the border of semi-elliptical surface flaws, particularly the singularity exponent. Stress freezing photoelasticity is employed to generate experimental data from nearly incompressible, elastic material. The technique of optical fringe multiplication is utilized to collect data from thin, closely spaced photoelastic slices.

A new quasi-linear algorithm for data analysis is developed and verified. The algorithm is implemented using the interactive and graphics capabilities of a microcomputer and digitizing tablet, saving time and reducing errors in photoelastic data analysis. By utilizing CRT graphics, the measurement zone producing the most consistent results is delineated.

Results obtained from a series of tests on both surface flaws and straight-front cracks bracket analytical values of the singularity exponent at the flaw border-free surface intersection. Suggestions to decrease variance in the results and possibly cause the results for all tests to coalesce to the analytical value(s) at the free surface are presented.

An algebraic formula is developed to account for the singularity exponent variation (3-D effect) by adjusting the magnitude of the classical LEFM mode I stress intensity factor, K_I. A discussion of the need to recognize and account for these effects in high-tech materials is also included.

For my mother, Helen,

my sisters, Dawn and Lynne,

and my grandmothers,

in the hope that some day I will live up

to all of your expectations.

ACKNOWLEDGEMENTS

The author thanks Drs. Smith, Post, and Czarnek for their help, encouragement, and most of all, their patience in completion of this thesis. Their experience and foresight have proven very valuable in meeting and overcoming the inevitable research obstacles encountered on an almost daily basis. The author also extends special thanks to the above Professors and their families for welcoming him into their homes.

Without the assistance of fellow research assistant Mohammed Rezvani, the author would still be collecting data from the first test. Thanks for everything "Mo". In addition, thanks are extended to many members of the ESM department faculty and staff for miscellaneous bits of information which helped keep the research moving forward, and not in circles.

Finally, special thanks to the author's sister, Lynne, who volunteered her time to assist with the completion of the figures, and grandmother, Louisa, for graciously volunteering space in her home where this work was completed.

W. Randolph Lloyd

September, 1986

TABLE OF CONTENTS

ILLUSTRATIONS

INTRODUCTION

1.1 Historical Perspective

The foundations of modern fracture mechanics were formed by C. E. Inglis [1] and A. A. Griffith [2] in the early part of this century. Subsequent work by, among others, H. M. Westergaard [3], M. L. Williams [4], and G. R. Irwin [5] served to advance the knowledge of stress fields local to crack tips and the associated analytical methods used to determine the stress intensity factor (SIF). It is important to note that this early work was all performed in the two-dimensional regime of plane elasticity. From about 1950 to the late 1960's, the majority of work centered around the solution of plane problems of increasingly complicated geometry, however, Green and Sneddon [6] did work on the three-dimensional problem of the embedded elliptical crack. Work also proceeded in applying the results of these solutions to the problem of fatigue related failure.

In the late 1960's, G. Sih and others [7] began to investigate three-dimensional cracked body problems. It was Sih who first suggested that the classical inverse square root stress singularity may be lost where the crack plane intersects a traction-free surface. He also noted the highly three-dimensional nature of the stress field in the vicinity of the crack front-free surface intersection, although his analysis was not valid in that region. Following Sih's initial work, analysts began to take a closer look at the crack front-free surface intersection (also called the "corner point" in the

literature) stress and displacement fields. Among the first to present analytical results were E. S. Folias [8] and J. P. Benthem [9]. Folias and Benthem performed their analyses independently. While both men agreed that the singularity exponent (or singularity order) was dependent upon a material's Poisson's ratio, there was, and still is disagreement [10] as to what the dependence is.

Following Folias' and Benthem's initial reports, several other researchers [11, 12] have attempted to solve the problem using various numerical techniques, such as finite difference and finite element methods and numerical integration schemes. Although reasonable agreement in numerical values of the singularity exponent has been achieved by several analysts independently [9, 11, 12], it is important to note that in all of the analytical formulations presented, some possible error is introduced through the use of numerical methods or by truncation of infinite series equations.

Due to the mathematical intractability of this three-dimensional problem, C. W. Smith [13] and his colleagues initiated a program to experimentally investigate the corner point problem in 1981. Besides establishing values for the singularity order at the free surface, it was hoped that a proposed transition zone (or boundary layer) where the singularity order varied continuously from its free surface value to the classical inverse square root value could be delineated.

Preliminary results of the experimental investigation were presented in 1983 [14]. Surface values of the singularity order agreed well with Benthem's analytical value, and an unexpectedly large transition zone was also reported.

During the time that Smith has been working on the problem experimentally, analysts have continued to seek a mathematically complete solution to the problem. Several different approaches to solving the problem have been followed, however no solutions have been proven to be mathematically complete.

1.2 Motivation for Current Research

There is general agreement among analysts [8, 9, 11, 12, 15] that the singularity order at the corner point depends on Poisson's ratio, and that as Poisson's ratio increases from zero, the singularity order continuously deviates from the classical linear elastic fracture mechanics (LEFM) value of 0.5. In particular, the work of Benthem [9, 15] indicates that a slow change in the singularity order occurs until Poisson's ratio exceeds about 0.4, when it begins to change more rapidly. When Poisson's ratio approaches 0.5, Benthem's results show the singularity order to be about one-third. This reduction of the singularity order results in considerable alteration of the stress and displacement fields near crack front-free surface intersections in nearly incompressible materials.

Consider now the following facts. The aerospace and defense industries are using increasing amounts of fiber reinforced composite materials in new designs. The matrix material in some epoxy based composites is nearly incompressible and may constitute over 50% of the volume of the material. The failure mechanism in these inhomogeneous, anisotropic materials is not yet well understood. The use of adhesives (typically having high Poisson's ratios), in place of conventional fasteners, is increasing. Most design codes concerned with failure due to brittle fracture and fatigue are based on LEFM principles. These principles are based entirely on two-dimensional theory, with most codes using a worst case assumption of the existence of generalized plane strain in the vicinity of the crack front (crack border). Current test procedures for determining the fracture toughness of materials rely on "thickness averaged" material behavior. The data obtained from many of the previously mentioned tests are in the form of surface measurements of displacement or strain.

If all of this information is combined, it indicates that the possibility exists for large errors to be made in the characterization of certain materials to be used in critical components of a structure. Inspection interval or life expectancy calculations could be affected through underestimation of effective stress intensity levels in a flawed component, which could lead to a catastrophic failure. The

probability of such failures could be reduced significantly if a more thorough understanding of the three-dimensional effects associated with the crack front-free surface intersection could be obtained. It is the prospect of increasing the understanding of this problem, and hence reducing the probability of future catastrophic failures, that motivates the current research efforts.

1.3 Problem Definition

The current experimental research is directed toward achieving two basic goals associated with three-dimensional effects in cracked high Poisson's ratio materials. The first goal is to determine stress singularity order distributions for naturally occurring surface cracks in elastic bodies having finite dimensions. In order to achieve this goal, several problems need to be solved, including the following. A suitable experimental method must be chosen or developed. A model geometry must be developed which will meet certain analytical criteria as well as be feasible to construct. A testing procedure must be developed. A method of collecting experimental data from the tests must be developed. Finally, a suitable algorithm must be developed to extract the desired parameters from the experimental data. It must be remembered that the entire experimental program should be developed so that consistent and repeatable results can be obtained.

The second goal is to overcome the following problem. The model equation for the stress field contains the singularity order as a variable. This presents no problem in itself. However, it is desirable that the results obtained from the use of this equation be incorporated into current design codes, which were developed for use with the LEFM-based stress intensity factor, K_I. The problem this presents concerns dimensional consistency. The coefficient of the singular term in the model equation, which has variable singularity order, does not have the same dimensional units as K_I when the singularity order is not equal to 0.5, e.g., at the free surface. A suitable formula or algorithm must be developed to convert this singular term coefficient (also referred to as "stress eigenfactor", D, or K_λ [14] in the literature) to a dimensionally correct "corresponding" SIF, K_{cor} (this is the notation used by Smith and Epstein for the mentioned quantity).

A program to study these problems was initiated in 1984, following the conclusion of initial work on straight front cracks by Epstein. Since then, considerable progress towards achieving the goals mentioned previously has been made. In addition to this progress, a large amount of well documented and accurate photoelastic data from surface flaw tests has been accumulated. This data base, in conjunction with this report, should serve as a good foundation for

future research on the three dimensional characteristics of surface flaws. In particular, work associated with the singularity order variation should benefit, since little other work of this nature is documented.

REVIEW OF LITERATURE

2.1 Introduction to Literature Review

The concept of the variable stress singularity order and associated three-dimensional effects has received relatively little attention compared to other topics in fracture mechanics. The work that has been published has been almost entirely analytically and/or numerically based. The analytical works are presented first in approximate chronological order. The only works published which have experimental foundations are those of Smith and his associates (see, for example [16]), and Ruiz and Epstein [17]. A review of this experimental work is also presented. Limtragool's Ph.D. dissertation [18] investigated the singularity order using holographic interferometry, however, a copy could not be obtained for review. The current research is an extension and refinement of the original experimental research performed by Epstein [14].

2.2 The Initial Work of Hartranft and Sih

In 1969, Hartranft and Sih [7] investigated the three dimensional stress field for a semi-infinite plane crack in an infinite solid (see figure 2.1). The problem was cast in circular cylindrical coordinates, with the axial coordinate, z, coincident with the crack border. They utilized the Williams stress eigenfunction in their solution. They proceeded to solve the three dimensional problem by first satisfying equilibrium conditions with the displacements, and subsequently

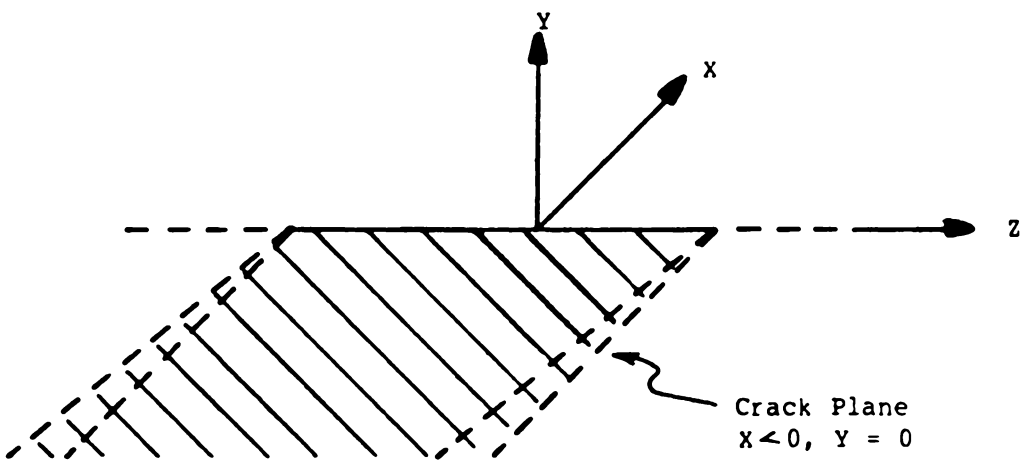

Semi-Infinite Plane Crack in
an Infinite Elastic Body
($-\infty < Z < \infty$)

Geometry of Hartranft and Sih's Analytical Model

Figure 2.1

converted the displacements into the three dimensional stresses.

Two important ideas are presented in this paper. It is the first time, according to the authors, that the three dimensional nature of the stress singularity is presented, i.e., the z component of stress (parallel to the crack border) exhibits singular behavior. Secondly, although the problem which is solved is infinite in three dimensions, the authors point out that the solution should be valid in the middle half of thick plates. Within the same comment, they also indicate a possibility of the singularity order differing from 0.5 as the surface of the plate is approached.

2.3 The Work of Bazant

In 1974, Bazant [19] presented a general method for the solution of three dimensional problems involving singularity rays (a crack front border in the present case). For his approach, he cast the problem in spherical coordinates (see figure 2.2). He then utilized a separation of variables approach, by which the singularity in the problem was eliminated. This resulted in a non-singular, non-symmetric eigenvalue problem in two dimensions, θ and ϕ, which could be solved using standard numerical procedures.

In 1978, Bazant and Estenssoro [11] presented solutions to the crack-free surface intersection problem. He utilized his previous

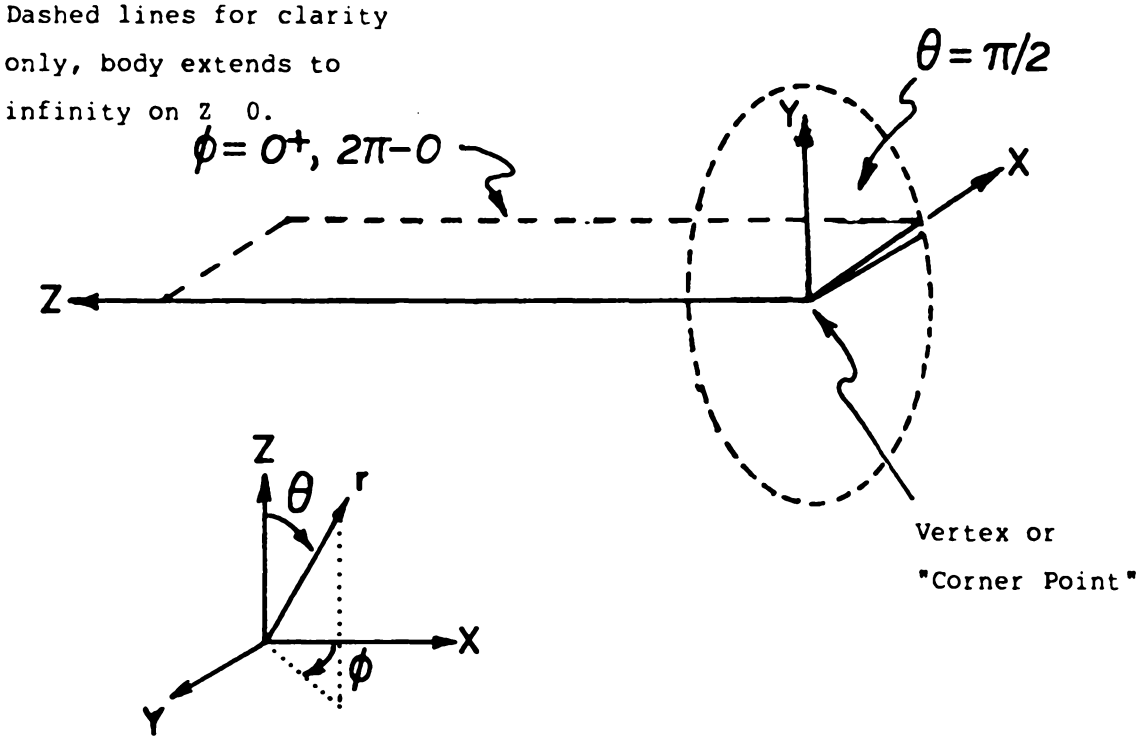

Quarter-Infinite Crack in an Elastic Half-Space

Geometry of Bazant, Swedlow, and Benthem's Model

Figure 2.2

method with some minor variations, which made his method of solution more suitable to the elasticity problem. In solving the problem, the boundary conditions were satisfied on surfaces traced out by radial lines, however no attempt was made to satisfy boundary conditions as r approached infinity in the problem domain. The results of his analysis yielded a value of the stress singularity order of 0.329 for a Poisson's ratio of 0.25, for a stationary crack. Through energy considerations, however, Bazant rationalizes that for a propagating crack in a linear, elastic, homogeneous material, the singularity order must return to 0.5.

2.4 The Work of Folias

In Folias' treatment of the three dimensional cracked body problem, as reported in 1975 [8], he uses a different approach than that of Bazant. His geometry is a thick, infinite plate containing a central through crack (see figure 2.3). His initial problem formulation is in terms of rectangular cartesian coordinates. His method of solution involves conversion of three coupled partial differential equations in three independent variables to a system of three ordinary differential equations in a single independent variable. He then writes the cartesian displacements in terms of semi-infinite integrals containing infinite series within the

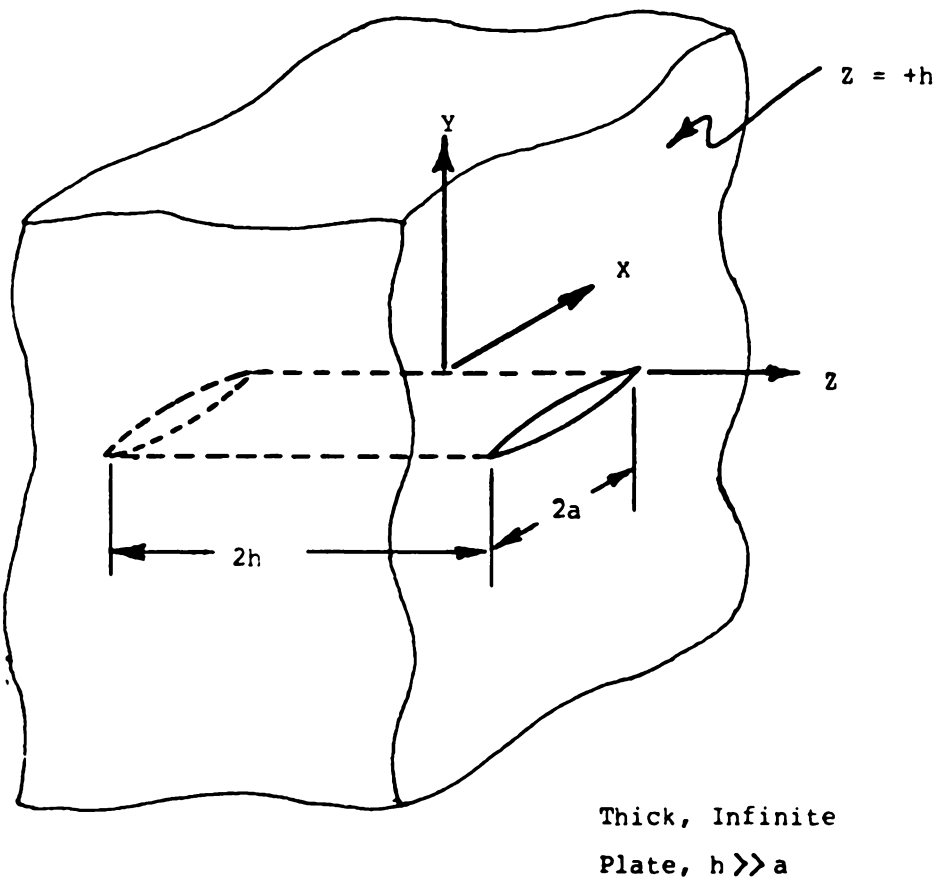

Geometry of Folias' Analytical Model

Figure 2.3

integrands. The final solution of the problem requires solution of an infinite system of equations with an infinite number of unknowns. Folias postulates that the singular part of the solution depends only on the leading coefficient in each equation. Subsequently, he truncates the system to a finite number of terms, which allows numerical determination of the leading coefficients.

After determining the approximate solution in cartesian coordinates for displacements and stresses, he states that the stress singularity order is Poisson's ratio dependent, and has the form

(2.4.1) $$\lambda = -\left(\frac{1}{2} + 2\nu\right)$$

where ν is the material's Poisson's ratio. This result is not in agreement with Bazant and Estenssoro [11] or Benthem [9, 15]. Folias also makes certain assumptions in terms of a spherical reference frame indicating that the stress singularity must vanish at the "corner point" due to the singularity occurring in the equation for the stress normal to the free surface. He also rationalizes, that because of unnatural behavior of his solution for certain values of Poisson's ratio, that linear elasticity theory is an insufficient basis for solution of the three dimensional problems. The results and

rationalizations of Folias prompted considerable disagreement among analysts doing related work [10].

In 1980, Folias published another paper [20] which attempts to clarify and/or justify some of his earlier statements. This paper also presents an overview of most work on the "corner point" problem that occurred in the period 1972-1979. The important points presented relating to his previous work include the following. He states that due to the mathematical intractability of solving certain integral equations, an unknown function exists in the singular term of the equation for the stress normal to the free surface. He states that it is possible for this function to vanish at the free surface, thereby allowing the singularity to exist at the free surface. He also states that his value of the stress singularity, equation (2.4.1) should be interpreted as a minimum value, and that the actual value may be closer to -0.5 than equation (2.4.1) suggests.

2.5 The Work of Benthem

In 1975, Benthem [9] reported the results of his investigation of the stress distribution around the vertex of a quarter-infinite crack in a half-space (see figure 2.2). His problem was cast in a spherical coordinate system, however, he used the cartesian components of stress. He began his investigation by seeking solutions to the coupled

system of three partial differential equations in three unknowns, the Navier-Cauchy equations. Seven solutions to this system were created by Boussinesq in the late 1800's. Four of the seven solutions are today known as the Papkovich-Neuber stress functions, due to the apparent independent discovery of the four solutions by Papkovich in 1932 and Neuber in 1934.

Using a combination of the known solutions, Legendre functions, and the technique of separation of variables in the spherical coordinate system, Benthem sought to satisfy the stress free boundary conditions on the plane $\theta = \pi/2$, and on the crack surfaces ($\phi = 0+$ and $\phi = 2\pi - 0$). After considerable effort, both analytically and with numerical computations, the theoretical singularity order at the corner point was obtained. Benthem's result of 0.3318 for incompressible materials prompted the initial experimental investigation by Epstein [14] which formed the foundation for the current work.

It is interesting to note that Benthem's analysis indicated that the normal stresses, σ_{xx} and σ_{yy} (for the case of an incompressible material), in the plane of the surface z = 0 along the line of crack extension under symmetric loading, should be identically zero. He then postulated that this could be easily verified by direct inspection of a photoelastic coating on a large rubber block, and hence validate his

numerical results. One photograph in his work does indicate a zero order fringe in the specified zone, however, the stresses σ_{xx} and σ_{yy} need only to be equal (assuming geometric symmetry and therefore zero shear stress, τ_{xy}) for this to occur. Indeed, Benthem's results for other Poisson's ratios indicate a different singularity order, but they also indicate equal non-zero stresses in the previously mentioned zone. This stress state would also lead to a zero order isochromatic, which leaves his experimental verification in question.

In a subsequent work, published in 1980 [15], Benthem approached the same general problem using a finite difference formulation. His results obtained from this work were in good agreement with his previous work and also with the work of Bazant and Estenssoro [11].

2.6 The Work of Swedlow and Associates

In 1978, Swedlow published an article [12] outlining a finite element formulation which could be adapted to the solution of the three dimensional variable singularity problem at a crack-free surface intersection (see figure 2.2). This work was based on Williams' [4] application of the Airy stress function with a variable singularity order to the plane sector problem. The finite element formulation involved the development and implementation of a special multi-sectored element which surrounds the singularity.

Burton and his associates, including Swedlow, published another work in 1984 [21] which implemented Swedlow's previous work, where the singularity order in the crack-free surface problem is investigated. Their numerical results are qualitatively similar to the results of Benthem and Bazant, however for Poisson's ratios in the range 0.0 to 0.4, their results indicate a weaker singularity than that of either Benthem or Bazant. The finite element results did coalesce with the results of the others for a Poisson's ratio of 0.0 (singularity order of 0.5).

2.7 The Recent Work of Takakuda

Takakuda [22] has recently investigated the crack border-free surface intersection using an integral equation method. His work includes evaluation of the singularity order for both wedge shaped cracks and surface cracks (see figure 2.4). Of particular relevance is his result for the surface crack where the crack border-free surface intersection angle is 90 degrees and the Poisson's ratio is 0.5. For this case, the singularity order reported is 0.3316, very close to the results obtained by Benthem and Bazant. It is interesting to note, however, that Takakuda's results indicate that the intersection angle strongly influences the singularity order, much more so than the material's Poisson's ratio.

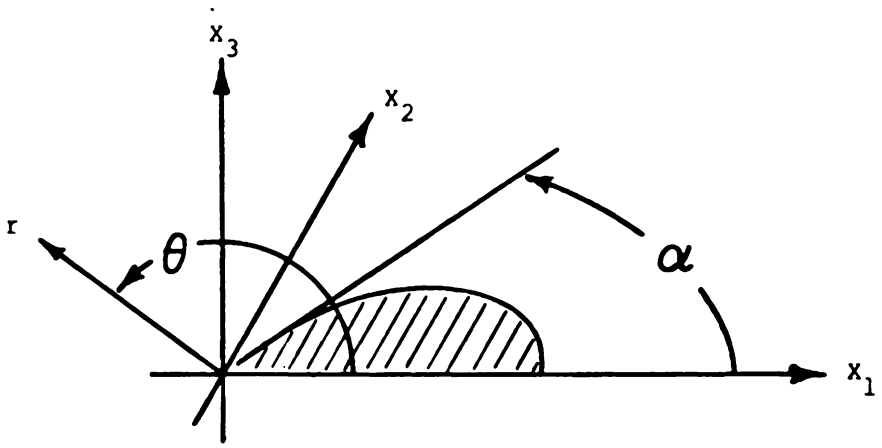

Geometry of Takakuda's Surface Flaw Model

Figure 2.4

2.8 Summary of the Analytical and Numerical Work

This analytical/numerical work which has been performed in the last ten or fifteen years shows general agreement in two areas. First, the work indicates that the singularity order in three dimensional cracked bodies tends to vary from the classical two dimensional value of 0.5 as the crack border intersects a free surface. Secondly, this variation is at least dependent on the material's Poisson's ratio. There are several other considerations which have not been mentioned that are pertinent to practical engineering applications.

It is understood that the mathematical aspects concerning the general solution to three dimensional cracked body problems are extremely complicated. However, as yet there are no solutions, analytical or numerical, which approach the problem of the singularity order transition from the accepted "interior" value of 0.5 to some different surface value. Also, the analysts have presented only minimal empirical verification of their results. These two facts prompted the original experimental work of Epstein [14] and Smith [23], whose work forms the foundation of this work.

2.9 Experimental Work of Epstein and Smith

In 1983, Epstein completed his doctoral dissertation [14] which was centered around an experimental program to verify the existence of a singularity order transition zone. His work also served to experimentally verify the analytical results of Bazant and Benthem, although Epstein's test geometry (figure 2.5) had finite dimensions that only approximated the semi-infinite geometry used in the analytical investigations.

Epstein's program consisted of testing several modified compact bending models, designed to simulate an ASTM E-399 3-point bend specimen. His work utilized the methods of stress freezing photoelasticity to measure three dimensional stress distributions, and moire interferometry to measure three dimensional displacement fields. By using the two methods independently to measure a parameter, λ, common to both, he was able to verify his own results.

While the work of Epstein was certainly an important contribution to the understanding of the three dimensional crack problem, a few questionable assumptions were noted in his formulation of an algorithm to extract the stress singularity order from experimental data. One of the purposes of the current work is to improve the methods of data analysis which Epstein developed.

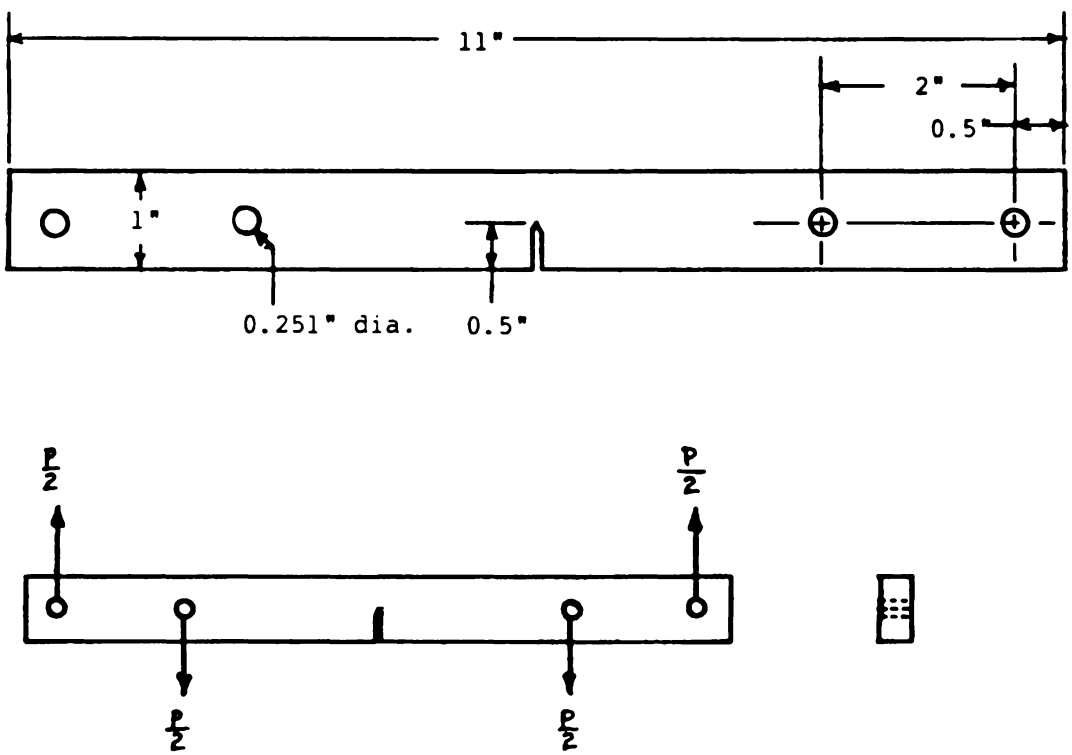

Epstein's Experimental Model Geometry

Figure 2.5

Subsequent to the completion of Epstein's dissertation, the current experimental program was initiated by C. W. Smith in parallel with a post-doctoral investigation by Ruiz and Epstein [17]. The achievements of the current program relating to the previous work of Epstein are presented elsewhere in this work.

TESTING PROGRAM

3.1 Introduction to Test Program Development

Several things needed to be considered in developing a test program for the study of surface flaws. These included material selection, model geometry, time required and cost of each test, and actual test procedure. A brief review of each of these follows.

In view of the success reported by Kirby [24] in performing three-dimensional photoelastic tests to determine the SIF distributions in surface flaws, it was decided to use a similar material. The stress freezing material to be used is PSM-9, a special epoxy material available in cast plate form from Photolastic Division of Measurements Group, Incorporated located in Raleigh, North Carolina. A description of the material properties can be found in appendix I.

3.2 Design of Model Geometry and Model Construction

The development of a satisfactory test geometry for testing natural surface flaws was time consuming. A model geometry which would minimize wasted material as well as be easy to manufacture was desired. It would also be required that the model geometry meet size requirements with respect to crack length to plate width and height ratios so as to simulate infinite boundaries. After consulting Sih's manual on stress intensity factors [25], it was found that a plate width to crack width ratio of 5 was sufficient to meet the requirements. No explicit information was found concerning plate

height. After reviewing the work of Kirby [24], it was found that a plate height of about 15 times the crack width produced a uniform uniaxial stress field between the crack plane and the points of load application. For the crack geometries to be considered (maximum width of 1 inch), the distance between loading points was chosen to be greater than 15 inches.

Kirby had originally used a large "dog bone" model geometry. In order to save material, a rectangular geometry was tested first. Due to stress concentrations around the loading pin holes, the first model cracked between these holes before the "starter crack" in the plate center began to propagate. The next shape tested was also rectangular, however fiberglass cloth was bonded to the model's surface around the load application area using PC-10 epoxy. The idea behind this approach was to reinforce the model to eliminate the cracking. However, due to the large mismatch between the thermal expansion coefficients of the fiberglass cloth and the epoxy model, severe cracking of the model occurred at the edge of the reinforcing layer during the initial heating cycle. Due to the test program schedule, further development of an improved model geometry was not pursued. The remainder of the test models were the "dog bone" type (figure 3.1), as used by Kirby.

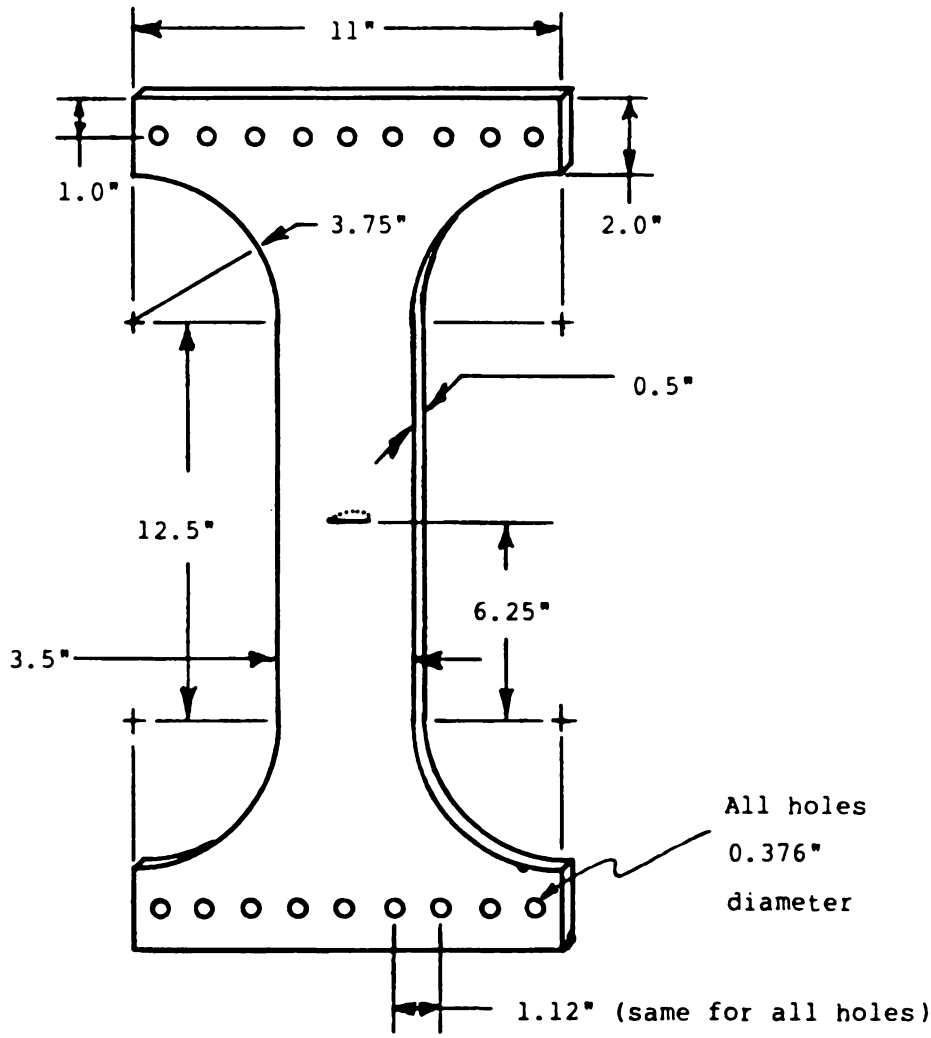

Surface Flaw Model Geometry

Figure 3.1

The "dog bone" models are cut from a precast sheet of the PSM-9 epoxy. The sheets are 24x24 inches (nominal dimensions) when purchased. This initial size is large enough to allow two complete models, including calibration specimens, to be fabricated from one sheet. The model and calibration specimen outlines are traced on the epoxy sheet using a felt tip pen. The models are cut from the sheet on a bandsaw using a 0.035 inch thick, high alloy, 13 tooth per inch bandsaw blade operated at low speed to avoid excessive heat. The models are cut out of the sheet by hand, using light cutting pressure. The model edges are then smoothed with sanding paper, starting with 80-grit and ending with 220-grit, always sanding parallel to the loading axis of the model. This smoothing is done to prevent crack initiation and propagation from the saw marks. See figures 3.1 and 3.2 for the shape and dimensions of the finished model and calibration specimens.

Due to the very high coefficient of thermal expansion of the epoxy material, and the required heating cycle, it is necessary to apply the loads through pins. The holes in the model which receive the 0.375 inch diameter steel pins are produced in the following manner. A slightly undersize hole is drilled in the epoxy plate using a "C" drill in a drill press at about 220 r.p.m. Next, a 90 degree countersink is used to lightly bevel the hole edges to remove any

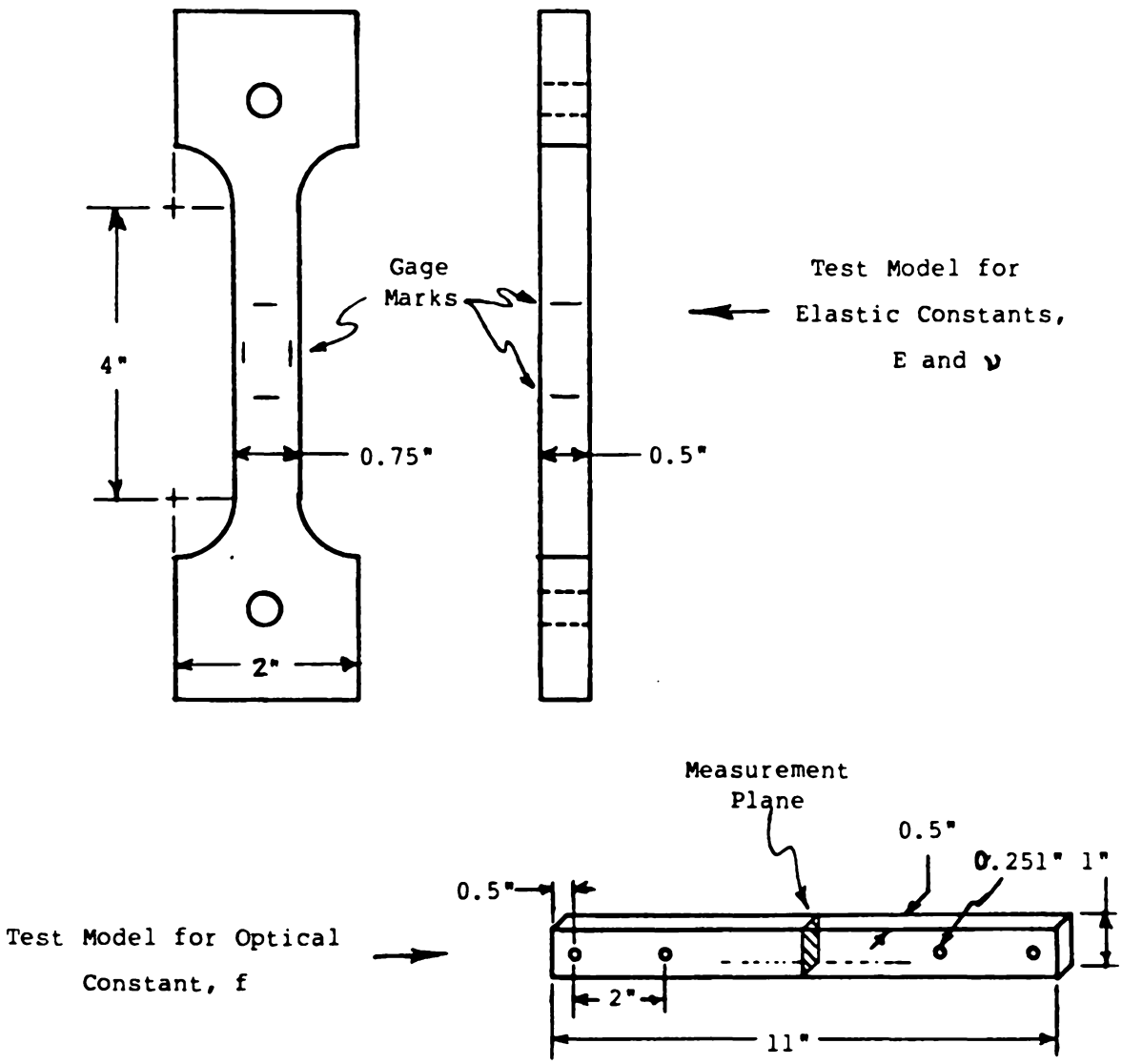

Models Used to Determine Material Properties

Figure 3.2

roughness or chip marks caused by the drilling operation. The holes are then finished to size using a 0.376 chucking reamer in the drill press at the slowest rotary speed. This allows a 0.001 inch clearance fit at room temperature.

The natural cracks are produced in the test models in the following manner. The model is placed on a rigid, flat surface. A special tool (see figure 3.3) is held normal to the plate surface and is struck with a 16 ounce dead-blow mallet. A starter crack will propagate a short distance ahead of the cutting edge of the tool and arrest. This procedure was performed many times on waste material to develop the striking technique which produced a suitable starter crack. Most starter cracks produced in this manner were nearly semi-circular in shape, regardless of the curvature of the cutting tool edge, and propagated about one quarter of the way through the depth of the plate. Once the starter crack is produced, the model is ready to be placed in the stress freezing oven.

The two types of calibration models used in the tests are produced using similar procedures as those used to fabricate the cracked model. The small "dog bone" specimen is used to measure the elastic modulus and Poisson's ratio of the stress freezing epoxy. The bending specimen is used to evaluate the material's photoelastic fringe constant (see figure 3.2). The only major difference in the construction of these

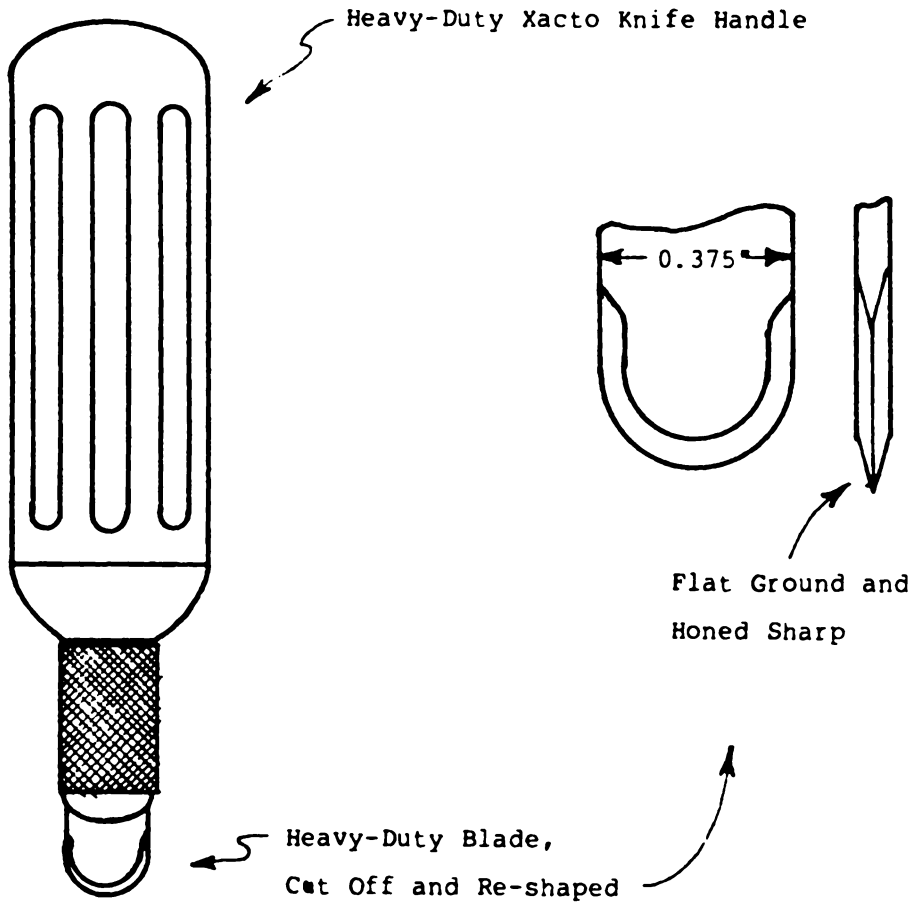

Special Tool for Initiating Surface Flaws

Figure 3.3

models is in the edge finishing. Instead of using sanding paper, the edges of the calibration models are smoothed using a high speed shaping router (available from Photolastic Division, Measurements Group, Inc.) with a 0.25 inch diameter, two flute end mill. This finishing procedure produces the final model dimensions accurately while maintaining a suitable surface finish. Dimensional control is accomplished by securing the roughed out model to a guide plate with thin, double-sided tape. The guide plate, which rides against a guide pin on the base of the router, has the correct finish dimension for the model. Models finished using this procedure showed dimensional variations of less than 0.2 percent.

3.3 Stress Freezing Test Procedure

Once the models are fabricated, they are placed in their respective loading fixtures (see figure 3.4) in the stress freezing oven (see appendix I). Particular care is taken to make sure the load is evenly distributed between the loading pins on the cracked model to prevent in-plane bending. Only a small load of about 5 pounds is applied to the cracked model prior to heating. This keeps a small amount of tension on the loading cables so that they remain in proper position. The load pins for the bend model are cleaned to insure minimum friction between the pins, the model, and the links (see figure 3.4).

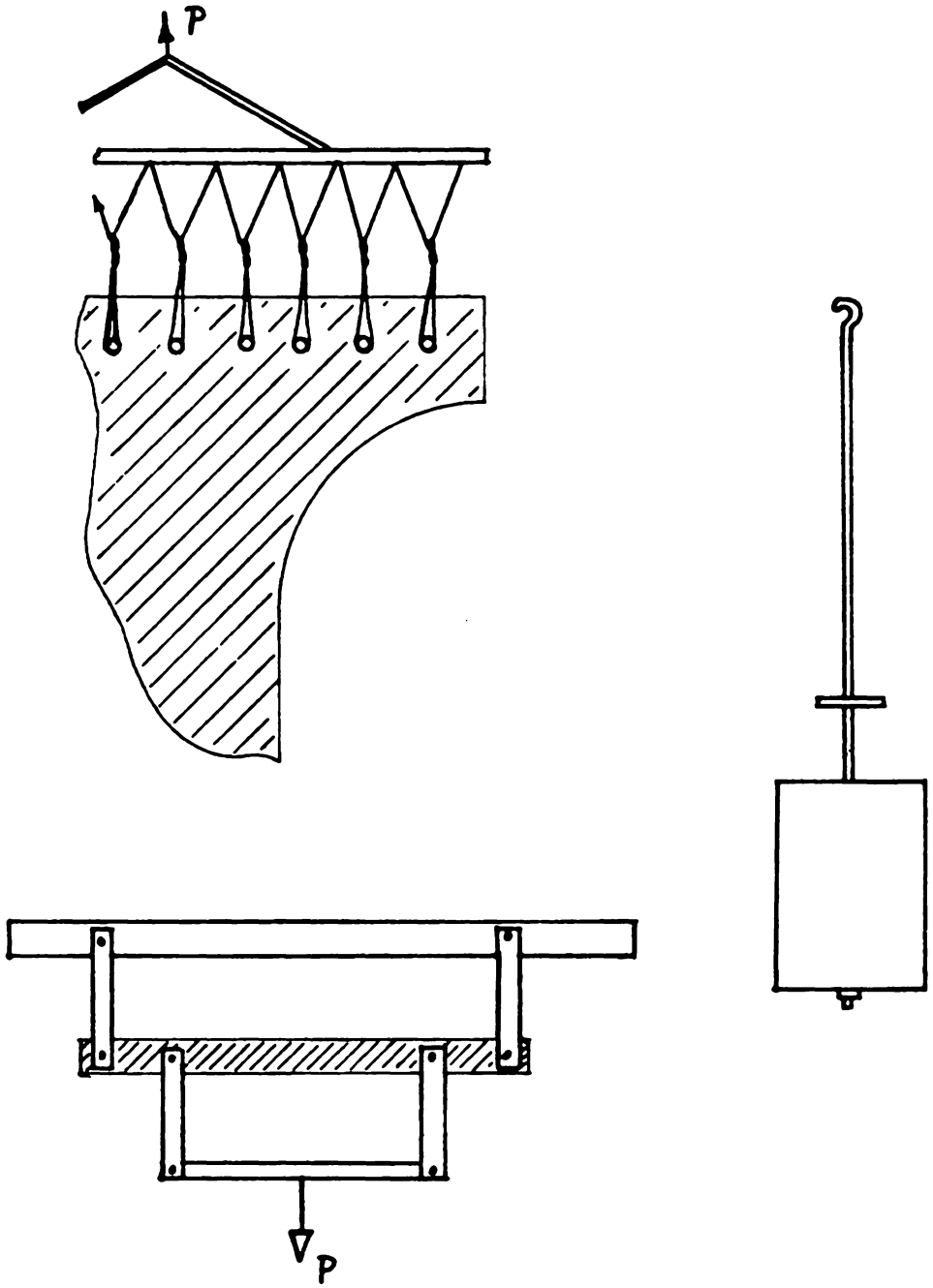

Load Application Fixtures for Stress Freezing

Figure 3.4

A load of 1 pound, producing a 1 inch-pound moment in the bend model, is applied as shown in the figure. This loading produces about 15 fringes per inch in the model, allowing accurate and repeatable determination of the material fringe constant (this procedure is covered in chapter 4). A 5 pound load is placed on the "dog bone" calibration model. This produces enough deformation for material property determination without inducing inelastic behavior.

The temperature control cam on the oven is set such that the servo control arm is adjacent to the "start" mark on the cam. The timer is adjusted for a 72 hour cycle time, and the oven is turned on. The control cam profile is designed to allow a 0.5 inch thick model to attain a uniform temperature of 105 degrees Centigrade in about six hours. A temperature-time profile for the entire test may be found in the appendix I, figure A1.1. Once the models reach uniform temperature, the cracked model is loaded to grow the crack.

The load is first increased to 50 pounds by adding iron weights to the loading fixture (see figure 3.4). This is done gradually while at the same time observing the starter crack to insure crack growth is not yet occurring. Once this is done, small increments of load are applied by adding small lead shot to a container affixed to the loading fixture. The load is increased very slowly in this manner while the starter crack is observed for the onset of crack extension.

Once crack extension begins, no additional load is added. Using this procedure, crack velocity is maintained at between 0.01 and 0.1 inch per minute. When the crack reaches the desired size, the load is reduced to one half the load required to maintain crack extension. This typically resulted in remote stresses of about 15 to 20 p.s.i. Only one of eight models loaded this way failed due to crack propagation after the load was reduced to this level.

Once this procedure is completed, the cooling portion of the stress freezing cycle is initiated. The temperature control cam reduces the oven temperature at a rate of 2 degrees Centigrade per hour until the temperature is reduced to 70 degrees Centigrade. The cooling rate is then increased to 5 degrees Centigrade per hour until the temperature reaches 45 degrees Centigrade. This temperature is then maintained to inhibit moisture absorption by the epoxy material until the models are ready to be analyzed (again, see figure A1.1 in appendix I). Moisture absorption can cause the formation of "time-edge" fringes. This phenomenon and its effect on the results of the tests are discussed briefly in Appendix I.

COLLECTION OF EXPERIMENTAL TEST DATA

4.1 Obtaining Material Properties

As mentioned in chapter three, two types of calibration models are run with each surface flaw model. A "dog bone" model is used to evaluate the material's elastic properties, and a four point bend model is used to evaluate the material's fringe constant (the constant coefficient in the stress-optic law). Each calibration model is removed from the stock plate material in a location adjacent to the central portion of the surface flaw model (see figure 4.1), since some variation in the material's properties may occur within a single plate. The calibration models undergo the same thermal cycle as the cracked model, although differences in the cycle should not have any effect on the measured properties. All measurements are made after the thermal cycle is completed with the models at room temperature.

Prior to beginning each test, the elastic constant test specimen is scribed with gauge marks so that post-test extensions can be measured (see figure 3.2). The distance between the marks is measured before and after the test using a Nikon profile projector. The projector has a magnification factor of ten, and is equipped with a micrometer stage graduated in 0.0001 inch increments. Very accurate and repeatable measurements can be made on these transparent models. Measurements can routinely be repeated to within 0.05 percent.

The longitudinal strain is calculated from the length measurements on the four sides of the small "dog bone" model. An average of these

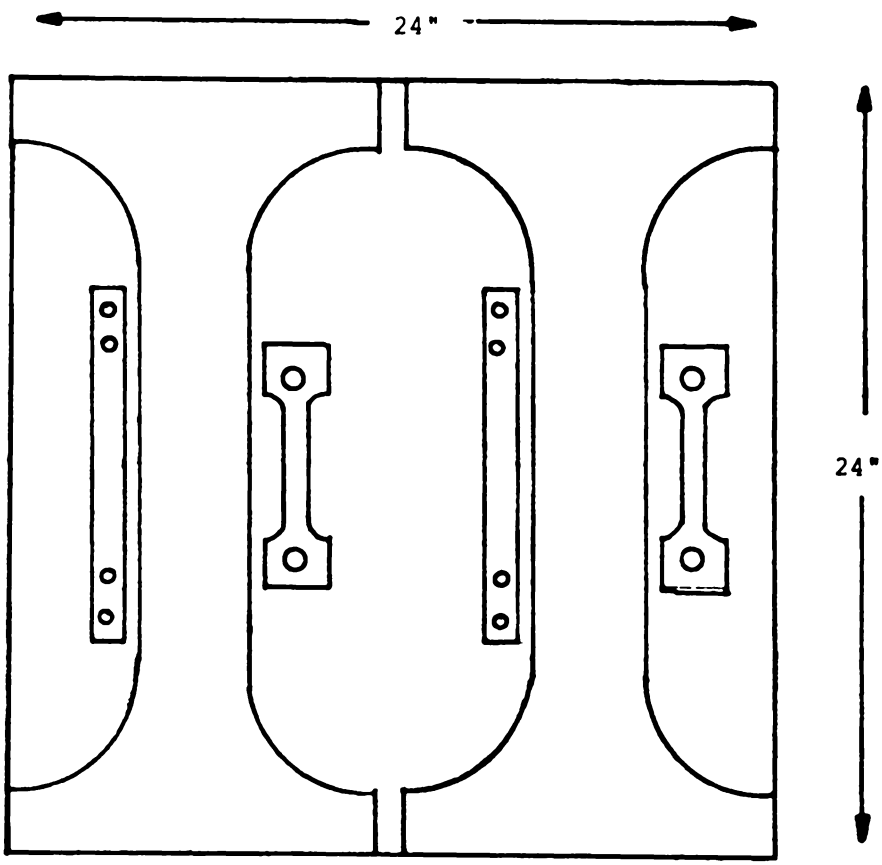

Pattern Used for Removing Models From Stock Material

Figure 4.1

four values is taken, which eliminates any effect a small amount of bending would have on the strain measurement. Measurements in a plane normal to the loading direction are also made and an average transverse strain is calculated. The longitudinal strain is substituted into the uniaxial Hooke's law, along with the effective load and cross sectional area at the midpoint between the longitudinal gauge marks, to obtain the elastic modulus of the material above its "critical" temperature (see appendix I). Typical values measured this way are about 2600 p.s.i. The longitudinal and transverse strains are also used to calculate the material's Poisson's ratio. Typical values varied from 0.47 to 0.49 at temperatures above the "critical" temperature.

Careful measurements are also made of the dimensions on the fringe constant calibration model. The measurements are also verified using micrometers or vernier calipers. The accuracy of these measurements is important if consistency in the experimental results is expected. Once the external dimensions are measured, the fringe spacing is measured in a direction normal to the beam's longitudinal axis using the Photolastic 051 polariscope. A plot of the fringe order, N, versus the distance from the neutral axis, y, is made (see figure 4.2).

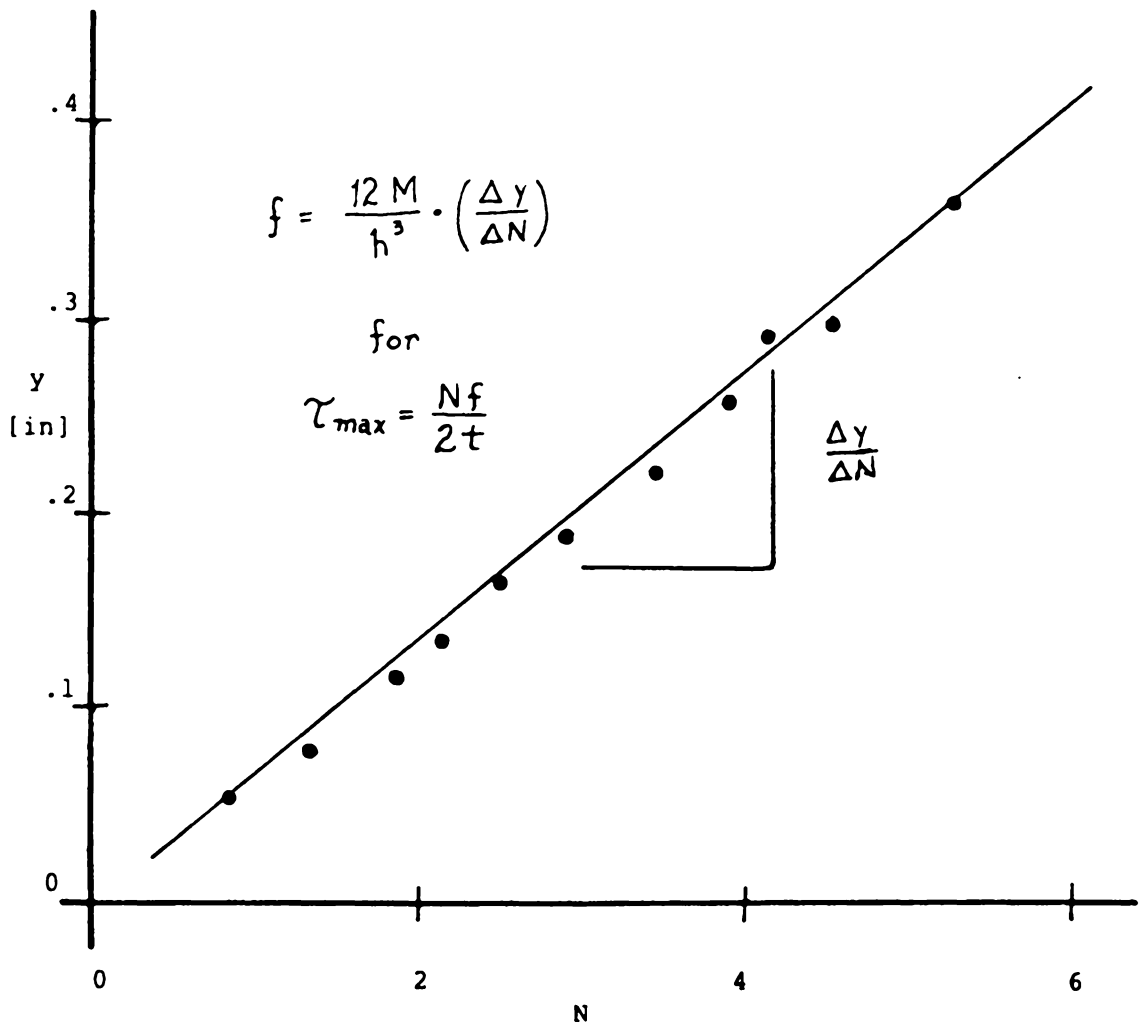

Graph of y vs. N for Determination of Fringe Constant

Figure 4.2

The slope, $\Delta y/\Delta N$, of the linear regression line through the points is substituted into

$$f = \frac{12\ M}{h^3} \cdot \frac{\Delta y}{\Delta N} \qquad (4.1.1)$$

to obtain the material fringe constant, f. In (4.1.1), M is the applied bending moment at the measurement plane, and h is the total beam depth. The values of f which were determined for the six tests (T2 - T7 inclusive) ranged from 1.83 to 2.00 #/in./fringe.

4.2 Sectioning the Three Dimensional Models

The algorithms which have been developed to determine the stress singularity exponent require maximum shear stress distributions in the n-z plane, in the z direction (see figure 4.3). This is accomplished by sawing the cracked section (see figure 4.4) from the test model using a standard band saw at a slow speed with a 14 tooth per inch blade. Care is taken not to overheat the model. After removing the cracked section with the large saw, the cracked section is gently clamped in the pivot arm of a Beuhler Isomet saw (see [26] for description), and the slice at maximum crack depth is removed. Each of the remaining two parts are, in turn, bonded to a special fixture (see figure 4.5) with Duco cement. The special fixture allows for the part

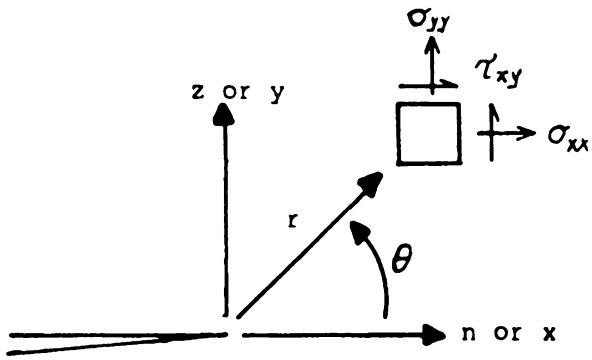

n-z-t is an orthogonal, curvilinear coordinate system. Z remains normal to the flaw plane, n remains normal to the flaw border.

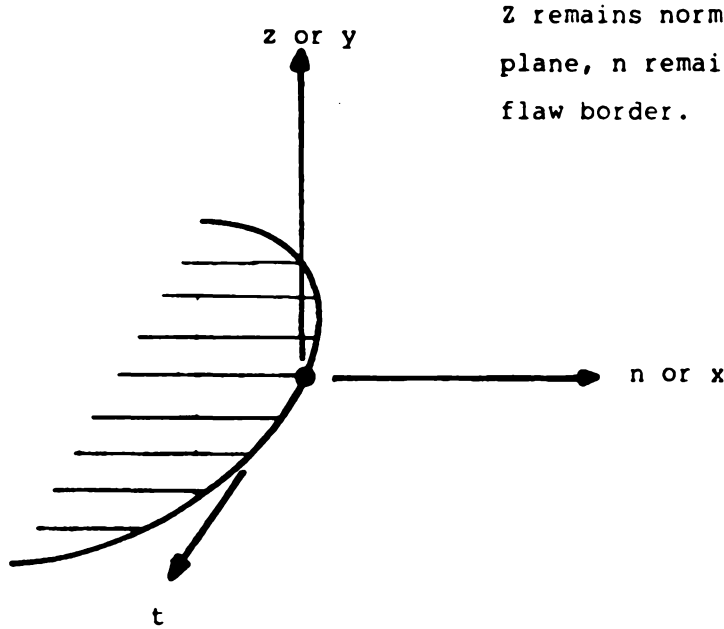

Local Coordinate System Relative to Flaw Border

Figure 4.3

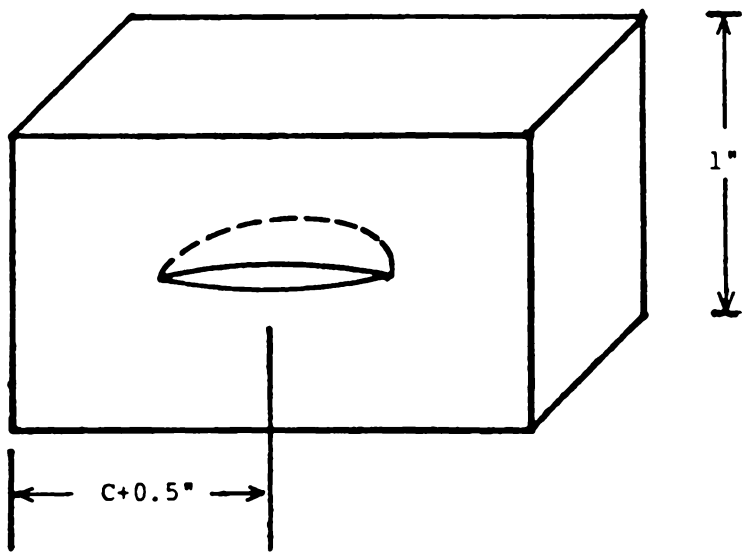

Section of Cracked Model Removed for Analysis

Figure 4.4

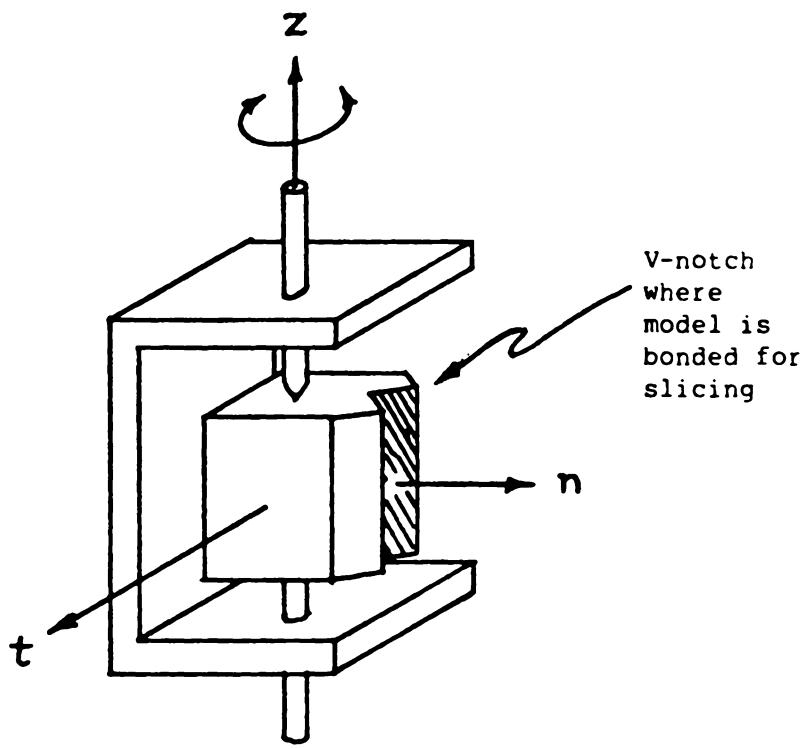

Saw arm moves in the z-t plane. Fixture translates in the n-direction. V-block mounted on needle bearing allows rotation about the z-axis.

V-Block Fixture Used for Slice Removal

Figure 4.5

to be rotated about the z-axis direction, simplifying the realignment procedure for cutting each slice. This fixture is mounted to the pivot arm of a Beuhler Isomet low speed saw. The saw is equipped with a 0.012 inch thick, 4.0 inch diameter blade, which is operated at a speed setting of 5 or 6. Previous work by Epstein [26] indicates that this cutting system does not induce residual stress in the epoxy material.

Using this system, thin slices approximately 0.020 inch thick are removed from the cracked section. Figure 4.6 illustrates the slicing planes and the usual order of slice removal. The individual slices are marked with an identification code using a Staedtler Lumocolor Superfine waterproof pen. A common identification code is utilized for all of the the tests. The code has the form

T n - xx $

where T stands for test, n is the test number, xx is the slice location in degrees (see figure 4.6), and $ is either R or L to specify whether the slice is from the right or left side of the crack's maximum depth. By using this common code, raw experimental data collected from each slice is easily organized, and it is not necessary to collect the data from each slice immediately after it is removed from the cracked model section.

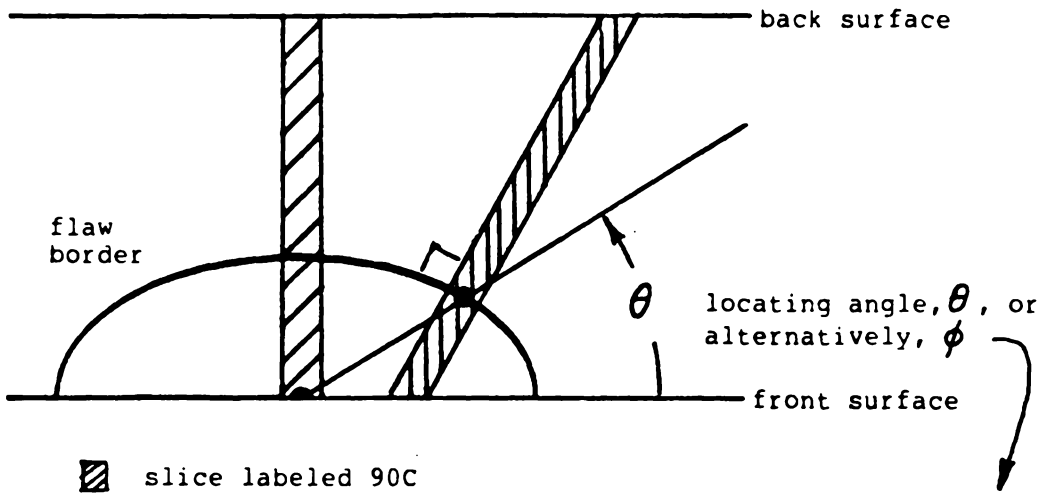

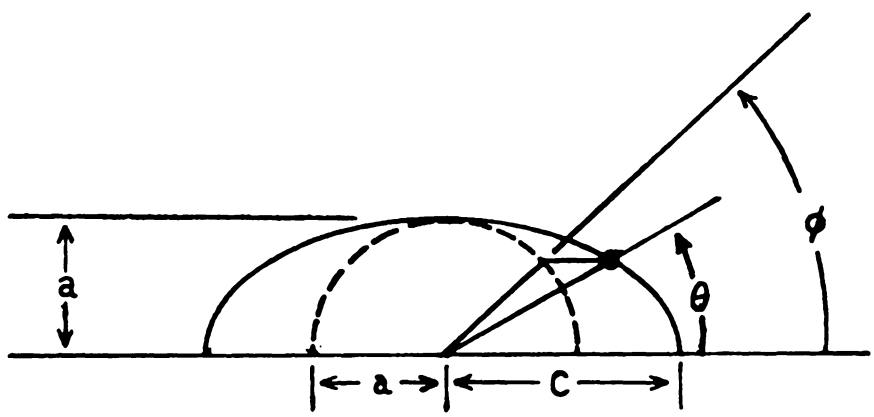

Slicing Planes and Slice Identification System

Figure 4.6

The thickness of each slice is measured with a 0 to 1 inch micrometer having 0.0001 inch increments. This thickness is measured over the crack tip area, and is then marked on the slice with the Lumocolor pen. All of the slice information is also copied on a data summary sheet, which contains all of the information from all of the slices in each test. Once all of the slices have been removed and marked, data from the isochromatic fringe patterns are collected.

4.3 Photoelastic Fringe Multiplication

Since the purpose of the experimental program is to measure an effect associated with the free surface-crack border intersection, it is necessary to collect as much information near this intersection point as possible. To accomplish this, very thin slices must be removed from the model (about 0.020 inch thick). Since the isochromatic fringe order is directly proportional to the slice thickness by

$$N = \frac{2\tau_{max}}{f} \cdot t \qquad (4.3.1)$$

and the maximum shear stresses in the models are small, only one fringe is usually visible when the slices are viewed through an ordinary circular polariscope. The use of the Tardy method [27] to

obtain fractional fringe orders was investigated, however, only five to eight data points could be collected this way. Also, due to the width of the single visible fringe, accurate location of the fringe center was not possible.

An alternative method of data collection yielding more data points with increased accuracy is the method of isochromatic fringe multiplication developed by Post [28, 29], and subsequently used by Epstein [14]. The fringe multiplication unit used by Epstein was a prototype developed by Epstein for use with three dimensional photoelastic slices in his investigation of the singularity order variation in a compact bending specimen. A modified version of the same unit used by Epstein is used in the present investigation of the surface flaw models.

The operating principle of a fringe multiplication unit is quite simple, while the design of a system to incorporate the principle can be tedious. The basic principle is this: Pass a light beam through a photoelastic model more than once, and the effective model thickness is increased the number of times the light passes through the model. An operating system which makes use of this principle must include: (1) an accurately collimated light source, (2) a circular polariscope, (3) a partial mirror system for multiple reflections, (4) an index matching oil bath contained within the partial mirror system, (5) a

device for selecting the desired beam multiple, (6) a method to focus the image, and (7) a method of viewing the image which allows measurements to be made on it. These are just the minimum design requirements. It is not difficult to see how much time is involved in the design and fabrication of such a system from the initial conception of the idea. To save time, the following approach was taken.

Several modifications were made to Epstein's unit which improved the image quality and allowed better repeatability of fringe location measurements (see figure 4.7). Where Epstein had used two pieces of cardstock to form a slit aperture to select the desired fringe multiple, a circular metallic aperture (0.040 inch diameter) was inserted. A 5 mW He-Ne laser was mounted directly to the unit, instead of using mirrors and a remote laser source, to minimize the amount of adjustments necessary to the system each time it was used. A more stable mounting base for the partial mirror unit was fabricated. This reduced the probability that the partial mirror unit would shift relative to the micrometer stage, causing errors in the direct measurement of the fringe locations. The original partial mirrors, which had a reflection ratio suitable for multiplication factors of greater than 15, were replaced with 50/50 reflection/transmission ratio mirrors which are better suited for multiplication factors of 3

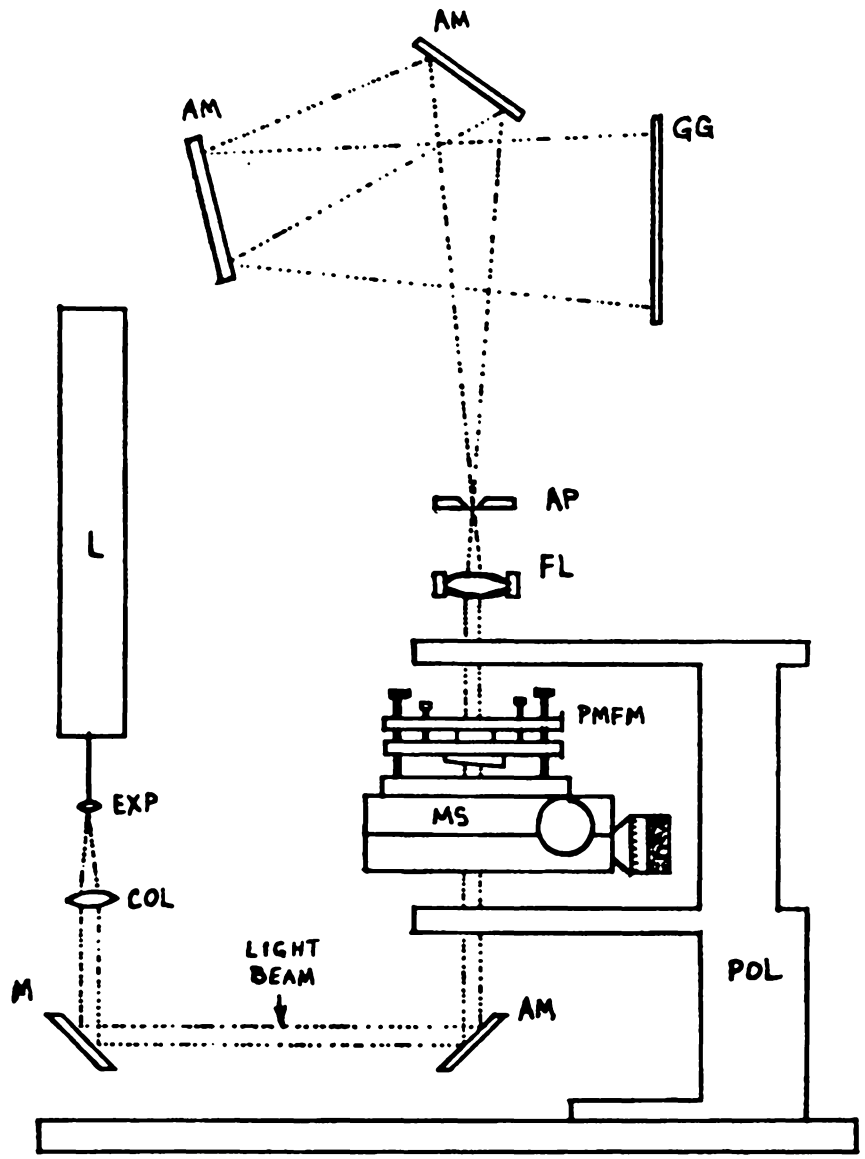

L - Laser
EXP - Expanding Lens
COL - Collimater
M - Mirror
AM - Adjustable Mirror
POL - "051" Polariscope
MS - Micrometer Stage
PMFM - Partial Mirror Fringe Multiplication Unit
FL - Focusing Lens
AP - 0.040" Circular Aperture
GG - Ground Glass Viewing Screen

Diagram of Fringe Multiplication Unit

Figure 4.7

to 7. The old mirrors had also been scratched because of contact with the slices and frequent cleaning. Finally, one of the image directing mirrors was relocated to allow an unobstructed field of view on the ground glass viewing screen. Due to time constraints, an improved focusing and viewing mechanism was not installed. These are all of the modifications which were made to Epstein's prototype unit.

Figure 4.7 shows a schematic diagram of the entire fringe multiplication system after all modifications have been performed. The figure shows all optical components, most structural components, and various auxiliary devices which aided in the operation of the unit. Most components are shown in their approximate relative orientation in the figure.

4.4 Manual Collection of Raw Data

All of the slices from the tests are analyzed using the multiplication unit. Multiplication factors of 5, 7, or 9 are commonly used, however multiplications as high as 21 have been successfully photographed. Several slices were analyzed using different multiplication factors in conjunction with varying increments of Tardy compensation to evaluate possible systematic errors associated with the optical system. The multiple data sets from each slice were plotted on a common plot to determine if any systematic error existed.

The largest variation in the data seemed to be associated with the human error incurred in locating the fringe centers. This variation became so small after analyzing several slices, that two data sets collected at different multiplications could not be directly distinguished from each other when plotted on the same graph of fringe order, N, versus radial distance, r.

The manual collection method works in the following way. The slice being analyzed is contained in the partial mirror unit which in turn is mounted to a micrometer stage. The stage has a central opening allowing the collimated, polarized light beam to pass through. An image of the light beam at the slice location is focused on a ground glass screen containing an aiming crosshair. By rotating the micrometers attached to the x-y stage, the mirror unit containing the slice is moved relative to the light beam, which remains stationary. This causes the image of the slice and its isochromatic pattern to move across the viewing screen. By aligning the crack tip with the crosshair and taking a reference reading, radial measurements to any location on the slice can be made. The image magnification for the current system set-up is measured to be 8.34x. The exact magnification factor is not required because measurements are taken from micrometers which are moving the slice directly.

Even though very accurate data is obtained using this method, collecting data with the manual method has proven to be both tedious and time consuming. It would not be uncommon for it to take over two hours to set up the system and collect data from one slice (see Appendix I for discussion of time-edge effects on measured values). If only one or two slices were to be analyzed this would present no problem, however, some of the test models were sectioned into twelve or fifteen slices. Although all of the initial data for this current series of tests has been collected using this method, another method which will save considerable time is suggested.

4.5 Semi-Automated Data Collection

This method still uses the fringe multiplication unit, however no measurements are made by directly moving the photoelastic slices. Instead, one or several photographs are taken of the isochromatic patterns, and data is collected from the photographs using an Altek AC 90 digitizing tablet. The tablet is connected to an IBM Personal Computer. An interactive computer program called DIGIFRNG.BAS (see appendix II) was written and thoroughly tested. The program allows data to be selectively collected, displayed, printed, and/or stored on a disk file for future use.

Data from several slices were collected using this system, and the total procedure, including the set-up of the multiplication unit, took less than 45 minutes, considerably faster than with the manual method. Accuracy of the data collected by the semi-automated system was comparable to that obtained using the manual method (section 4.4). This method of collecting and storing optical data has been adopted by several other experimental mechanics researchers. Joh [30] has reported greatly reduced data collection time and improved accuracy in the collection of displacement data from interferometric fringe patterns.

DEVELOPMENT OF A MATHEMATICAL MODEL

5.1 Development of Stress Field Equations

In 1952, Williams [4] formulated a stress function which could be applied to the two dimensional problem of an infinite sector with a variable vertex angle. The stress function has the form

$$\chi(r,\theta) = r^{(2-\lambda)}\, g(\theta) \tag{5.1.1}$$

By satisfying the biharmonic equation, along with specifying finite strain energy around the crack tip, the functional form of $g(\theta)$ is found [34]. Further, by imposing conditions of symmetry in the vicinity of the crack tip, there results an infinite number of possible solutions. The resultant stresses are in the form of infinite series, where the exponents of r were found to be functions of the sector vertex angle for a sharp notch in an infinite plate. In 1957, Williams used this stress function to solve the problem of an infinite plate containing a crack, i.e. a sector of angle 2π (also called a branch cut in mathematical references). For this problem, he found the exponent of r in the leading term of the stress series to be -0.5, corresponding to the classical LEFM stress singularity value of -0.5.

Since more recent work suggests a variation of the singularity order, and the Williams stress function allows this variation in two dimensions, the problem formulation using this stress function, employed by Epstein [14] and subsequently corrected by Olaosebikan

[31] will be employed in the present work. By eliminating all terms in the series containing powers of r greater than or equal to 0.5, this formulation yields stresses close to the crack tip in a local rectangular cartesian reference system (see figure 4.3) in the form

$$\sigma_{ij} = D\, r^{-\lambda} F_{ij}(\lambda,\theta) \tag{5.1.2}$$

where the σ_{ij} represent components of the symmetric stress tensor, and a constant term is commonly added to σ_{xx} to account for biaxial load effects.

From the theory of photoelasticity [32] it is known that the isochromatic fringes represent lines of constant principal stress difference (or maximum shear stress) in the plane normal to the direction of light propagation. The governing relation is

$$\frac{\sigma_1 - \sigma_2}{2} = \tau_{max} = \frac{N f}{2 t} \tag{5.1.3}$$

where

σ_1 , σ_2	are the principal stresses,
τ_{max}	is the maximum shear stress,
N	is the fringe order,
f	is the material fringe constant,
t	is the model thickness.

A derivation of this equation may be found in Experimental Stress Analysis by Dally and Riley, pp. 409-411.

By placing equations (5.1.2) into the equation for the maximum in-plane shear stress

$$4\tau_{max}^2 = (\sigma_{yy}-\sigma_{xx})^2 + 4\tau_{xy}^2 \tag{5.1.4}$$

an equation which may be applicable to modeling photoelastic data obtained from the singular stress field surrounding the crack tip is obtained:

$$\tau_{max}^2 = H^2 + H\sigma_o \sin((\lambda+1)\theta) + \frac{\sigma_o^2}{4} \quad , \quad H = \frac{D\lambda \sin(\theta)}{r^{\lambda}} \tag{5.1.5}$$

It is obvious that this equation is non-linear and cannot be solved in a direct manner. However, by observing that σ_o is always less than H, dividing through (5.1.5) by H^2, and ignoring the quadratic term, the binomial expansion may be used to take the square root of the right hand side, leading to the approximate form

$$\tau_{max} = \frac{D\lambda \sin(\theta)}{r^{\lambda}} + \sigma_o \sin((\lambda+1)\theta) \tag{5.1.6}$$

This is the approximation made by Smith [35] in his Two-Parameter

Method, which is widely used in photoelastic analysis. This approximation is reasonable as a first order correction from a state of biaxial tension. The error introduced by the approximation leading to equation (5.1.6) yields conservative (increased) values of the stress eigenfactor, D (K_I when $\lambda=0.5$). In view of this "safe" error, and the computational simplification which the approximation allows, (5.1.6) is adopted as the basic model equation for the present experimental investigation.

5.2 Significance of Model Equation Parameters

There are three parameters, D, λ, and τ_o, in the model equation (5.1.6) which must be determined from analysis of the experimental photoelastic data, N_i and r_i. In order to develop a suitable algorithm for determination of the parameters, their physical significance with respect to the stress field and their influence on the data distribution, i.e. isochromatic fringe pattern, are examined.

The parameter D, the stress "eigenfactor", is assumed to be a linear function of the remote load applied normal to the crack plane and a smooth, unknown function of geometry. The stress singularity order (or eigenvalue), λ, is assumed to be independent of in-plane geometry, coordinate system, and loading. However, it is assumed to vary smoothly in a direction normal to the n-z plane (the "t"

direction). The parameter τ_o represents the deviation of the remote stress field from a state of biaxial tension. It should be noted that as the value of the non-singular term, τ_o, goes to zero, that the error associated with using approximate equation (5.1.6) vanishes.

In order to gain further physical insight into the mathematical problem, the effect of variation of each of the three parameters upon the isochromatic patterns, or "fringe signatures" [33], is investigated. In order to accomplish this, an interactive graphics program called "LOOPS.BAS" (see appendix II) is developed. The program allows comparison of up to four isochromatic patterns generated by the model equation (5.1.5) with variations in the parameters. After entering the desired parameters for one set of fringe loops, the program calculates the coordinates of the lines which represent the center of the isochromatic fringes. These "theoretical fringes" are then displayed on the CRT monitor. A copy of the CRT display of theoretical fringes, generated using equation (5.1.5), is shown in figure 5.1. It is then possible to alter one or more of the parameters by an arbitrary amount, and overlay the pattern associated with the altered parameters onto the original pattern, allowing relative changes in maximum shear stress distribution to be visualized. It is noted in passing that only the mode I stress field was modeled, since this is the only type of loading currently being

considered, however, the code could easily be modified to model Mode II or Mode III loading.

This visual interpretation of the maximum shear stress distribution revealed the following. Changes in the non-singular stress component in (5.1.6) causes a tilting of the fringe loops, with an associated enlargement or reduction in the average radial distance to points on a loop (an example is shown in figure 5.2). This behavior is documented by Liebowitz, Lee, and Eftis [34].

The dominant variation of the fringe pattern caused by changing the stress eigenfactor, D, is an increase or decrease in the radial distance to the farthest point on the loop from the crack tip. This variation is identical to the change in maximum shear stress caused by varying the LEFM K_I value. The most interesting aspect of this study is the fringe pattern change caused by a variation of the singularity order, λ.

An isochromatic associated with a singular point (crack tip) has three well defined stationary points existing on a continuous curve, one with respect to angular variation, $\partial \tau_{max}/\partial\theta = 0$, and two with respect to linear variation, $\partial \tau_{max}/\partial y = 0$ (see figure 5.3). Referring to this figure, the ratio of length L to length T is defined to be the fringe loop aspect ratio. As the magnitude of the singularity order decreases, this aspect ratio increases.

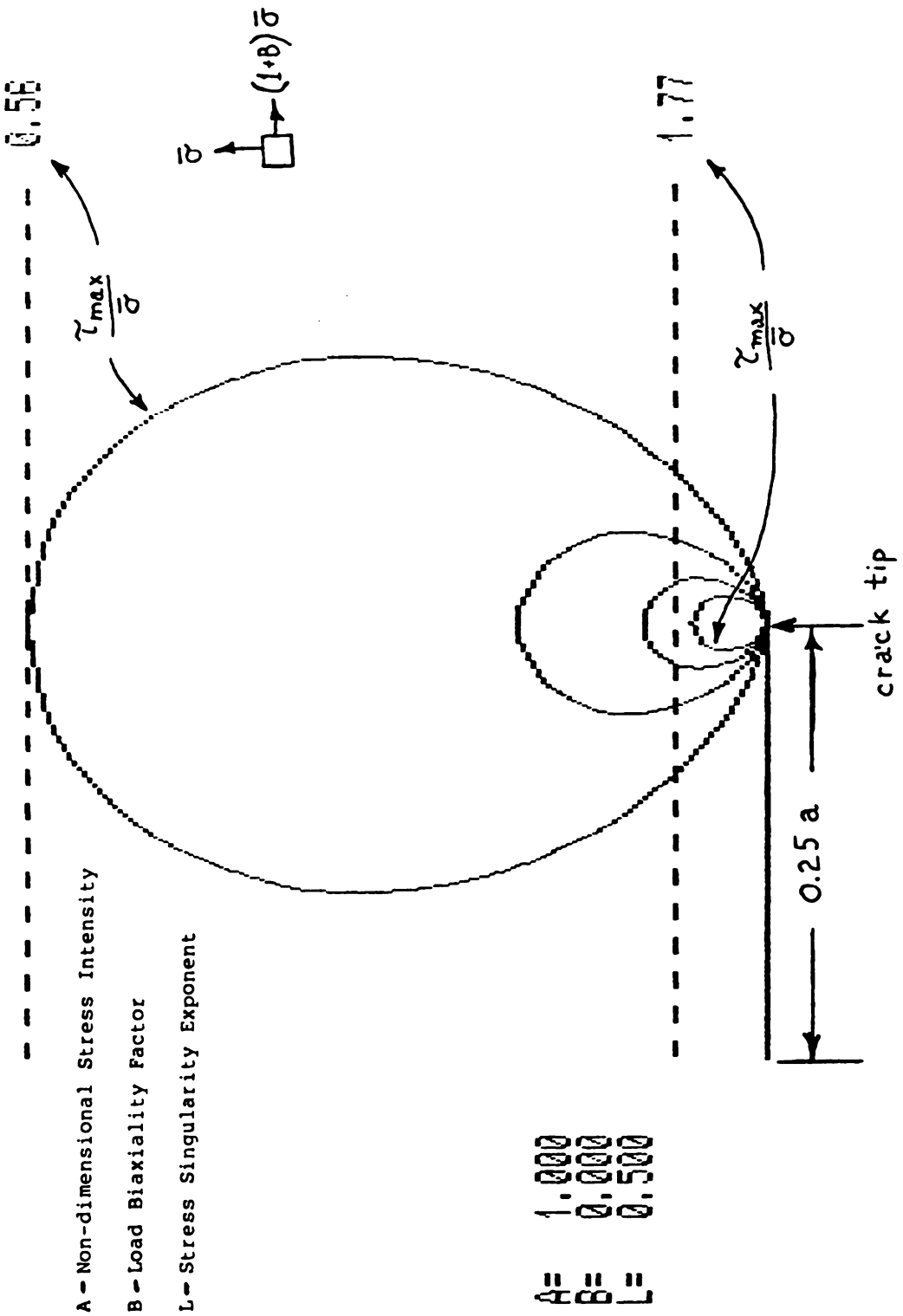

Theoretical Fringe Pattern Generated by Computer

Figure 5.1

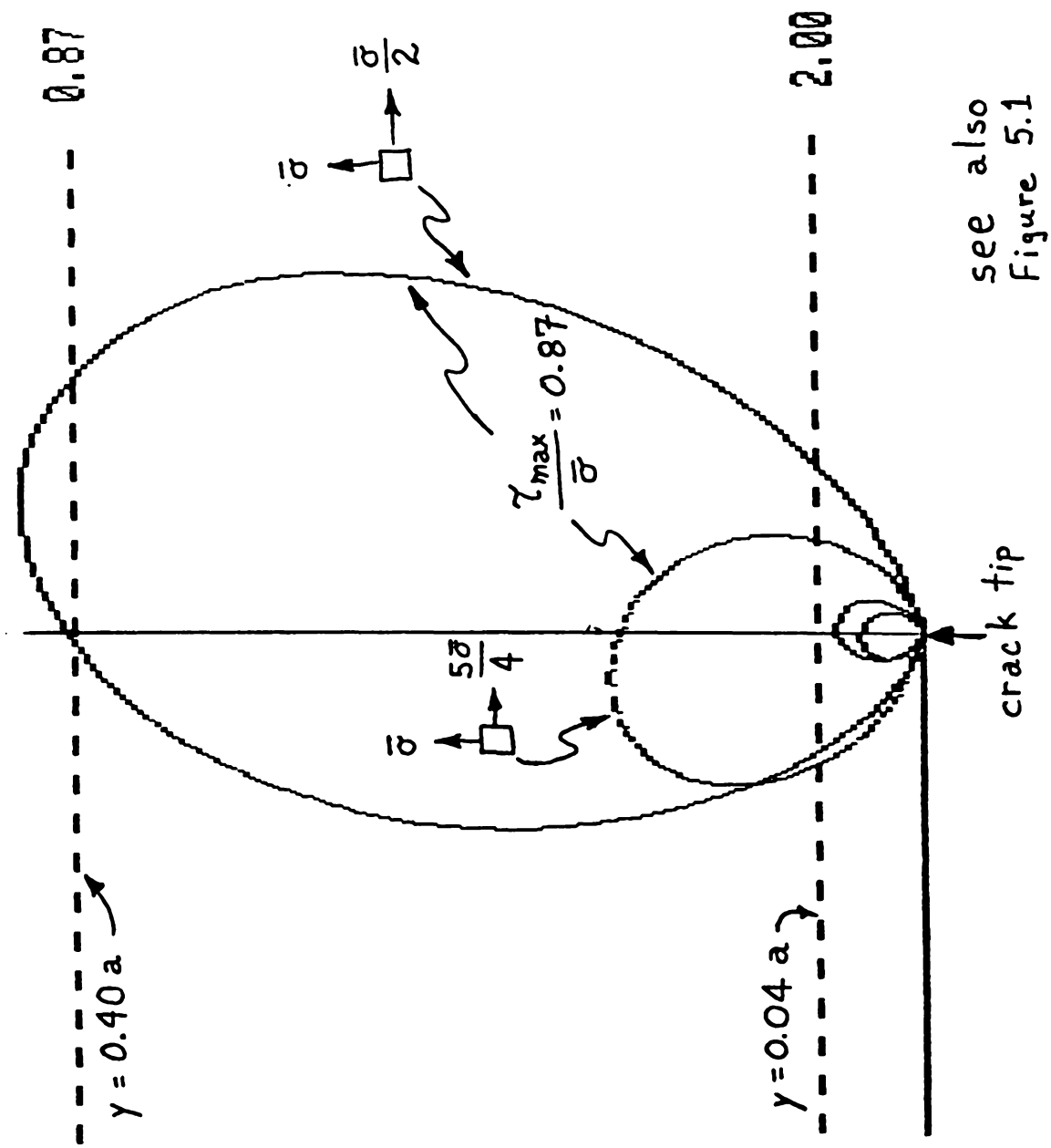

Theoretical Fringe Pattern Showing σ_o Effect

Figure 5.2

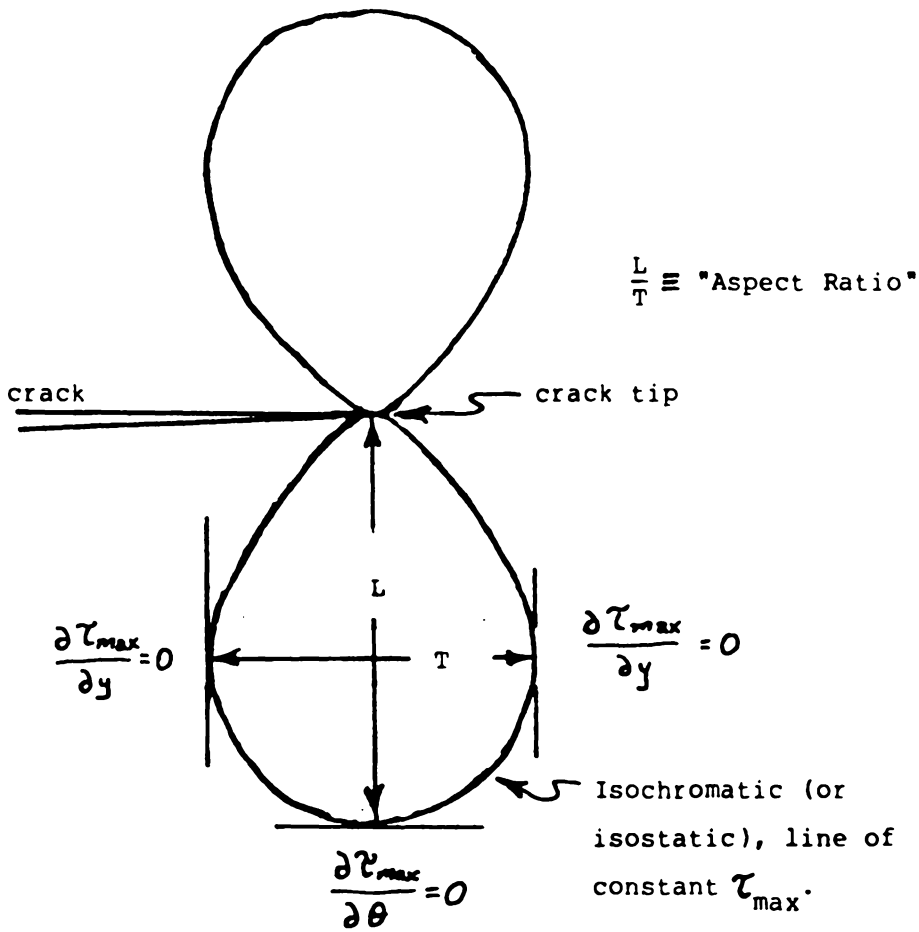

Representative figure only. Not to scale. Additional isochromatics omitted for clarity.

Fringe Loop Geometry Showing Stationary Points

Figure 5.3

Reasonable correlation was found between experimental fringe patterns and theoretical fringe loops generated by the computer, with respect to this aspect ratio. This physical phenomenon looked to provide a promising approach to developing a data analysis algorithm, however no algorithm based on this phenomenon has been developed at this time.

SOLUTION OF THE NON-LINEAR PROBLEM

6.1 Extracting the Singularity Order from Experimental Data

There are two fundamental problems which must be solved in order to obtain an empirical solution to equation (5.1.5) or (5.1.6). The first problem involves the mathematical treatment of an overdetermined, non-linear system. It will be covered in this section. The second problem involves selection of the appropriate zone surrounding the crack tip from which experimental data should be collected. This problem is discussed in section 6.2. There is also a third problem to be solved before the results obtained from (5.1.5) or (5.1.6) can be applied to practical problems. It is related to the variable dimensions of the stress eigenfactor, D, and a solution is proposed in section 6.3. Section 6.4 explains the application of the method developed in this chapter to analyze experimental data.

For the following discussions, the experimentally determined values of isochromatic fringe order, N_i (equivalently maximum shear stress, $(\tau_{max})_i$, by equation (5.1.3)), and corresponding polar coordinates, r_i and θ_i, will be referred to as the problem data. The variable parameters of the model equation (5.1.6), D, λ, and τ_o, will be referred to as stress field parameters.

It is easily recognized that equation (5.1.6) can not be directly linearized. This is equivalent to saying that all three parameters are not mathematically independent. Any one of the three parameters can be solved for directly, but the remaining two parameters will be

dependent on each other. Epstein [14] overcame this difficulty by assuming the non-singular term, which he called σ_o, to be vanishingly small which reduced equation (5.1.6) to a linearizable form. He also collected data only along the radial line $\theta = \pi/2$, which further simplified (5.1.6) to

$$\tau_{max} = \frac{D\lambda}{r^{\lambda}} \tag{6.1.1}$$

or after linearization

$$\ln(\tau_{max}) = \ln(D\lambda) - \lambda \ln(r) \tag{6.1.2}$$

While this approximation was initially thought to be valid, subsequent testing (TlD) and analysis indicate that the non-singular stresses must be accounted for.

In an effort to avoid the complexity and time involved in the formulation and testing of an iterative non-linear least squares algorithm to solve equation (5.1.5) or (5.1.6), the following approach is taken. It is assumed that for any geometry meeting fracture toughness testing requirements (ASTM E-399), a condition of plane strain will exist at the point on the crack border farthest from the free surface. This assumption is based on the analytical work of Sih

[7] which indicates the LEFM singularity order of -0.5 is recovered in the middle half of thick plates with through cracks. By setting the singularity order λ to -0.5 in equation (5.1.6), which makes the equation linear in $r^{-0.5}$, the data collected at maximum crack depth can be analyzed using Smith's Two-Parameter Method [35], a linear least squares procedure. The non-singular stress parameter τ_o which gives the theoretical singularity order of -0.5 at maximum crack depth is thus recovered.

Once the value for τ_o is recovered, it can be substituted into the rearranged form of equation (5.1.6)

$$\ln(\tau_{max} - \tau_o) = \ln(D\lambda) - \lambda \ln(r) \tag{6.1.3}$$

as a known quantity, which makes (6.1.3) linear in the unknown parameters D and λ. In order for this linearization to be valid, the value of the non-singular shear stress, τ_o, must be independent of r along $\theta = \pi/2$ (the "z" direction).

6.2 Determination of the Data Collection and Analysis Zone

The experimental data, which exists as an infinite number of sets $(N, r, \theta)_i$, i=1,2,3,... for each photoelastic slice, must be reduced to a finite number of sets in order for a numerical analysis scheme to

be employed to satisfy the model equation. In fact, only two sets are required to calculate the unknown parameters D and λ. However, due to the unknown random error associated with each data set (or data point, since each data set represents a geometric point and a scalar quantity associated with that point), it is appropriate to choose the method of least squares (a description of this method can be found in most books on statistics, probability, or numerical methods), which allows an arbitrary number of data sets to be used to obtain a solution. Briefly, this method allows unknown parameters of a model equation to be calculated such that the square of the difference between the experimental dependent variable and the value of this variable predicted by the model equation is minimized. For the two parameter model under investigation, equation (6.1.3), this method is the so called "best straight line fit " through the data points.

An investigation of the literature concerning photoelastic determination of stress intensity factors reveals a study by Doyle [36] suggesting that for the case of mode I loading, data collection should be restricted to the zone near $\theta = \pi/2$ (see figure 6.1) to minimize errors. The frequently used Two Parameter Method of Smith [35] restricts data collection to the same zone. In view of this previous work, data is collected along $\theta = \pi/2$. This minimizes not only errors, but also simplifies the model equation and reduces

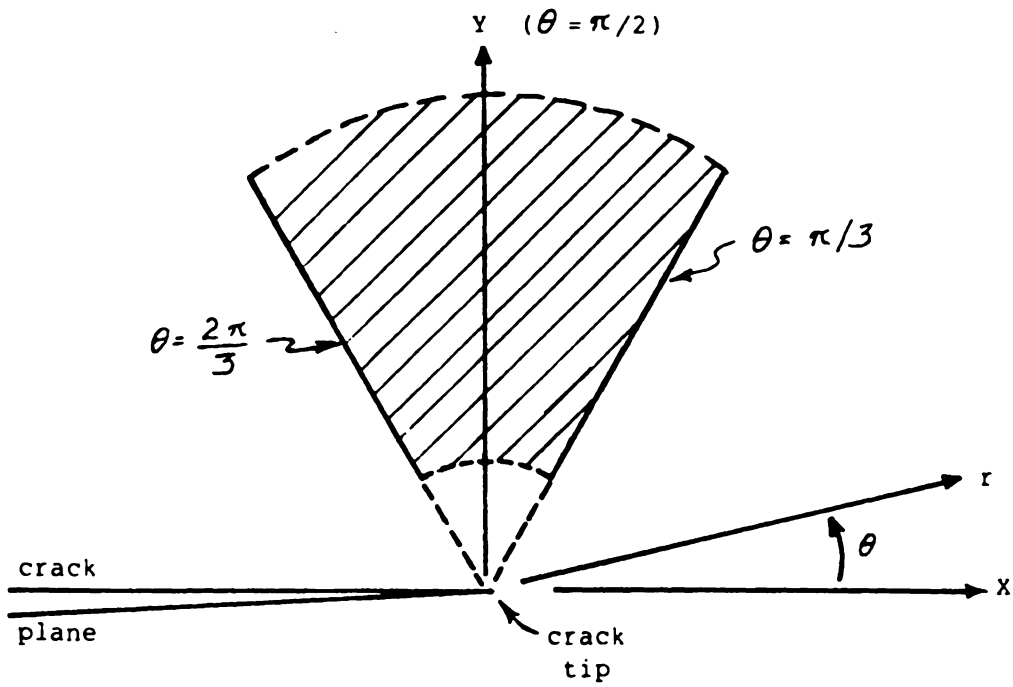

Angular Zone for Data Collection

Figure 6.1

complications in the experimental data collection procedure (data need only be collected along a straight line, and not over a two dimensional field. There are some who believe this is a waste of information [37], however, accuracy and repeatability of results must dictate the methods to be used in experimental work.

After having eliminated the angular variation in the data, it is now necessary to consider the radial variation. The primary concern here is to establish inner and outer radial limits on the data (figure 6.2), such that the data in the interval or "measurement zone" behaves in a manner which the model equation predicts. There are two factors which influence the location of these "end points". First, the model equation is an approximation, initially based on a crack in an infinite domain. Without adding additional terms to the model equation, the outer limit (or end point) must be restricted to avoid the influence of the finite boundaries. Secondly, optical non-linearities occur in the high stress region surrounding the crack tip. The inner limit must be sufficiently removed from the crack tip to avoid this region, since the model equation is not developed to account for the non-linear behavior.

Earlier work in LEFM applications of photoelasticity by Smith and associates indicates an inner limit for the "linear zone" to be located about six percent of the crack length from the crack tip

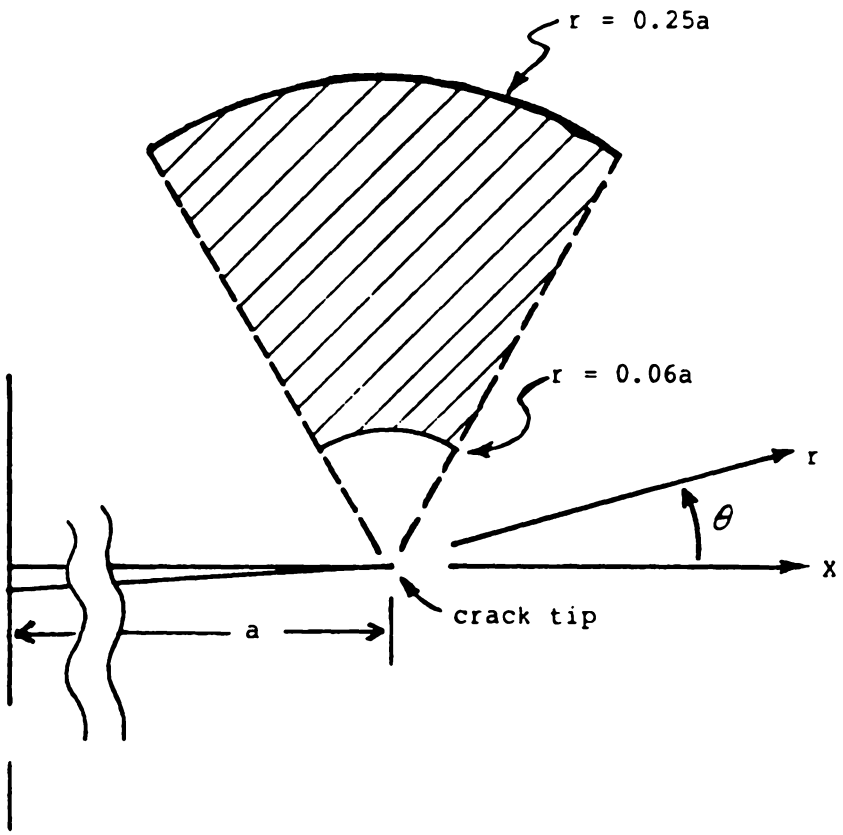

Radial Zone for Data Collection

Figure 6.2

(r_{min}=0.06a). Epstein [14] reports a similar figure. In order to verify the previously determined values, data is collected as close to the crack tip as possible. No definitive work on the location of the outer limit of the "linear zone" (LZ or MZ [14]) could be located. Data is collected either to the edge of the photoelastic slice or to the maximum distance permitted by the size of the viewing area in the fringe multiplication unit in order to establish the existence of an outer radial limit for the measurement zone.

The procedure used for determining the limits on the measurement zone is simple and effective. The experimental data is plotted in a manner so as to be consistent with the model equations (which are linear). The data points, so plotted, which form a reasonable straight line and also yield parameters which are within the expected range (determined from prior experimental or analytical work), delineate the measurement zone. This procedure is performed for each slice from each test using both equation (5.1.6) and equation (6.1.3) as models. The end points of the measurement zones determined in this manner are then averaged. Figure 6.3 shows the extent of the measurement zone and corresponding statistical values for each end point after values from all six tests are averaged. The values obtained from the SIF graphs (Smith's Two Parameter Method) show good correlation with the values obtained from the log-log graphs (equation (6.1.3)) for singularity

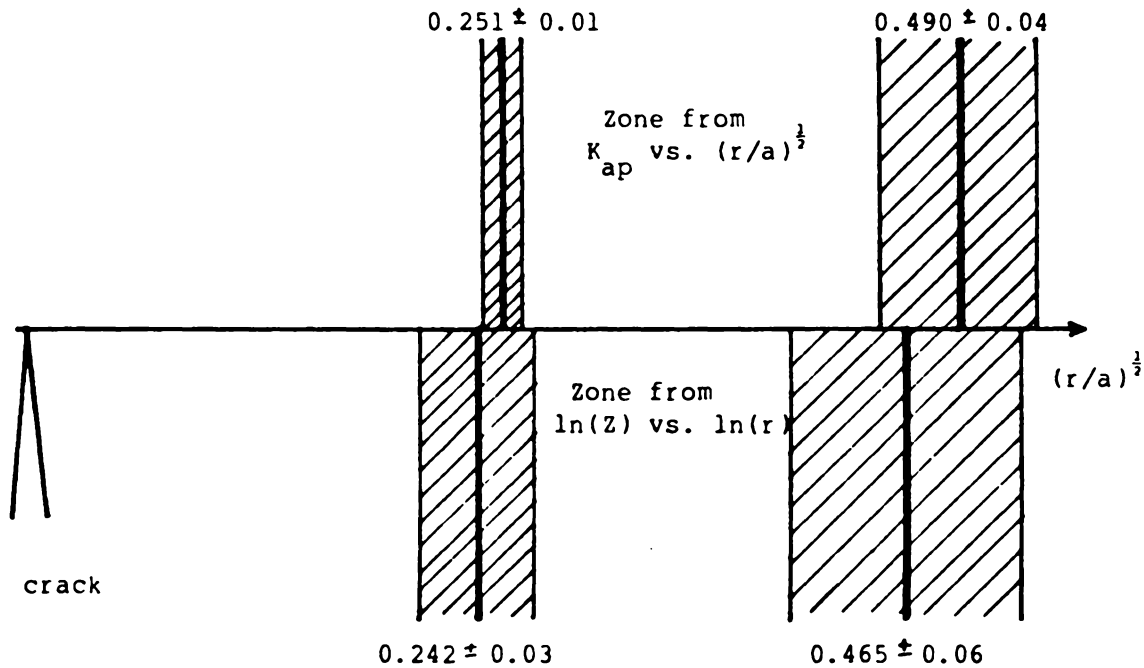

Measurement Zone Limits and Statistical Data

Figure 6.3

order determination, the values from the log-log graphs being about 3% smaller. No correlation was noted between measurement zone limits and position along the crack border.

Intuition indicates that the outer limit would be strongly dependent on the finite geometry of the photoelastic model. However, the present results do not lead to this conclusion due to the independence of the outer limit of the measurement zone from the crack border location of the slices collected from the surface flaw models.

6.3 Accounting for a Variable Singularity Order With a Corresponding Stress Intensity Factor

The development of the non-linear model equation (5.1.6) allows for the analysis of experimental photoelastic data to determine the stress singularity order, λ. The analysis also yields a stress "eigenfactor", D, which functions much like the stress intensity factor, K_I, in LEFM. However, the value D has units of pressure multiplying a variable fractional power of length, where the variable power is the stress singularity exponent. Mathematically, this is not a problem. However, it is desirable to allow incorporation of the experimentally determined parameters into design codes based on the LEFM stress intensity factor, K_I. In order to accomplish this, the

dimensional variation in the stress eigenfactor, D, must be corrected to constant dimensions of the stress intensity factor, pressure multiplying square root of length. Toward this end the following mathematical formulation is developed. For $\theta = \pi/2$, define a corresponding "apparent" stress eigenfactor, D_{ap}, where

$$D_{ap} = \frac{\tau_{max}\, r^{\lambda}}{\lambda} = D + \frac{\tau_o g(\lambda)\, r^{\lambda}}{\lambda} \tag{6.3.1}$$

Dimensionally map D_{ap} to a corresponding $(K_{cor})_{ap}$ by

$$D_{ap}\, r^{(\frac{1}{2} - \lambda)} = \frac{\tau_{max}\, r^{1/2}}{\lambda} = \frac{(K_{cor})_{ap}}{(2\pi)^{\frac{1}{2}}} \tag{6.3.2}$$

This leads to the following relation between $(K_{cor})_{ap}$ and the experimental data ...

$$(K_{cor})_{ap} = \frac{\tau_{max}\, (2\pi r)^{\frac{1}{2}}}{\lambda} = K_{cor} + A\, r^{\frac{1}{2}} \tag{6.3.3}$$

From Smith's Two-Parameter LEFM formulation, the relation

$$(K_I)_{ap} = \frac{\tau_{max}\, (2\pi r)^{\frac{1}{2}}}{\frac{1}{2}} = K_I + \sigma^* r^{\frac{1}{2}} \tag{6.3.4}$$

is known. By comparing (6.3.3) with (6.3.4), the equivalent relation

(6.3.5) $$K_{cor} = \frac{K_I}{2\lambda} \qquad \text{where} \qquad A = \frac{\sigma^*}{2\lambda}$$

is obtained. From (6.3.5), it is apparent that K_{cor} will coalesce with K_I when the singularity order goes to 0.5. Equation (6.3.5) will also yield conservative estimates of a stress intensity according to the experimental results obtained to date. It is further noted that Epstein [14] proposed a similar type of argument, however his method required an additional two data plots for each photoelastic slice to determine K_{cor}, the reason being that he did not perform the equivalence leading from equation (6.3.3) to (6.3.5). Besides being an inconvenience, it did not permit the direct conversion of known LEFM values of K_I to K_{cor} by only knowing the singularity order distribution and the LEFM stress intensity distribution. By this reasoning, the present method is argued to be valid as well as faster to apply.

6.4 Application of the Data Analysis Algorithm

The method of data analysis proposed in sections 6.1 through 6.3 has been used to analyze photoelastic slices from seven new tests. It has also been used to re-analyze data collected by former peers in an effort to validate the method. An overview of the basic procedure used to analyze the data for a single test is presented in this section.

The method, as presented here, requires considerable hand calculation to implement. After initial analyses were performed which showed promising results, an interactive computer code employing the computational and graphical capabilities of the IBM Personal Computer was developed. The program "TAU-PLOT.BAS" performs all of the data reduction, produces all of the graphs, and carries out all calculations necessary to do the complete analysis. The program user has considerable control over program branching at several points, and has control of a graphics cursor, allowing the user to delineate the "linear zone" on which the least squares analysis is carried out. The ability to manually delineate the measurement zone was included because of the problem covered in section 6.2. It was desirable to examine a variety of measurement zones to see if a common zone existed which gave self-consistent results, since such a zone was not known a priori. A copy of "TAU-PLOT.BAS" appears in Appendix II.

For the purpose of this overview, it is assumed that photoelastic data points, $(N,r)_i$, have been collected along $\theta = \pi/2$ for several photoelastic slices obtained from a common stress frozen test model (see figure 6.4), using the methods described in chapter 2. The first step in the analysis is to take the data from each slice and average the r values corresponding to the same fringe orders on either side of the crack plane (see figure 6.5)(This step was found to significantly

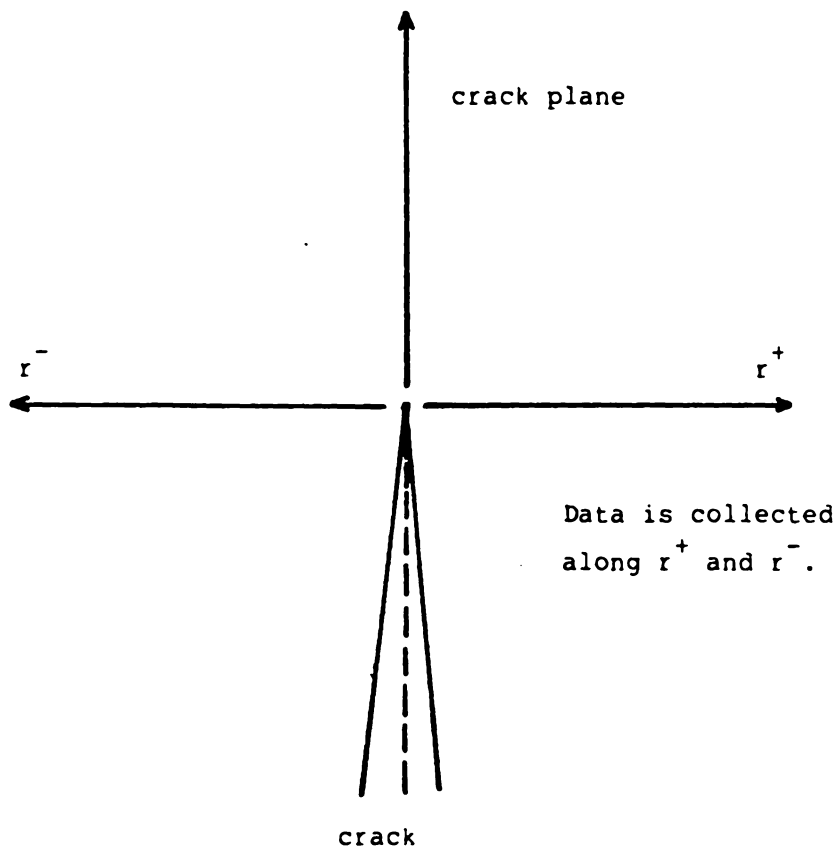

Direction of Data Collection

Figure 6.4

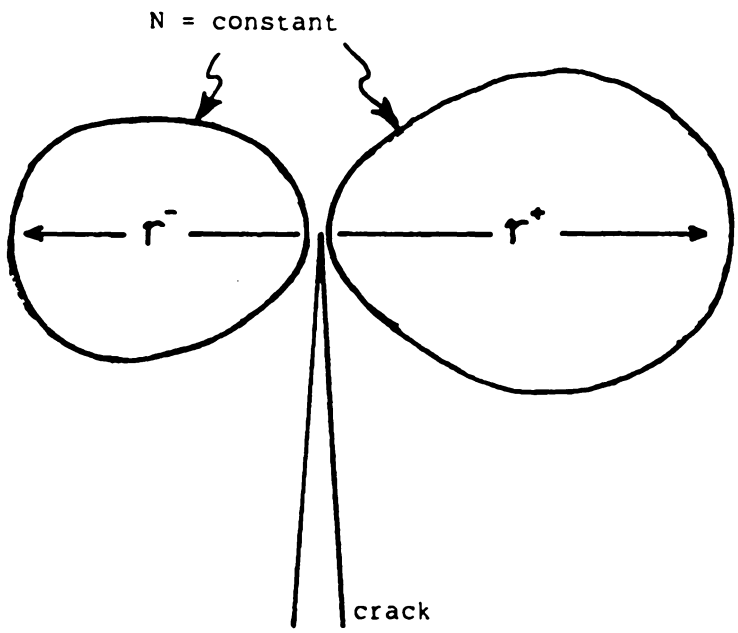

$$\bar{r} = \frac{r^+ + r^-}{2}$$

Averaging Process for r^+ and r^- Values

Figure 6.5

reduce the apparent scatter in the final results of the analysis). Once this has been done, Smith's Two Parameter Method [35] is applied to all data. This yields two important results. First, it gives the K_I distribution along the crack border. Secondly, and more importantly, the distribution of the non-singular stresses, σ^*, are recovered.

The distribution (in a point to point sense) of the non-singular stresses is then examined. Typically, a considerable amount of variance exists in the distribution (see figure 6.6). In order to obtain the desired value to be used in equation (6.1.3), a numerical average of several values near the maximum crack depth is calculated. This average value is renamed τ_o, to differentiate it from the variable σ^*. A plot of $\ln(\tau_{max} - \tau_o)$ versus $-\ln(r)$ for each slice is then made. The slope of the linear portion of the curve, calculated using the least squares linear regression formulae, is the stress singularity order. Figure 6.7 shows a hard copy of the computer display of the log-log distribution for a particular slice, along with the parameters of equation (6.1.3). The vertical lines on the graph delineate the measurement zone from which the values of the parameters are determined. This step is repeated for the data from each slice. The result is a distribution of points indicating the approximate variation of the singularity order along the crack border. Figure 6.8 shows representative distributions for both a naturally grown surface

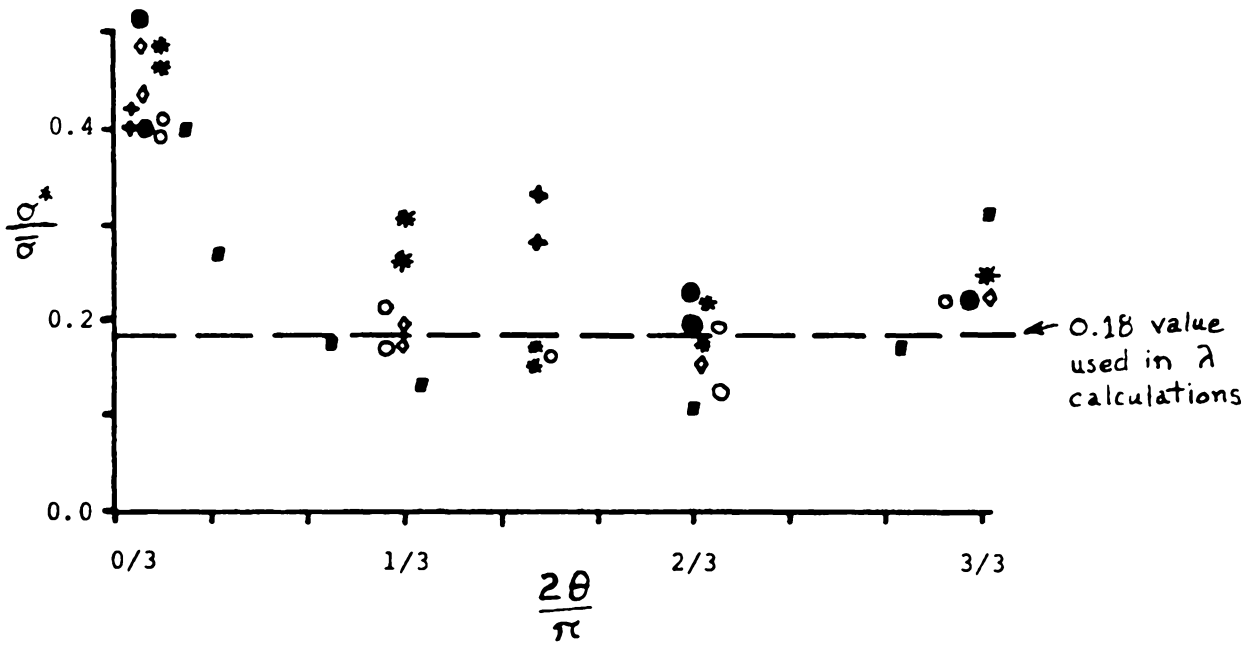

TEST	SYMBOL	a/c
T2	+	1.03
T3	◇	0.83
T4	●	0.89
T5	*	1.11
T6	o	0.87
T7	■	0.89

$\bar{\sigma}$ - Remote Normal Stress

Distributions for Tests T2 Through T7 From LEFM

Figure 6.6

$$Z = (\tau_{max} - \tau_o)$$

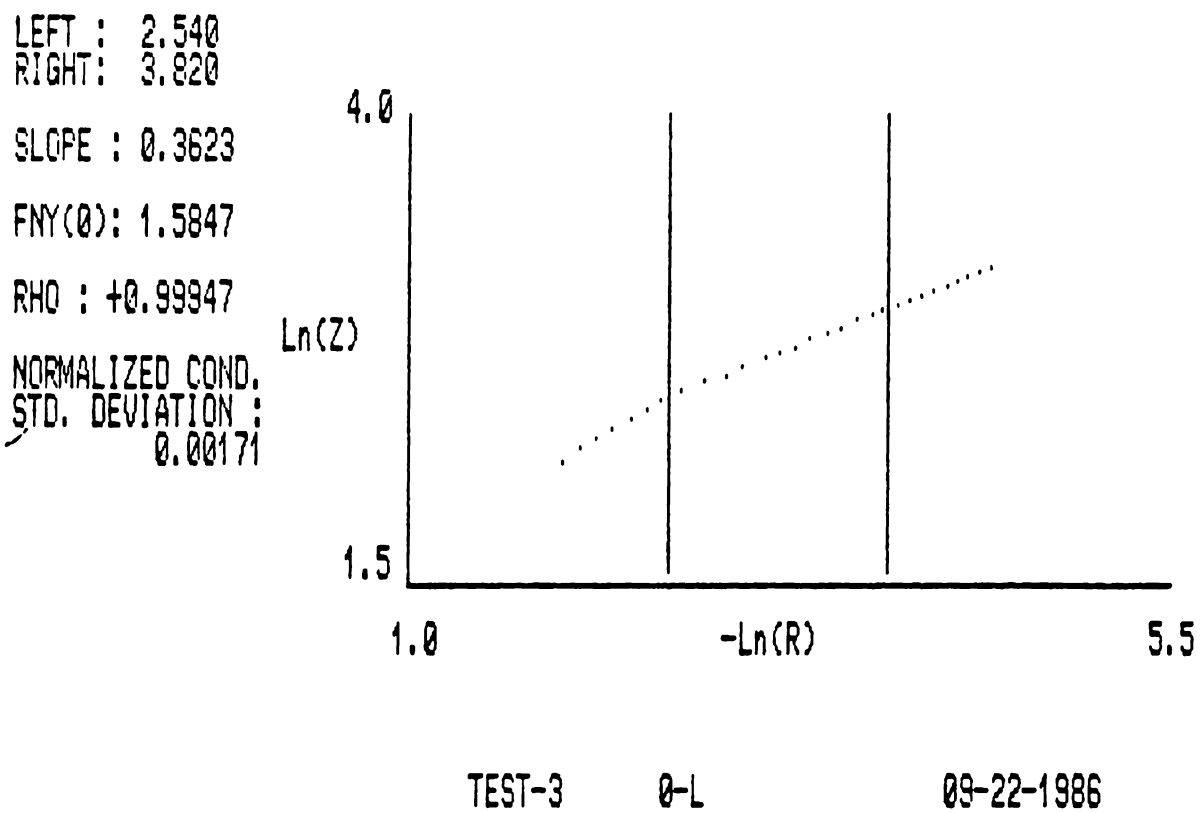

Log-Log Graph for Singularity Order Determination

Figure 6.7

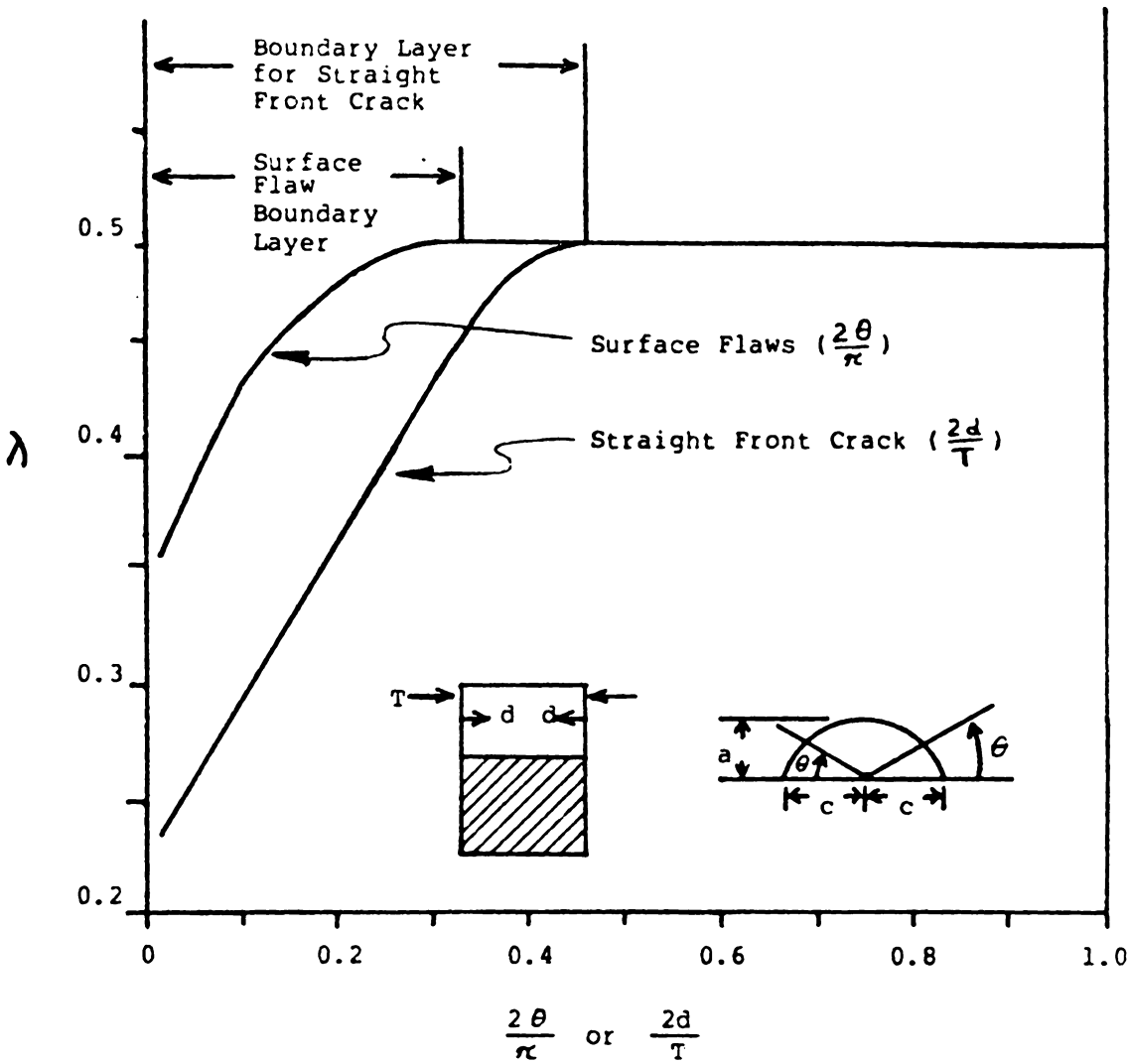

Representative Singularity Order Distributions

Figure 6.8

flaw loaded in tension and a machined "V"-shaped edge notch loaded by bending (both Mode I).

There will be random scatter in the experimentally determined values. As such, model geometries should be selected which are symmetrical with respect to the point of maximum crack depth if possible. This allows some of the error to be "averaged out" by plotting all values from a single test on a graph where distance is measured with respect to the geometric center of the model. A smooth curve can then be drawn through the points which will represent an improved singularity order distribution. Points are then selected from this curve to convert the K_I distribution obtained in the first step to the equivalent K_{cor} distribution by using equation (6.3.5) in a point by point manner. Figure 6.9 shows the K_I and associated K_{cor} distributions from test T3 obtained in this manner.

In applying this method of analysis, τ_o has been assumed constant along the entire crack border, while σ^* varies according to the result shown in figure 6.6 where λ is held constant at 0.5. It is necessary to hold τ_o constant to maintain the linearity of equation (6.3.1).

The results of Epstein's work on straight front cracks, where the quantity called σ_o in this work was set to 0, suggests that τ_o may tend to 0 as the free surface is approached. By setting τ_o to 0 and reanalyzing some surface slices for both surface flaws and straight

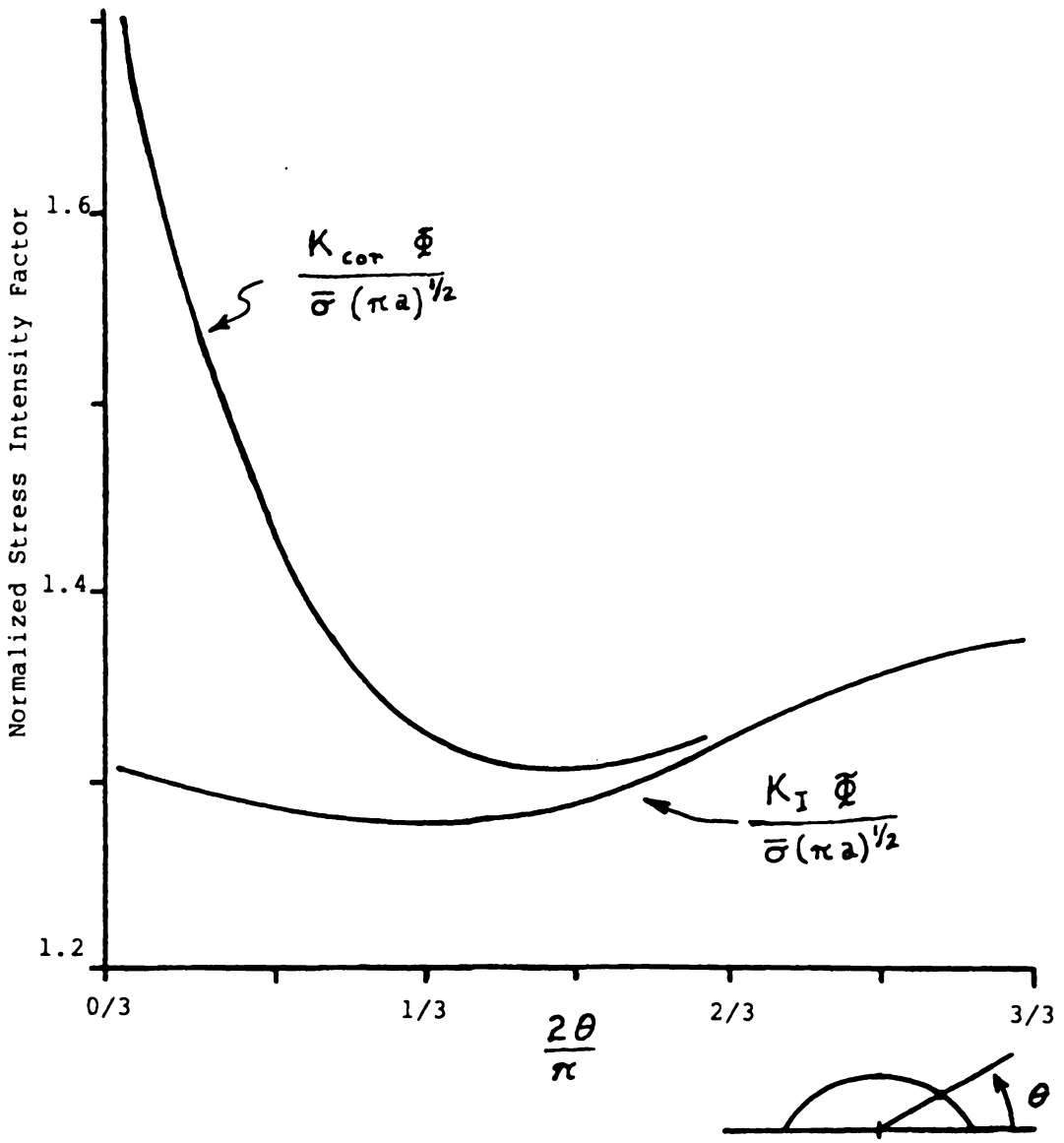

K_I and K_{cor} Distributions for Test T3

Figure 6.9

front cracks, values of λ approached 0.32 for both geometries. This is very close to the generally accepted analytical value of 0.33

Since it is very likely that τ_o does tend to vary as the surface is approached, another method must be incorporated to determine λ in this region. Epstein's application of moire interferometry [14] in his study of the problem is a likely choice. If the displacement equation for U_z obtained from the stress function which generates equation (5.1.5) is examined, the first term is found to contain $r^{(1-\lambda)}$ and subsequent terms to contain higher powers of r. If data is collected close to the crack tip, all terms except the leading term will make insignificant contributions to the displacement. This eliminates the non-linearity associated with the stress equation (5.1.6) thus allowing solution by linear methods. It would still remain necessary to develop experimental techniques yielding sufficiently accurate data for the analysis to work.

TEST RESULTS AND DISCUSSION

7.1 Stress Singularity Order Distributions for Surface Flaws

Seven surface flaw tests were performed. The results from the first test (T1) are somewhat erratic. This is attributed to a lack of practical experience, required to perfect testing and data collection procedures. Of the remaining six tests, two have aspect ratios, a/c, greater than 1.0 (T2, 1.03 and T5, 1.11)(see figure 4.6). This causes the SIF (K_I) distribution to be somewhat different than what is normally expected for semi-elliptical flaws with the major axis parallel to the free surface (aspect ratio less than 1.0), however, as shown subsequently, the singularity order distribution is independent of the aspect ratio a/c. The remaining four surface flaw tests, T3, T4, T6, and T7, have aspect ratios from 0.83 to 0.89. These tests have experimentally determined SIF distributions similar in shape to the distributions predicted by the equations of Newman and Raju [38] (see figure 7.1). The Newman and Raju equation is developed for Poisson's ratio of 0.3 while the model material used in the testing has a Poisson's ratio of 0.48. The higher Poisson's ratio is the reason for the increase in the average value of stress intensity calculated from the experiments.

The singularity order distributions for the surface flaw tests are presented in figure 7.2. The abcissa in the graph represents a non-dimensional parametric angle, which is described in the inset, where zero represents the free surface location, and 1.0 represents

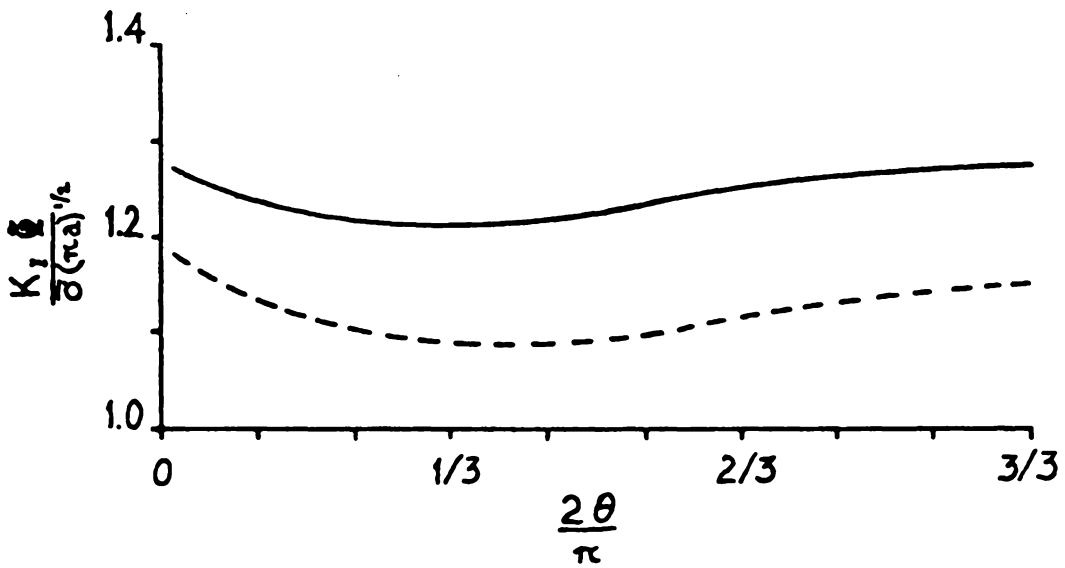

— Test T4 a/c = 0.89 a/T = 0.4 ν = 0.48

--- Newman and Raju equation [38] ν = 0.30

See Figure 6.9 for definition of θ

$$\Phi = \int_0^{\frac{\pi}{2}} \left[\sin^2\phi + \left(\frac{a}{c}\right)^2 \cos^2\phi\right]^{1/2} d\phi$$

$$\phi = \tan^{-1}\left[\frac{a}{c}\tan\theta\right]$$

SIF Distributions for Aspect Ratio Less Than 1.0

Figure 7.1

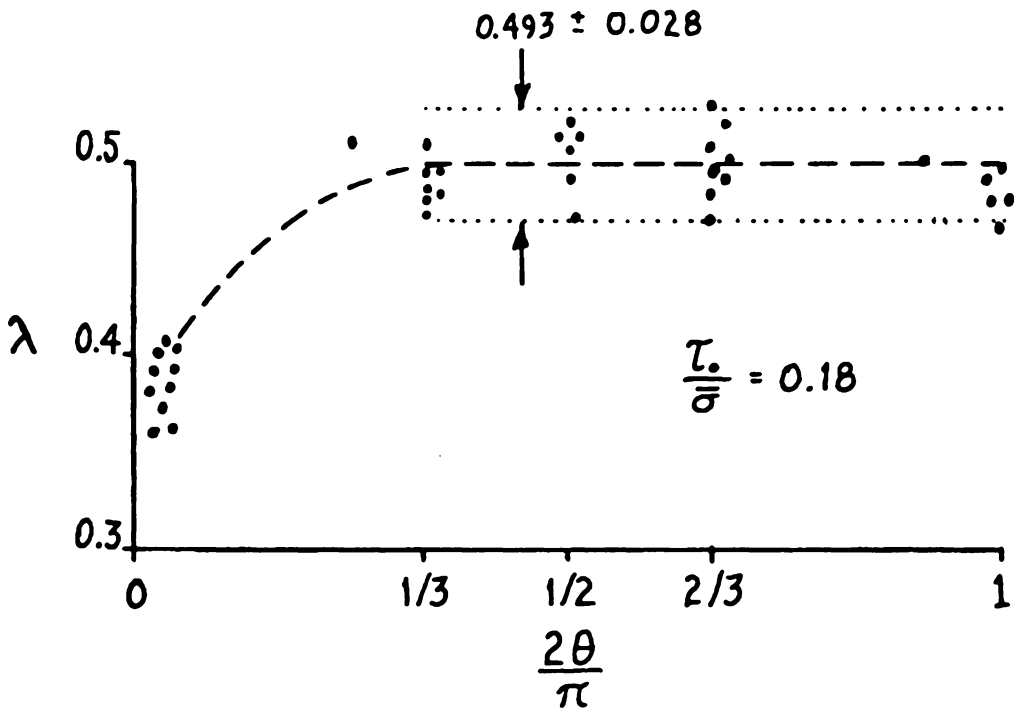

Composite Results from Test T2 Through Test T7

Singularity Order Distributions for Surface Flaws

Figure 7.2

the maximum crack depth location. There are several points to be discussed concerning this distribution. It can be seen in figure 7.2 that there is a small but consistent decrease of the apparent singularity order in the vicinity of maximum crack depth. This raises the question, Is the singularity order maximum at some point other than the maximum crack depth? On first inspection, the answer may be yes. However, if the algorithm for determining the distribution is examined, it is found to contain a parameter which is a measure of the in-plane, non-singular component of maximum shear stress. This parameter, τ_o , is assumed constant around the entire crack border for the present method of analysis. Intuitively, this is not a good assumption, due to the widely varying distance to the free boundary ahead of the crack tip in the plane of analysis of each individual slice. However, due to the complexity of determining even an approximate solution for the three dimensional stress field, the present method is retained for its simplicity.

There is an argument in favor of continued use of the present algorithm. For all of the values of the singularity order shown in figure 7.2, the non-singular stress component, τ_o, is precisely 18% of the remote applied normal stress. This ratio, $\tau_o / \bar{\sigma}$ is a constant, regardless of the elliptical aspect ratio and the crack length (see figure 6.6). This independence from the physical geometry of the

problem does present a great advantage in experimental work. If the non-singular stress component can be shown to be insensitive to moderate changes in geometry, the process of data analysis is further simplified, resulting in savings of time and money.

The next point concerns the value of the singularity order at the free surface. In view of the finite thickness of the "surface" photoelastic slice, a true surface value is not obtainable by photoelastic investigation. Even though techniques have been developed which allow photoelastic analysis of slices as thin as 0.01 inch, some type of extrapolation must be performed to obtain "true" surface values. To date, this has been achieved by graphically extrapolating a curve from the experimentally determined points near the surface to the surface. This method is adopted because: (1) no radical changes in the first or second derivative of the line through the interior values have been observed, (2) a reasonable estimate of the "scatter band" (see figure 7.2) has been established, (3) the distribution is not understood well enough to formulate a mathematical interpolating/extrapolating function, and (4) thickness averaged experimental values are obtained within 0.01 inch of the free surface.

By using the graphical extrapolation method of the previous paragraph, "surface" values of the singularity order which average 0.37 for the surface flaws are obtained. Obviously this differs from

the values obtained analytically for the semi-infinite straight front crack. This fact, combined with the uncertainty associated with the interior distribution, prompts the following question. If the present method is used for further analysis, is the quantity τ_o chosen such that: (1)the maximum singularity order is 0.5, or (2) the singularity order is 0.5 at maximum crack depth, (3) the value τ_o is allowed to vary such that both (1) and (2) are retained, or (4) the analytical value is achieved at the free surface? This is an interesting philosophical question. However, for the present analytical methods it may be redundant. The present methods utilized to determine the singularity order only yield results accurate to within about 10%. Since the experimental error is a significant portion of the overall variation of λ, it would seem logical to investigate a method to reduce the overall error first, since this may involve formulation of a new algorithm.

It is suggested that a linear or quadratic variation in the non-singular component inside the boundary layer be investigated. By utilizing the present algorithm from maximum depth out to a point where the boundary layer is detected (singularity order begins to change), and then letting the non-singular component vary to 0 as the surface is approached, an improved distribution of the singularity order may be recovered.

A second alternative would be to employ the process of "annealing" moire (as used by Epstein [14]) in the boundary layer region. The model equation for the displacement in the "z" direction may be truncated to a linear form and used with confidence so long as it is applied only close to the crack tip (small values of r). Although the displacement measuring technique is more time consuming than the photoelastic method, it eliminates the problems associated with the non-singular component of stress without the need for developing a non-linear data analysis algorithm.

7.2 Comparison of Results for Surface Flaws and Straight-Front Cracks

The algorithm which is used to analyze the surface flaw singularity order distributions is also applied to data which has been collected by Epstein from the single edge notch (simulated crack) bend specimen (see figure 7.3). An additional model, identical to the model tested by Epstein, has been tested (test T1D) in order to verify the validity of Epstein's data. Application of the present algorithm to both the recently generated data and Epstein's data produce similar results. These results from test T1D are presented in figure 7.4.

Four differences are apparent when comparing the results of the tests on surface flaws and straight-front cracks. When the previously described method (section 6.4) of selecting the non-singular stress

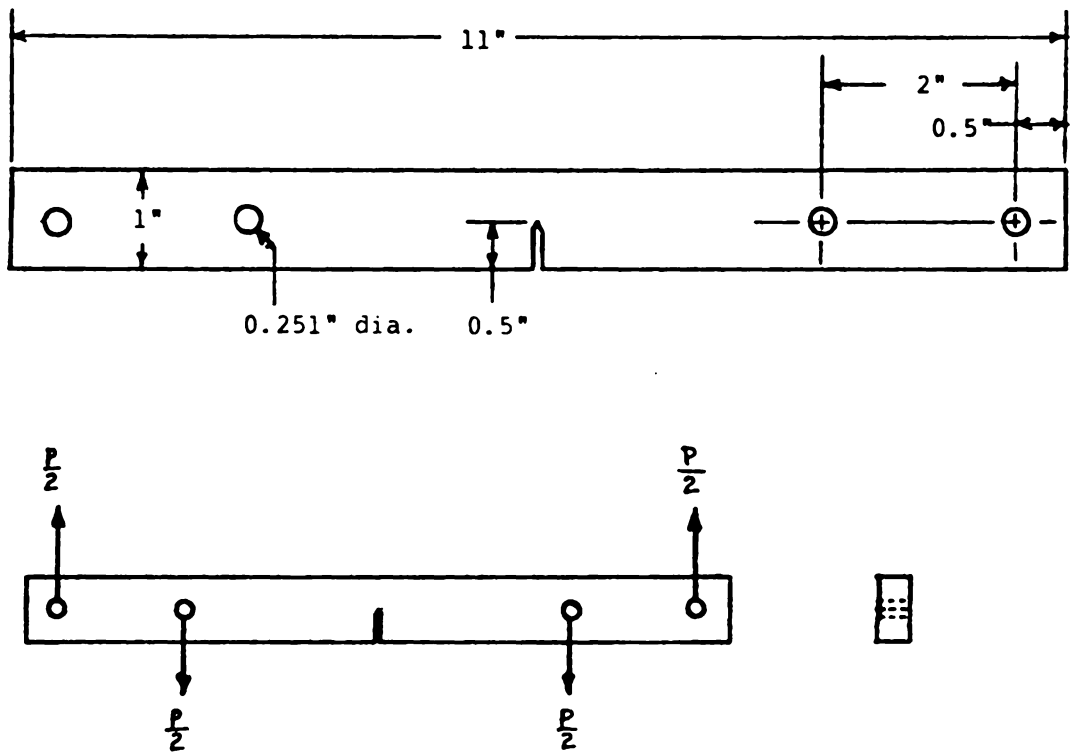

Single Edge Notch (SEN) Bend Model Geometry

Figure 7.3

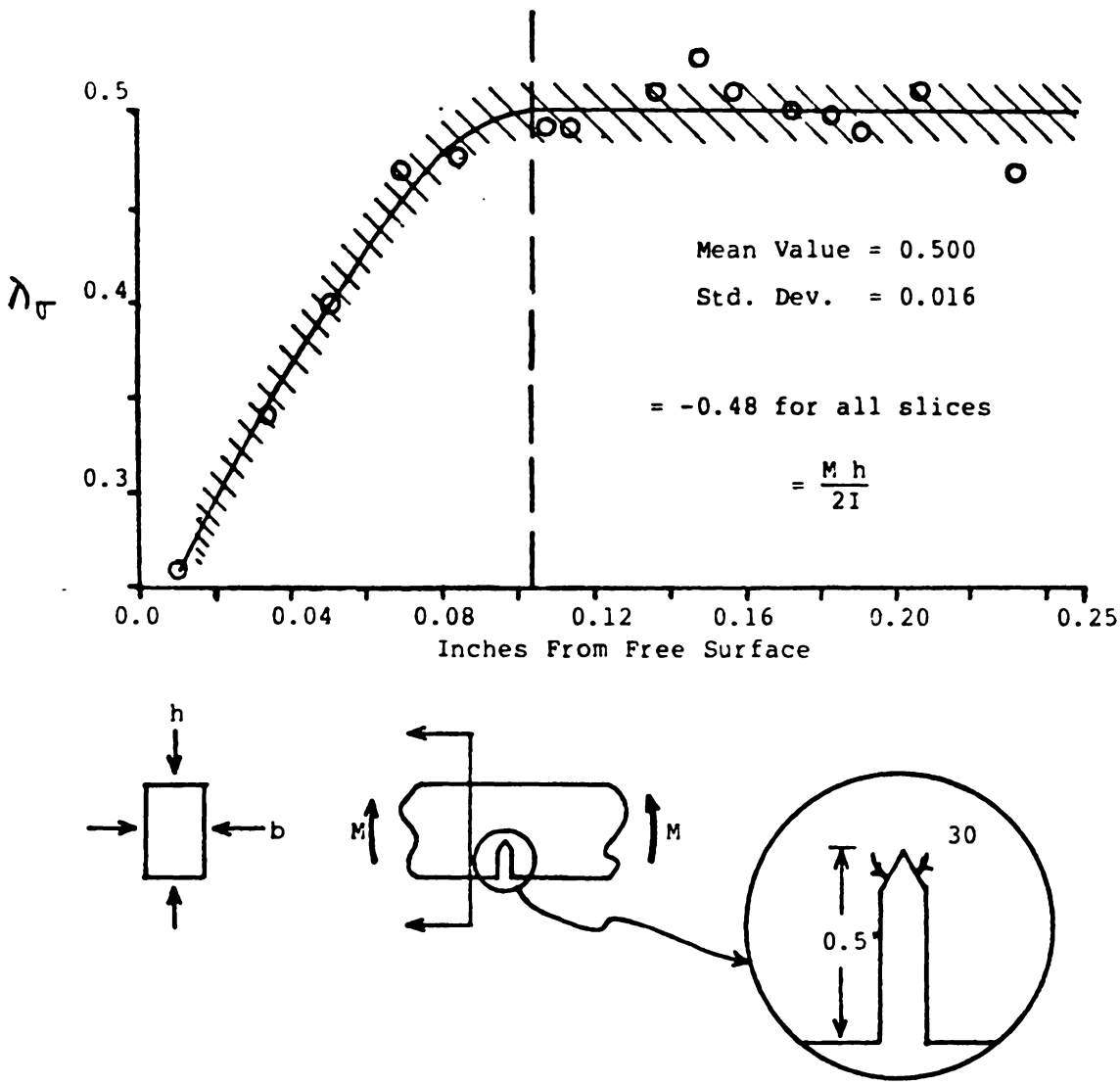

All data taken from 15 slices from test T1D

Singularity Order Distribution for SEN Model

Figure 7.4

term for the algorithm is applied, there is a difference in the singularity order near the surface for the two different geometries (0.37 for the surface flaw, 0.25 for the SEN geometry). The decrease in λ which is apparent at maximum crack depth in the surface flaw models (previous section) is not apparent in the straight-front crack models. The ratio of the non-singular stress term to the remote normal stress (M*c/I)for the single edge notch (SEN) specimen is -0.48, compared to +0.18 for the surface flaws (τ_0*A/P). Finally, the extent of the singularity order "boundary layer" is found to be smaller for the surface flaws than for the straight front crack.

Concerning the difference in surface values of the singularity order, the values obtained experimentally for the two geometries bracket the (approximate) analytically determined values of Benthem, Bazant, Takakuda, and Burton. One possible explanation concerns the algorithm used to analyze the experimental data. The present method assumes a constant value for the non-singular stress component along the entire crack border. Comparison of the actual fringe patterns obtained from surface slices with computer generated theoretical fringe patterns suggests a possible variation in the non-singular component of stress as the surface is approached. While there is no analytical or empirical foundation on which this variation can be based, a more detailed investigation of the phenomenon may be in

order. It is noted here that Ruiz and Epstein [17] reported surface values of the singularity for both the SEN geometry and the surface flaw geometry near 0.33, however their method of analysis was less refined than the method used in the present work. They also showed a completely different interior distribution for the surface flaw. The results presented herein are from six independent tests and show very good correlation. It is postulated that the results given by Ruiz and Epstein may have been distorted by random experimental error, which went undetected due to lack of repeat tests to form a statistical base.

The slight decrease in the apparent singularity order at maximum crack depth is most likely attributable to a moderate variation in the non-singular stress component which is not accounted for in the algorithm presented in chapter six. The variation which may cause the decrease would likely be small enough that only a more mathematically rigorous non-linear equation solution algorithm would be able to detect the variation.

The large difference in the non-singular stress component is not surprising. Large differences in the non-singular stress field surrounding the zone dominated by the singularity exist, and these differences cause the variation in the non-singular term, σ^*. There is a possible relation, however, between the variation in the

singularity order at the free surface and the difference in the non-singular stress for the two different geometries tested. Referring to figure 6.8, it can be seen that the singularity order for the two geometries diverge as the surface is approached. By examining equation 6.1. , however, it is obvious that by allowing the non-singular stress component to go to zero as the free surface is approached, the singularity order distributions for the two geometries tend to coalesce. This approach was utilized on several surface slices for both geometries, and resulted in the singularity order coalescing to an average value of 0.32, much closer to the analytical results.

The extent of the boundary layer (figure 6.8) may also be related to the non-singular stress component, τ_o. The values of singularity order obtained using the present algorithm (section 6.4) are directly related to the choice of τ_o. If, as mentioned previously, τ_o tends to zero as the free surface is approached, the extent of the boundary layer may be more nearly the same for both geometries. Whether or not this is the case, a more rigorous algorithm which determines τ_o and λ independently would certainly be beneficial.

7.3 "Corresponding" Stress Intensity Distributions

The method for converting LEFM stress intensity distributions to a corresponding K_{cor} presented in chapter five is dependent directly on the singularity order distribution. As mentioned in section 7.1, there is some question concerning the accuracy of the singularity order distribution in the boundary layer. The results and discussion presented here are based on the algorithm presented in chapter 6, keeping in mind that the corresponding SIF may be slightly larger (surface flaw) or smaller (straight front) due to changes in the singularity order near the free surface.

The distribution of K_{cor} for the straight front crack is approximately constant (within the limits of experimental error), while the LEFM K_I distribution shows a decrease as the free surface is approached (figure 7.5). This amounts to an effective increase in the SIF of over 50% at the surface. Consider the new methods being developed for the performance of highly accurate surface measurements. The advantage of the accuracy is effectively nullified if outdated and inaccurate methods of analysis are used to analyze the data. As such, consideration of the three dimensional effects, manifested in the elevation of K_{cor} near the surface, must be included in future experimental investigations, particularly ones involving nearly incompressible materials.

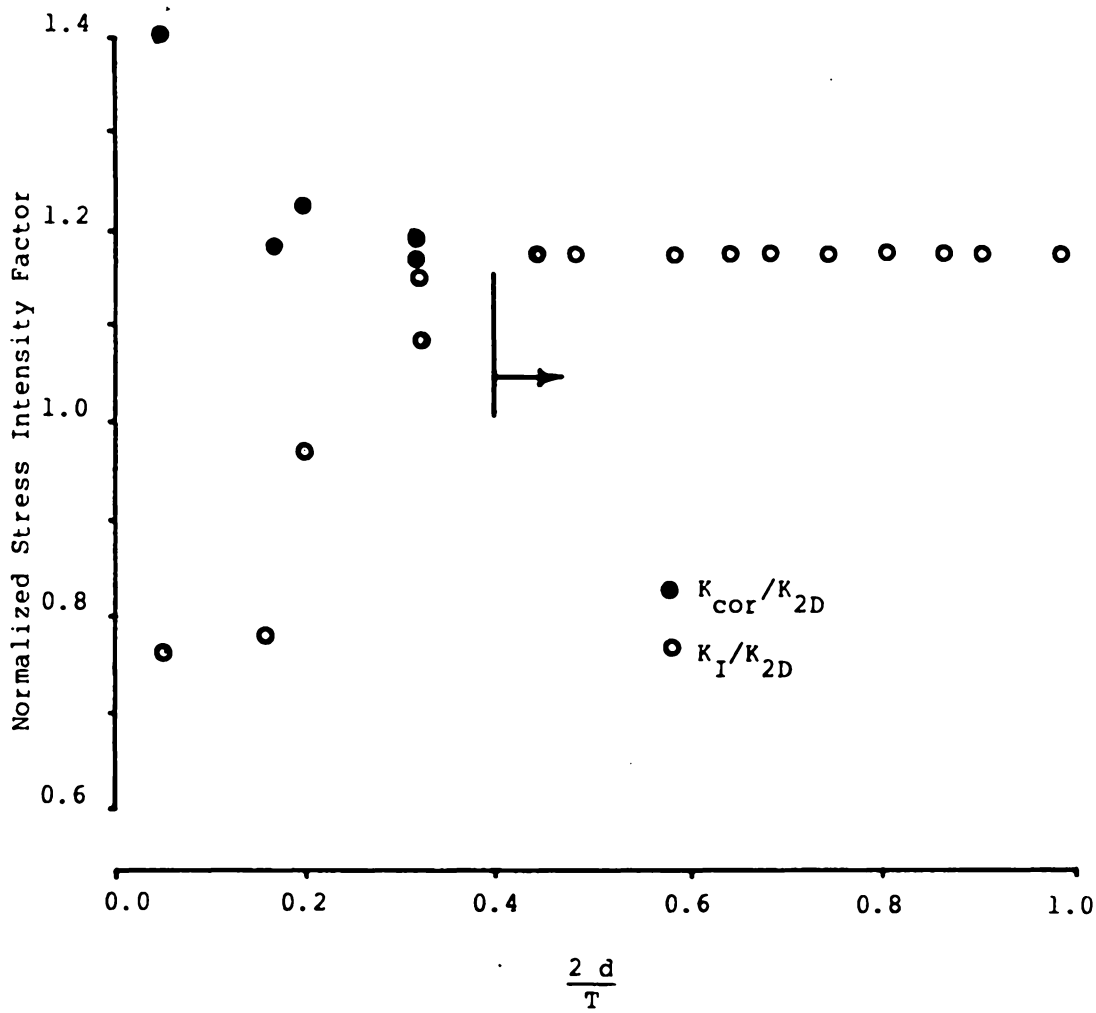

K_I and K_{cor} Distribution for a Straight Front Crack

Figure 7.5

The increase of K_{cor} over K_I for the surface flaw is not as dramatic due to the higher values of λ as the surface is approached (see figure 6.9). However, due to equation (6.3.5) and the assumptions presented in chapter six, K_{cor} will always be larger than or equal to K_I, with their values coalescing as the singularity order approaches 0.5. As such, the corresponding stress intensity, K_{cor}, is a conservative (larger) value of stress intensity which accounts for the three dimensional effects observed in high Poisson's ratio materials, and it is applicable to existing design codes and life prediction methods.

CLOSURE

The goals set forth in the introduction, namely: (1) determining the distribution of the singularity order for surface flaws, and (2) developing a method to account for three dimensional effects using LEFM (two dimensional) concepts and design codes, have been achieved. In the course of achieving these goals, several important methods, techniques, and data analysis algorithms have been developed. The quasi-linear algorithm (section 6.4 and equations (5.1.6) and (6.1.3)) was a major accomplishment in that it allowed reasonably consistent results to be obtained from two dissimilar cracked body geometries. The development of a simple formula which allows LEFM stress intensity factors to be adjusted to a corresponding stress intensity, K_{cor}, accounting for the singularity order boundary layer is an important accomplishment. Until the three dimensional problem is more fully understood, this formula allows for a conservative adjustment to be made to K_I, where K_I has been calculated from surface values of displacement or stress. This in turn, may prevent unexpected failures from occurring, where surface K_I values grossly underestimate the actual interior values of stress intensity.

In order to apply the K_{cor} correction, the singularity order distribution must be known a priori. Until a more powerful analytical method is developed, this distribution must be determined experimentally. Testing hundreds of different models is obviously an

extremely time consuming task. Part of this difficulty may be alleviated by considering the preliminary results presented in chapter seven. By looking at the results obtained from a variety of test geometries, it becomes apparent that the singularity order distribution is relatively insensitive to moderate changes in crack shapes or remote boundaries. If this is verified in future tests on different geometries, a significant reduction in the number of tests required to establish an empirical base for the engineering community would result.

The remaining question left to answer concerning experimental determination of the singularity order distribution concerns the assumptions and approximations incorporated into the development of the data analysis algorithm. It is obvious from the experimental results obtained so far that the algorithm represents a fairly good model of the actual behavior everywhere except possibly at the free surface. This judgement is made on the basis that the analytical results for surface values are appropriate for the finite geometry of the experimental model. The fact that the experimental results, obtained from two different geometries but using the same analysis method, bracket the analytical values tend to strengthen this judgement.

In order to obtain a more accurate singularity order distribution from the experimental photoelastic data, it will be necessary, at minimum, to develop and implement a non-linear algorithm for data analysis. This current model equation (5.1.6) could be utilized for the preliminary study. It is possible, however, that a new model equation will be needed which will allow more variation of the local stress field, if preliminary results prove to be erratic.

Finally, it is hoped that the methods, techniques, and results presented in this report will serve as a foundation on which future work on the three dimensional nature of the stress field around surface flaws can be built. Past work of others was very helpful and enlightening during the work which culminated in this report. Hopefully, this work will serve the same purpose for others in the future.

REFERENCES

[1] Inglis, C. E., "Stresses in a plate Due to the Presence of Cracks and Sharp Corners", Transactions of the Institute of Naval Architects, v.60, 1913, p.219.

[2] Griffith, A. A., "The Phenomenon of Rupture and Flow in Solids", Phil. Trans., Royal Society of London, v.221, 1921, pp.163-198.

[3] Westergaard, H. M., "Bearing Pressures and Cracks", J. Appl. Mech., Trans. ASME, v.61, 1939, pp.A49-A53.

[4] Williams, M. L., "Stress Singularities Resulting from Various Boundary Conditions in Angular Corners of Plates in Extension", J. Appl. Mech., Trans. ASME, v.19, n.4, 1952, pp.526-528.

[5] Irwin, G. R., "Analysis of Stresses and Strain Near the End of a Crack Transversing a Plate", J. Appl. Mech., Trans. ASME, v.24, 1957, pp.361-364.

[6] Green, A. E. and Sneddon, I. N., "The Distribution of Stress in the Neighborhood of a Flat Elliptical Crack in an Elastic Solid", Proc. Cambridge Philos. Soc., v.46, 1950, pp.159-164.

[7] Hartranft, R. J. and Sih, G. C., "The Use of Eigenfunction Expansions in the General Solution of Three-Dimensional Crack Problems", J. Mathematics and Mechanics, v.19, n.2, 1969, pp.123-138.

[8] Folias, E. S., "On the Three-Dimensional Theory of Cracked Plates", J. Appl. Mech., Trans. ASME, September 1975, pp.663-674.

[9] Benthem, J. P., Three-Dimensional State of Stress at the Vertex of a Quarter-Infinite Crack in a Half-Space, Report WTHD No. 74, Department of Mechanical Engineering, Delft University of Technology, The Netherlands, September 1975.

[10] Benthem, J. P. and Koiter, W. T., (discussion), Folias, E. S., (closure), J. Appl. Mech., Trans. ASME, v.43, pp.374-375, 1976.

[11] Bazant, Z. P. and Estenssoro, L. F., "Surface Singularity and Crack Propagation", Int. J. Solids Structures, v.15, pp.405-426, 1979.

[12] Swedlow, J. L., "Singularity Computations", Int. J. Numerical Methods in Engineering, v.12, pp.1779-1798, 1978.

[13] Personal communication with C. W. Smith, 1985.

[14] Epstein, J. S., "On the Variation of the First Classical Eigenvalue of Fracture Mechanics in Three-Dimensional Transitory Stress Fields", Ph.D. dissertation, Virginia Polytechnic Institute and State University, 1983.

[15] Benthem, J. P., "The Quarter-Infinite Crack in a Half-Space, Alternative and Additional Solutions", Int. J. Solids and Structures, v.16, n.2, pp.119-130, 1980.

[16] Smith, C. W. and Epstein, J. S., "Measurement of Three Dimensional Effects in Cracked Bodies", Proc. of Fifth Int. Congress on Experimental Mechanics, pp.102-110, 1984.

[17] Ruiz, C. and Epstein, J. S., "On the Variation of the Stress Intensity Factor Along the Front of a Surface Flaw", Int. J. Fracture, v.28, pp.231-238, 1985.

[18] Limtragool, J., "Investigation of the Three-Dimensional Behaviour of a Crack Tip Singularity by Holographic Interferometry", Ph.D. dissertation, Carnegie-Mellon University, 1982.

[19] Bazant, Z. P., "Three-Dimensional Harmonic Functions Near Termination or Intersection of Gradient Singularity Lines: A General Numerical Method", Int. J. Engng. Sc., v.12, pp.221-243, 1974.

[20] Folias, E. S., "Method of Solution of a Class of Three-Dimensional Elastostatic Problems Under Mode I Loading", Int. J. Fracture, v.16, n.4, pp.335-348, 1980.

[21] Burton, W. S., et. al., "On the Implications for LEFM of the Three-Dimensional Aspects in Some Crack/Surface Intersection Problems", Int. J. Fracture, v.25, pp.3-32, 1984.

[22] Takakuda, K., "Stress Singularities Near Crack Front Edges", Bull. JSME, v.28, n.236, pp.225-231, 1985.

[23] Smith, C. W. and Epstein, J. S., "Experimental Boundary Layer Studies in Three Dimensional Fracture Problems", Advances in Aerospace Structures, Materials, and Dynamics, ASME-AO-06, pp.119-126, 1983.

[24] Kirby, G. C., III, "SIF Distribution for Natural Flaws Grown Under Mode I Loading Using 3-D Photoelasticity", Ph.D. dissertation, Virginia Polytechnic Institute and State University, 1982.

[25] G. C. Sih, Handbook of Stress Intensity Factors for Researchers and Engineers, Lehigh University, 1973.

[26] Epstein, J. S., Post, D., and Smith, C. W., "Three Dimensional Photoelastic Measurements with Very Thin Slices", Experimental Techniques, pp.34-37, December 1984.

[27] Tardy, M. L. H., "Methode Pratique d'Examen de Mesure de la Birefringeneces des Verres d'Optique", Ref. d'Optique, v.8, pp.59-69, 1929.

[28] Post, D., "Isochromatic Fringe Sharpening and Fringe Multiplication in Photoelasticity", Proc. SESA, v.12, n.2, pp.143-156, 1955.

[29] Post, D., "Photoelastic Fringe Multiplication for Ten-Fold Increase in Sensitivity", Experimental Mechanics, pp.3-10, 1970.

[30] Personal communication with D. Joh, December 1985.

[31] Personal communication with O. Olaosebikan, October, 1985.

[32] Dally, J. W. and Riley, W. F., Experimental Stress Analysis, Second Ed., pp.406-446, McGraw-Hill, 1978.

[33] Smith, C. W., et.al., "Experimental Near Tip Methods of Analysis in Fracture Mechanics", Proc. SEM Spring Conference on Experimental Mechanics, June 1986.

[34] Liebowitz, H., et.al., "Biaxial Load Effects in Fracture Mechanics", Engineering Fracture Mechanics, v.10, n.2, pp.315-335, 1978.

[35] Smith, C. W. and Olaosebikan, O., "On the Extraction of Stress Intensity Factors from Near Tip Photoelastic Data", Proc. SESA Spring Conference, 1983.

[36] Doyle, J. F., et.al., "Error Analysis of Photoelasticity in Fracture Mechanics", Experimental Mechanics, pp.429-435, November 1981.

[37] Personal communication with C. Burger at Mid-West Graduate Conference on Experimental Mechanics, Purdue University, September 1984.

[38] Newman, J. C., Jr. and Raju, I. S., "Stress Intensity Factor Equations for Cracks in Three-Dimensional Finite Bodies Subjected to Tension and Bending Loads", NASA TM 85793, 1984.

APPENDIX I

PHOTOELASTIC STRESS FREEZING

Photoelastic stress freezing is a method by which the internal stress distribution for arbitrary model geometries can be obtained. The method requires the use of materials which are both double refracting and di-phasic. By utilizing both properties, in conjunction with techniques to be explained, internal stress distributions can be obtained quite accurately.

Double refraction or birefringence as it is sometimes called, is an optical phenomenon observed in many transparent, non-crystalline materials. When polarized light is passed through the stressed material, it is divided into two orthogonal components, aligned with the directions of principal stresses in the plane normal to the direction of light propagation. The refractive index is different in the two directions, and as a result, one of the components undergoes a relative retardation with respect to the other, giving rise to the well known isochromatic fringes. A complete mathematical derivation and explanation may be found in Dally and Riley's Experimental Stress Analysis.

The term di-phasic refers to materials exhibiting two different sets of properties at different temperatures. For the polymeric material used in the present investigation, the transition takes place in the neighborhood of 100 degrees Centigrade. At room temperature the

material is rather brittle, has a Poisson's ratio of about 0.40 [14] and has an elastic modulus of about 300 ksi. The optical fringe constant is about 25 pounds/inch/fringe. Above the material's transition or "critical" temperature, the properties change drastically. It becomes nearly incompressible, rubbery, and the elastic modulus drops to about 2500 psi. The optical fringe constant also decreases to about 2.0 pounds/inch/fringe. Physically, the process consists of the breaking of secondary molecular bonds, while primary bonds remain intact, retaining the model's shape.

This transition can be utilized to examine three dimensional stress distributions in the following manner. The model is machined or cast from the di-phasic material at or near room temperature. The model is then placed in a programmable, servo-controlled oven (Blue M Manufacturing Co.). A control cam, which produces the time-temperature profile shown in figure A1.1, is used to slowly increase the models temperature above the transition temperature. At this point, live loads (stationary) are applied to the model, which create stress and deformation in the model. The temperature is then slowly decreased through the transition temperature so that residual thermal stresses are not "frozen" in the model with the stresses resulting from the live loads (the coefficient of thermal expansion also increases by an order of magnitude above the material's critical temperature).

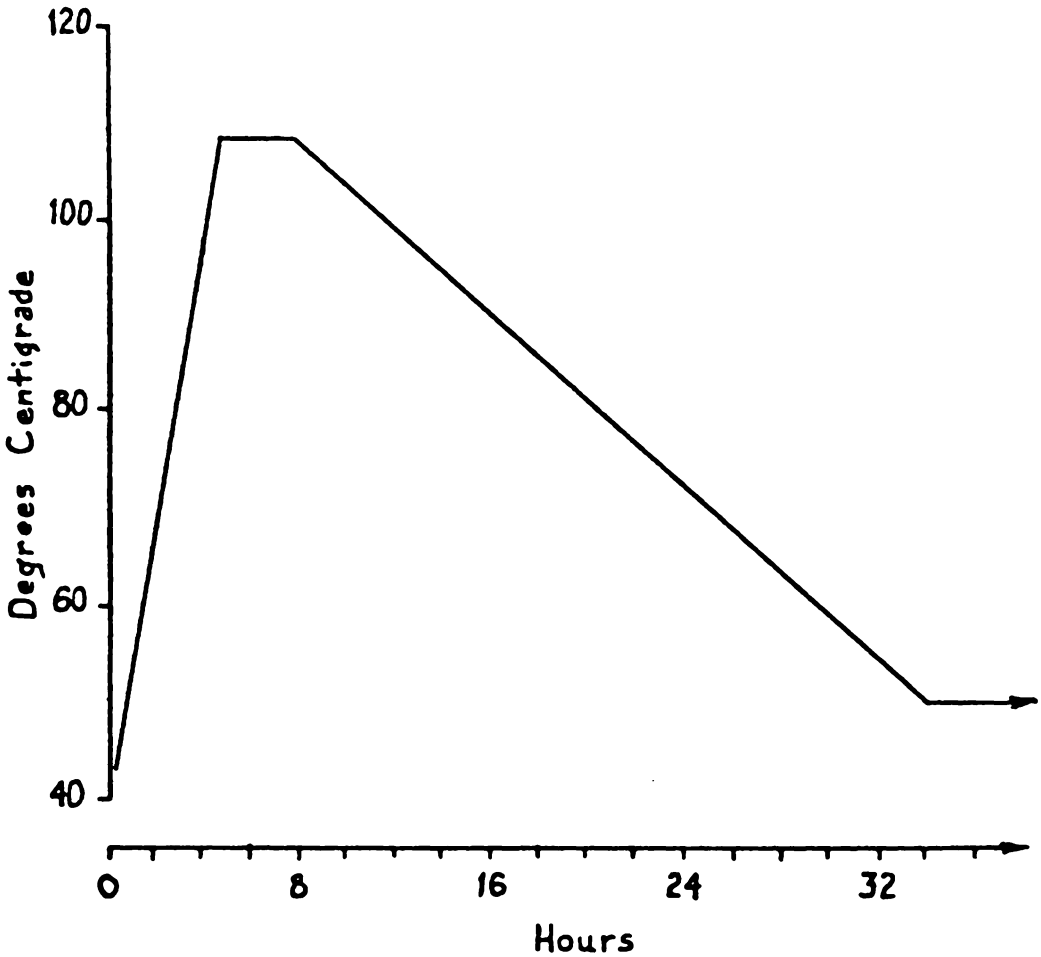

Time-Temperature Profile for Stress Freezing

Figure A1.1

Once the temperature is reduced below the transition temperature, the loads may be removed. Due to the large change in elastic modulus, only an insignificant change in deformation occurs when the loads are removed. An even smaller change occurs in the isochromatic distribution. The model may now be sectioned using appropriate cutting tools and the deformations and associated isochromatic patterns will be retained, allowing analysis of the internal stress distribution in the model (in the plane of the sections removed from the model.

There is one problem which must be accounted for in this procedure. When the temperature of the model is elevated, internal moisture is driven from the model. When the temperature is then lowered, moisture infuses back into the model until equilibrium is established. However, at room temperature, it may take from hours to months for equilibrium to be re-established. During the period while equilibrium is being established, residual stresses and deformation due to the spatial variation of moisture content occur in the slices or sections. These are normally manifested in isochromatics appearing parallel to the slice borders (or erratic displacement contours in the case of "annealing" moire). To date, no problem has been encountered with respect to this time-edge effect in analyzing the thin slices. This is attributable to the rapid return to equilibrium of the

moisture content in the slices due to the short distance moisture must infuse (or diffuse). Care should be taken when analyzing thicker slices, however.

APPENDIX II

INTERACTIVE COMPUTER PROGRAMS

All three of the programs contained in this section were originally written in a version of MicroSoft Advanced Basic (BASICA), which runs on the 8088 family of microprocessors. Subsequently, the program "DIGIFRNG.BAS" was modified to be compiled with the MS QuickBasic Compiler. All of the programs have been utilized extensively in the reduction and analysis of photoelastic data, resulting in less time spent crunching numbers, and more time spent doing productive research, not to mention the reduced eye strain from not having to stare at dim fringe patterns continuously for two hours.

The program "DIGIFRNG.BAS" allows photoelastic data to be recorded digitally, directly from a photoghraph of a fringe pattern. This program is also applicable to recording displacement fringe patterns, particularly ones having very high fringe density.

The program "TAU-PLOT.BAS" is the main data reduction and analysis program used in connection with this research project. The program allows direct user control of the display and program branching, and is simple to use. Prompts appear on the screen requesting input where it is required. Because the program is constructed in a modular fashion, it would be no problem to incorporate new algoritms (linear) into the program. This has already been done, and basically involves inserting model equations in the program at three different places.

The program "LOOPS.BAS" is basically an equation plotting program.

For the version contained in this appendix, the program plots a rearranged form of equation (5.1.5) which has been solved for the variable r.

It was anticipated that all three of these programs would be merged into one master analysis program, however, time ran out and the task could not be accomplished prior to completion of this report. It is probable that this compilation will occur in the future, and possibly even incorporate a digital video camera and interface to record information directly from the polariscope. This would allow immediate results to be obtained, as well as allow the possibility of analyzing quasi-dynamic two dimensional models.

```
$

REM - THIS IS THE PROGRAM TO DIGITIZE PHOTOELASTIC FRINGES AND PERFORM
REM - STORAGE AND PLOTTING. THIS IS SOURCE CODE FOR THE MS-BASIC COMPILER.
      OPTION BASE 1
      COMMON SHARED PI#,XO,YO,MAG,CST#,SNT#,RTOD#,DTOR#,ITOMM,KO
      DIM NRT(100,3)
      PI#=3.141592654# :RTOD#=180#/PI# :DTOR#=1#/RTOD# :ITOMM=.0254
3     CALL TABLET
      M=1
4     CALL INITIAL (NNEXT,FINC)
      J=0 :KO=0
5     CALL RDPNT (X,Y,F$)
      CALL CHFLAG (F$,FO)
      IF FO=2 THEN CALL CHGINC (FINC,NNEXT) :GOTO 5
      IF FO=3 THEN CALL CHGN (NNEXT) :GOTO 5
      IF FO=4 THEN GOTO DATASAVE:
      CALL CONVERT (X,Y,XI,YI,RI,TI)
      CALL STORE (NNEXT,FINC,RI,TI,NRT(),J)
      CALL UPDATE (X,Y,RI,TI,NNEXT,FINC,J)
      GOTO 5
DATASAVE: CALL SETPRNT (NRT(),J,ID$,DO)
      IF DO=1 THEN 4
      CALL SETPLOT (NRT(),J,M,ID$)
      M=M+1
      CALL SETFILE (NRT(),J,ID$)
      CALL RST (DO)
      ON DO GOTO 4,3
      END
REM   ************************************************************************
      SUB RDPNT (X,Y,F$) STATIC '*************************************
      REM - THIS ROUTINE READS A (X,Y) COORDINATE FROM INPUT BUFFER #2 *
      D$=INPUT$(15,#2)
      F$=LEFT$(D$,1)
      X=VAL(MID$(D$,3,5))
      Y=VAL(MID$(D$,9,5))
      END SUB
```

```
REM  ************************************************************************
     SUB CONVERT (X,Y,XI,YI,RI,TI) STATIC '*****************************
     REM - THIS ROUTINE CONVERTS TABLET (X,Y) TO IMAGE COORDINATES ****
     XT=(X-XO)*MAG :YT=(Y-YO)*MAG
     XI=CT#*XT-ST#*YT :YI=ST#*XT+CT#*YT
     RI=SQR(XI^2+YI^2) :TI=ATN(YI/XI)
     CALL CONANG (TI,XI,YI)
     END SUB
REM  ************************************************************************
     SUB TABLET STATIC '*************************************************
     REM - SETS UP TABLET-IMAGE COORDINATE TRANSFORM PARMAMETERS *******
     REM - THESE PARAMETERS ARE COMMON TO THE WHOLE PROGRAM ************
     SCREEN 0 :COLOR 2 :CLS
     OPEN "COM2:9600,O,7,1,RS,DS" AS #2
     PRINT "AFFIX IMAGE TO TABLET. MAKE SURE CONTROLLER IS TURNED ON."
     PRINT :PRINT "PLACE CURSOR AT IMAGE (0,0) AND PRESS ANY BUTTON."
     CALL RDPNT (XO,YO,F$)    'XO,YO ARE THE ORIGIN OFFSET COORDINATES
     PRINT
     INPUT "ENTER (X,Y) OF KNOWN POINT ON IMAGE FROM KYBD:",X2,Y2
     PRINT :PRINT "PLACE CURSOR AT (";X2;","Y2;") AND PRESS A BUTTON."
     CALL RDPNT (X1,Y1,F$)
     X1=X1-XO :Y1=Y1-YO
     R2=SQR(X2^2+Y2^2) :R1=SQR(X1^2+Y1^2) :MAG=R2/R1  'LINEAR MAG.
     T1=ATN(Y1/X1) :T2=ATN(Y2/X2)
     CALL CONANG(T1,X1,Y1)          'CONVERT ANGLE TO 0 < ANGLE < 2*PI
     CALL CONANG(T2,X2,Y2)
     PHI=T2-T1
     CST#=COS(PHI) :SNT#=SIN(PHI)
     PRINT :PRINT "AXIS ROTATION ANGLE: ";PHI*RTOD#;" DEGREES"
     PRINT :PRINT "LINEAR MAGNIFICATION: ";MAG*1000
     CALL NEXTSCR (24,1)
     END SUB
REM  ************************************************************************
     SUB CONANG(T,X,Y) STATIC '*****************************************
     REM - CONVERTS ANGLE TO RANGE (0,2*PI) GIVEN (X,Y) COORD. *********
     IF X<0 AND Y>0 THEN T=T+PI#
```

```
      IF X<0 AND Y<0 THEN T=T+PI#
      IF X>0 AND Y<0 THEN T=T+2#*PI#
      END SUB
REM   ************************************************************************
      SUB NEXTSCR (ROW,COL) STATIC '*****************************************
      IF ROW>24 THEN ROW=24
      IF COL>40 THEN COL=40
      LOCATE ROW,COL
      PRINT "PRESS ANY KEY TO CONTINUE .....";
10    Z$=INKEY$
      IF LEN(Z$)=0 THEN 10
      COLOR 2 :CLS
      END SUB
REM   ************************************************************************
      SUB INITIAL (NNEXT,FINC) STATIC '**************************************
      REM - SET SCREEN FOR DATA COLLECTION ***********************************
      COLOR 2 :CLS
      PRINT "LAST 'N' VALUE:"
      LOCATE 1,40 :PRINT "LAST (R,i) COORDINATE:"
      LOCATE 3,1 :PRINT "CURRENT 'N' VALUE:"
      LOCATE 3,40 :PRINT "LAST DIGITIZER COORDINATES:"
      LOCATE 5,1 :PRINT "CURRENT 'N' INCREMENT:"
      LOCATE 5,40 :PRINT "NO. DATA POINTS COLLECTED:"
      LOCATE 7,1 :PRINT "STATUS:"
      LOCATE 7,9 :PRINT "INITIALIZE VALUES"
      LOCATE 9,1 :INPUT "ENTER FIRST FRINGE ORDER TO READ: ",NNEXT
      LOCATE 3,20 :PRINT USING "+###";NNEXT
      LOCATE 9,1 :PRINT
      LOCATE 9,1 :INPUT "ENTER FRINGE INCREMENT: ",FINC
      LOCATE 5,24 :PRINT USING "+###";FINC
      LOCATE 9,1 :PRINT
      LOCATE 7,9 :PRINT :LOCATE 7,9 :PRINT "READ"
      LOCATE 20,1 :PRINT "INSTRUCTIONS:"
      LOCATE 21,1 :PRINT "PRESS ANY NUMERIC BUTTON ON CURSOR TO READ."
      LOCATE 22,1 :PRINT "PRESS 'C' TO CHANGE CURRENT 'N' VALUE."
      LOCATE 23,1 :PRINT "PRESS 'A' TO CHANGE THE INCREMENT."
```

```
      LOCATE 24,1 :PRINT "PRESS 'F' TO TERMINATE DATA COLLECTION."
      END SUB
REM   ************************************************************************
      SUB CKFLAG (F$,FO) STATIC '*************************************************
      FO=1
      IF F$="A" THEN FO=2
      IF F$="C" THEN FO=3
      IF F$="F" THEN FO=4
      END SUB
REM   ************************************************************************
      SUB CHGN (NNEXT) STATIC '***************************************************
      LOCATE 7,9 :PRINT "CHANGE CURRENT 'N'"
      LOCATE 9,1 :INPUT "CHANGE CURRENT 'N' TO WHAT: ",NNEXT
      LOCATE 9,1 :PRINT
      LOCATE 3,20 :PRINT USING "     ";" "
      LOCATE 3,20 :PRINT USING "+###";NNEXT
      LOCATE 7,9 :PRINT :LOCATE 7,9 :PRINT "READ"
      END SUB
REM   ************************************************************************
      SUB CHGINC (FINC,NNEXT) STATIC '*********************************************
      LOCATE 7,9 :PRINT "CHANGE 'N' INCREMENT."
      LOCATE 9,1 :INPUT "CHANGE INCREMENT TO WHAT: ",IO
      LOCATE 9,1 :PRINT
      NNEXT=NNEXT-FINC+IO
      FINC=IO
      LOCATE 3,20 :PRINT USING "+###";NNEXT
      LOCATE 5,24 :PRINT USING "+###";FINC
      LOCATE 7,9 :PRINT :LOCATE 7,9 :PRINT "READ"
      END SUB
REM   ************************************************************************
      SUB STORE (NNEXT,FINC,RI,TI,NRT(2),J) STATIC '***********************
      REM - STORES N,R,i IN ARRAY FOR LATER USE ************************
      J=J+1
      NRT(J,1)=NNEXT
      NRT(J,2)=RI
      NRT(J,3)=TI*RTOD#     'SAVES ANGLE IN DEGREES
```

```
      NNEXT=NNEXT+FINC      'INCREMENT FRINGE ORDER FOR NEXT DATA POINT
      END SUB
REM   ************************************************************************
      SUB UPDATE (X,Y,RI,TI,NNEXT,FINC,J) STATIC '************************
      REM - UPDATES DATA COLLECTION DISPLAY SCREEN ***********************
      LOCATE 1,65 :PRINT USING "##.###  ###.#";RI;TI*RTOD#
      LOCATE 3,69 :PRINT USING "##### #####";X;Y
      LOCATE 1,17 :PRINT USING "+###";(NNEXT-FINC)
      LOCATE 3,20 :PRINT USING "+###";NNEXT
      LOCATE 5,68 :PRINT USING "###";J
      IF J<99 THEN EXIT SUB
      IF J=99 THEN BEEP :LOCATE 16,1 :COLOR 20,0,0 : _
         PRINT "NEXT POINT IS LAST READABLE POINT (100)" :COLOR 2,0,0
      IF J=100 THEN BEEP :LOCATE 16,1 :PRINT "MAX POINTS INPUT. PRINT"
         CALL NEXTSCR (17,1) :KO=1 :EXIT SUB
      END SUB
REM   ************************************************************************
      SUB SETPRNT (NRT(2),J,ID$,DO) STATIC '*********************************
      REM - DISPLAY DATA ARRAY ON SCREEN. LPRINT OPTIONAL. ***************
      CLS :PRINT "DATA ARRAY - (N, R, i) - JUST COLLECTED:"
      R=2 :C=1
      FOR I=1 TO J
         IF I=20 OR I=40 OR I=60 OR I=80 THEN R=2 :CALL NEXTSCR (24,1)
         LOCATE R,C
         PRINT USING "+###   ##.###   ###.##   +#.####   +#.####"; _
            NRT(I,1);NRT(I,2);NRT(I,3);LOG(NRT(I,1));LOG(NRT(I,2))
         R=R+1
      NEXT I
      LOCATE 24,1 :PRINT "IF DATA IS O.K., PRESS Y, IF NOT, PRESS N";
1     Z$=INKEY$
      IF Z$="Y" OR Z$="N" THEN 2 ELSE 1
2     IF Z$="N" THEN DO=1 :EXIT SUB ELSE DO=0
      CLS :PRINT "ENTER AN I.D. STRING (MAX.78 CHAR.) FOR DATA SET"
      INPUT "",ID$
      PRINT "MAKE SURE PRINTER IS CONNECTED AND ON-LINE"
      PRINT :PRINT "PRESS ANY KEY WHEN READY ....."
```

```
25    Z$=INKEY$
      IF LEN(Z$)=0 THEN 25
      LPRINT CHR$(27)+"A"+CHR$(16)+CHR$(27)+"N"+CHR$(6)
      LPRINT ID$ :LPRINT
      LPRINT "          N        R        THETA     LN(N)      LN(R)"
      LPRINT
      FOR I=1 TO J
      LPRINT USING "      +###     ##.###     ###.##    +#.###    +#.###"; _
         NRT(I,1);NRT(I,2);NRT(I,3);LOG(NRT(I,1));LOG(NRT(I,2))
      NEXT I
      BEEP :CLS :PRINT "PRINTING DONE. PRESS ANY KEY TO CONTINUE."
30    Z$=INKEY$
      IF LEN(Z$)=0 THEN 30
      CLS
      END SUB
REM - ************************************************************************
      SUB SETPLOT (NRT(2),J,M,ID$) STATIC '*****************************
      REM - THIS PLOTS THE DATA SET IN LOG-LOG FORM **********************
      REM - USE STANDARDIZED PLOT SCALE FOR CONSISTENCY ******************
      STATIC P(3),K(1)
      DIM P(100,2,4),K(4)
      IF M=5 THEN CLS :PRINT "ONLY FOUR SETS CAN BE PLOTTED TOGETHER" _
         :PRINT "SET COUNTER IS RESET TO 1" :M=1
      K(M)=J
      FOR I=1 TO K(M)
         P(I,1,M)=LOG(NRT(I,1))
         P(I,2,M)=-LOG(NRT(I,2))
         NEXT I
      CLS :CALL SCRNSET (M)
      REM - THIS SECTION PLOTS THE DATA POINTS
QUERYSET: LOCATE 1,18 :INPUT "PLOT WHICH SET (0 TO PRINT):",S
      IF S<0 OR S>M THEN LOCATE 1,18 :PRINT :GOTO QUERYSET:
      IF S<>0 THEN GOTO PLOT:
      REM - USE PRTSC TO DUMP GRAPHICS TO PRINTER
      LPRINT CHR$(27)+"A"+CHR$(8)
40    Z$=INKEY$
```

```
      IF Z$="C" THEN 50 ELSE GOTO 40
50    LPRINT CHR$(27)+"A"+CHR$(18)
      SCREEN 0 :COLOR 2 :CLS :EXIT SUB
PLOT: FOR I=1 TO K(S)
         PSET (P(I,2,S),P(I,1,S))
         NEXT I
60    LOCATE 1,20 :INPUT "ENTER SET ID (22 CHAR. MAX.):",S$
      LOCATE 1,20 :PRINT
      IF LEN(S$)>22 THEN 60
      LOCATE 1,S+16 :PRINT USING "&";S$
      GOTO QUERYSET:
      END SUB
REM   ************************************************************************
      SUB SCRNSET (M) STATIC '*****************************************
      REM - THIS SETS UP THE GRAPHICS SCREEN FOR PLOTTING LN(N)-LN(R) **
      SCREEN 2 :CLS
      PRINT "DATE: "+DATE$
      LOCATE 3,1 :PRINT "TIME: "+TIME$
      VIEW (200,8)-(639,199)
      WINDOW (-.05,-1.18)-(5.5,3.5)
      LINE (0,0)-(5.5,0) :LINE (0,0)-(0,3.5) 'DRAW AXES
      FOR I=0 TO 5.5 STEP .5
      LINE (I,0)-(I,-.05)
      NEXT I
      FOR J=0 TO 3.5 STEP .5
      LINE (0,J)-(-.05,J)
      NEXT J
      LINE (0,-.58)-(5.5,-.58)
      FOR I=0 TO 5.5 STEP .5
      LINE (I,-.58)-(I,-.63)
      NEXT I
      LOCATE 20,26 :PRINT "0"
      LOCATE 20,35 :PRINT "-1"
      LOCATE 20,45 :PRINT "-2"
      LOCATE 20,49 :PRINT "LN(R)"
      LOCATE 20,55 :PRINT "-3"
```

```
      LOCATE 20,65 :PRINT "-4"
      LOCATE 20,75 :PRINT "-5"
      LOCATE 23,26 :PRINT "1.0"
      LOCATE 23,35 :PRINT ".37"
      LOCATE 23,45 :PRINT ".14"
      LOCATE 23,55 :PRINT ".05"
      LOCATE 23,65 :PRINT ".02"
      LOCATE 23,75 :PRINT ".007"
      LOCATE 3,24 :PRINT "3"
      LOCATE 8,24 :PRINT "2"
      LOCATE 11,21 :PRINT "LN(N)"
      LOCATE 13,24 :PRINT "1"
      LOCATE 19,24 :PRINT "0"
      LOCATE 23,19 :PRINT "R [IN]"
      END SUB
REM   ************************************************************************
      SUB SETFILE (NRT(2),J,ID$) STATIC '*********************************
      REM - SAVES DATA SET ON DISK FILE
      SCREEN 0 :COLOR 2 :CLS
      INPUT "ENTER FILENAME FOR DATA STORAGE:",FILE$
      IF LEN(FILE$)=0 THEN EXIT SUB
      OPEN "O",#1,FILE$
      PRINT#1, USING "&";ID$
      PRINT#1,"  N      R [IN]      THETA"
      FOR I=1 TO J
      PRINT#1, USING "+###     ##.####     ###.##"; _
         NRT(I,1);NRT(I,2);NRT(I,3)
      NEXT I
      CLOSE #1
      END SUB
REM   ************************************************************************
      SUB RST (DO) STATIC '*************************************************
      REM - RESETS VARIABES TO START NEW DATA COLLECTION SEQUENCE
80    SCREEN 0 :COLOR 2:CLS
      PRINT "COLLECT ANOTHER SET - ENTER 1"
      PRINT "START ON NEW IMAGE  - ENTER 2"
```

```
PRINT "TERMINATE PROGRAM   - ENTER 3"
PRINT :INPUT "ENTER OPTION NUMBER: ",DO
IF DO<1 THEN 80
IF DO<2 THEN EXIT SUB
IF DO<3 THEN EXIT SUB
IF DO>3 THEN 80
CLS
END SUB
```

```
10 ' ********** PROGRAM "TAU-PLOT.BAS" ****************************************
20 OPTION BASE 1
30 DIM N(40),R1(40),R2(40),LG(40,2),KD(40,2),P(40,2),CURSOR(30),DLT(40)
35 DIM XD(40,2)
40 GOSUB 510
50 GOSUB 1690                  'ACCESS TEST DATA ENTRY/STORAGE ROUTINE
60 JO=0
70 GOSUB 1850                  'ACCESS SLICE DATA ENTRY/STORAGE ROUTINE
80 GOSUB 350                             'CALCULATE VALUES FOR PLOTS
90 SCREEN 2 :CLS :KEY OFF
100 LOCATE 1,1 :PRINT "ENTER EITHER Plot, Data, or End"
110 LOCATE 3,1 :PRINT "ENTER 'P' TO GO TO THE PLOTTING ROUTINES"
120 LOCATE 4,1 :PRINT "ENTER 'D' TO GO TO THE DATA ENTRY/STORAGE ROUTINES"
130 LOCATE 5,1 :PRINT "ENTER 'E' TO HALT PROGRAM EXECUTION"
140 LOCATE 1,40 :INPUT D$
150 IF D$="E" THEN CLS :STOP
160 IF D$="P" THEN 240
170 IF D$<>"D" THEN 90
180 CLS :LOCATE 1,1 :PRINT "ENTER EITHER 'T' OR 'S'"
190 LOCATE 3,1 :PRINT "ENTER 'T' FOR TEST DATA ACCESS FOR A DIFFERENT TEST"
200 LOCATE 5,1 :PRINT "ENTER 'S' FOR SLICE DATA ACCESS FOR THE CURRENT TEST"
210 LOCATE 1,30 :INPUT DTA$
220 IF DTA$="T" THEN 50
230 IF DTA$="S" THEN 70 ELSE 100
240 CLS :LOCATE 1,1 :PRINT "ENTER EITHER 'K' OR 'L' OR 'X'"
250 LOCATE 3,1 :PRINT "ENTER 'K' TO PLOT Kap vs. SQR(r/a)"
260 LOCATE 5,1 :PRINT "ENTER 'L' TO PLOT Ln(tau) vs. -Ln(r)"
265 LOCATE 7,1 :PRINT "ENTER 'X' TO PLOT Klambda vs. R^lambda"
270 LOCATE 1,34 :INPUT PLOT$
280 GOSUB 430
290 GOSUB 560
300 GOSUB 1230
310 LB=0
```

```
320 GOSUB 740
330 GOSUB 1300
340 GOTO 90
350 'CALCULATE VALUES ***************************************************************
360 CO=SQR(2!)*F*PHI/(TS*SIG*MF)
362 INPUT "ENTER A VALUE FOR LAMBDA :";LAMBDA
364 INPUT "ENTER A VALUE FOR TAU-ZERO (@ MAX CRACK DEPTH):";TAU
370 FOR I=1 TO M
380 LG(I,1)=LOG((N(I)*F/(2!*MF*TS))-TAU)
390 LG(I,2)=-LOG(ABS(R1(I)-R2(I))/2!)
400 KD(I,2)=SQR(ABS(R1(I)-R2(I))/(2!*A))
410 KD(I,1)=CO*N(I)*KD(I,2)
412 XD(I,2)=EXP(-LAMBDA*LG(I,2))
413 XD(I,1)=N(I)*F*XD(I,2)/(2!*MF*TS)
420 NEXT I
430 'TRANSFER VALUES TO PLOTTING ARRAY P( , ) ***********************************
440 IF PLOT$="K" THEN 480
445 IF PLOT$="X" THEN 501
450 FOR I=1 TO M
460 P(I,2)=LG(I,1) :P(I,1)=LG(I,2)
470 NEXT I :RETURN
480 FOR I=1 TO M
490 P(I,2)=KD(I,1) :P(I,1)=KD(I,2)
500 NEXT I :RETURN
501 FOR I=1 TO M
502 P(I,2)=XD(I,1) :P(I,1)=XD(I,2)
503 NEXT I :RETURN
510 'CURSOR SET-UP ******************************************************************
520 SCREEN 2 :VIEW :CLS
530 LINE (5,5)-(5,101)
540 GET (5,5)-(5,101),CURSOR
550 CLS :RETURN
560 'SCREEN SET-UP FOR PLOTTING *****************************************************
570 SCREEN 2 :VIEW :CLS :KEY OFF
```

```
580 VIEW (200,1)-(630,120)
590 IF PLOT$="K" THEN 670
595 IF PLOT$="X" THEN 731
600 WINDOW (1!,1.5)-(6!,4.5)
610 X0=1.05 :X1=5.5 :Y=4! :X=3.3 :DX=.04
620 LINE (1!,4!)-(1!,1.5) :LINE -(5.5,1.5)
630 LOCATE 3,22 :PRINT "4.0" :LOCATE 9,18 :PRINT "Ln(Z)"
640 LOCATE 15,22 :PRINT "1.5"
650 LOCATE 17,25 :PRINT "1.0" :LOCATE 17,46 :PRINT "-Ln(R)"
660 LOCATE 17,73 :PRINT "5.5" :LOCATE 1,1 :RETURN
670 WINDOW (0!,1!)-(.9,3.2)
680 X0=.03 :X1=.85 :Y=2.85 :X=.4 :DX=.01
690 LINE (0!,3!)-(0!,1!) :LINE -(.85,1!)
700 LOCATE 3,22 :PRINT "3.0" :LOCATE 9,22 :PRINT "Kap"
710 LOCATE 15,22 :PRINT "1.0"
720 LOCATE 17,25 :PRINT "0.0" :LOCATE 17,45 :PRINT "(R/A)^.5"
730 LOCATE 17,73 :PRINT "0.85" :LOCATE 1,1 :RETURN
731 WINDOW (0!,3!)-(.65,11!)
732 X0=.04 :X1=.6 :Y=10.5 :X=.3 :DX=8.000001E-03
733 LINE (0!,10.5)-(0!,3!) :LINE -(.6,3!) :LOCATE 2,21 :PRINT "10.5"
734 LOCATE 9,18 :PRINT "(K')ap" :LOCATE 15,22 :PRINT "3.0" :LOCATE 17,25
735 PRINT "0.0" :LOCATE 17,46 :PRINT "R^lambda" :LOCATE 17,73
736 PRINT "0.6" :LOCATE 1,1 :RETURN
740 'LOCATE LINEAR ZONE AND BAD DATA ********************************************
750 ON KEY(1) GOSUB 890 :KEY(1) ON                    'LEFT ENDPOINT
760 ON KEY(2) GOSUB 930 :KEY(2) ON                  'RIGHT ENDPOINT
770 ON KEY(3) GOSUB 970 :KEY (2) ON                 'DELETE BAD POINT
780 ON KEY(4) GOSUB 1030 :KEY (4) ON                 'EXIT SUBROUTINE
790 ON KEY(9) GOSUB 1070 :KEY (9) ON                 'SLOW CURSOR
800 ON KEY(10) GOSUB 1090 :KEY (10) ON               'SPEED CURSOR
810 ON KEY(12) GOSUB 1110 :KEY (12) ON               'CURSOR MOVE LEFT
820 ON KEY(13) GOSUB 1150 :KEY (13) ON               'CURSOR MOVE RIGHT
830 DIR = SGN(P(M,1)-P(1,1))
840 IF DIR < 0 THEN I1=M :I2=1 ELSE I1=1 :I2=M
```

```
850 L6=0 :PUT (X,Y),CURSOR
860 WHILE L8=0
870 WEND
880 RETURN
890 'READ LEFT END
900 XLT=X :LOCATE 1,1 :PRINT "                    "
910 LOCATE 1,1 :PRINT USING "\     \  #.###";"LEFT :";X
920 RETURN
930 'READ RIGHT END
940 XRT=X :LOCATE 3,1 :PRINT "                    "
950 LOCATE 2,1 :PRINT USING "\     \  #.###";"RIGHT:";X
960 RETURN
970 'DELETE BAD POINTS
980 L6=L6+1 :BEEP
990 FOR I=I1 TO I2 STEP DIR
1000 IF P(I,2) > X THEN DLT(L6)=I :GOTO 1020
1010 NEXT I
1020 RETURN
1030 'EXIT SUBROUTINE
1040 L8=1 :KEY(1) OFF :KEY(2) OFF :KEY(3) OFF :KEY(4) OFF :KEY(9) OFF
1050 KEY(10) OFF :KEY(12) OFF :KEY(13) OFF :PUT(X,Y),CURSOR
1060 RETURN
1070 'SLOW CURSOR
1080 DX=DX#2!/3! :RETURN
1090 'SPEED CURSOR
1100 DX=DX#3!/2! :RETURN
1110 'MOVE TO LEFT
1120 PUT(X,Y),CURSOR :X=X-DX :GOSUB 1190
1130 IF L7=1 THEN X=X+DX :BEEP
1140 PUT(X,Y),CURSOR :RETURN
1150 'MOVE TO RIGHT
1160 PUT(X,Y),CURSOR :X=X+DX :GOSUB 1190
1170 IF L7=1 THEN X=X-DX :BEEP
1180 PUT(X,Y),CURSOR :RETURN
```

```
1190 'TEST FOR OUT OF BOUNDS
1200 L7=0
1210 IF (X<=X0) OR (X>=X1) THEN L7=1
1220 RETURN
1230 'PLOT DATA POINTS ************************************************************
1240 LOCATE 21,60 :PRINT DATE$
1250 FOR I=1 TO M
1260 PSET(P(I,1),P(I,2))
1270 NEXT I
1280 LOCATE 21,30 :PRINT USING "\       \     \       \";TEST$;SLICE$
1290 RETURN
1300 'PERFORM REGRESSION ANALYSIS ON GOOD DATA IN LINEAR ZONE ******************
1310 N0=0 :SX=0! :SX2=0! :SY=0! :SY2=0! :SXY=0!
1320 FOR I=I1 TO I2 STEP DIR
1330 IF(P(I,1)<=XLT) OR (P(I,1)>=XRT) THEN 1400
1340 FOR J=1 TO L6
1350 IF I=DLT(J) THEN 1400
1360 NEXT J
1370 N0=N0+1
1380 SX=SX+P(I,1) :SX2=SX2+P(I,1)^2 :SXY=SXY+P(I,1)*P(I,2)
1390 SY=SY+P(I,2) :SY2=SY2+P(I,2)^2
1400 NEXT I
1410 XM=SX/N0 :YM=SY/N0
1420 SLOPE=(SXY-N0*XM*YM)/(SX2-N0*XM^2)
1430 INCPT=YM-SLOPE*XM
1440 VARYX=(SY2-2!*YM*SY+N0*YM^2-SLOPE^2*(SX2-2!*XM*SX+N0*XM^2))/(N0-2)
1450 VARY=(SY2-2!*YM*SY+N0*YM^2)/(N0-1)
1460 RHO=SQR(1!-(N0-2)*VARYX/((N0-1)*VARY))
1470 SDYX=SQR(VARYX)/YM                          'NORMALIZED CONDITIONAL STD. DEV.
1480 'PLOT REGRESSION ENDPOINTS AND PRINT STATISTICAL VALUES ******************
1490 PUT (XLT,Y),CURSOR
1500 PUT (XRT,Y),CURSOR
1510 LOCATE 4,1 :PRINT USING "\      \ #.####";"SLOPE :";SLOPE
1520 LOCATE 6,1 :PRINT USING "\      \ #.####";"FNY(0):";INCPT
```

```
1530 LOCATE 8,1 :PRINT USING "\    \ +#.#####";"RHO :";RHO
1540 LOCATE 10,1 :PRINT "NORMALIZED COND."
1550 LOCATE 11,1 :PRINT "STD. DEVIATION :"
1560 LOCATE 12,1 :PRINT USING "          #.######";SDYX
1570 IF PLOT$="K" OR PLOT$="X" THEN 1620
1580 PI=3.141593 :S12=(SIN(PI*SLOPE/2!))^2 :S22=(SLOPE*SIN((SLOPE+1)*PI/2!))^2
1590 C12=(COS(PI*SLOPE/2!))^2 :C22=(COS((SLOPE+1!)*PI/2!))^2
1620 LOCATE 24,1 :PRINT "FOR HARD COPY, PRESS 'O', THEN Shift-PrtSc, AND/OR 'C'
TO CONTINUE";
1622 Z$=INKEY$
1624 IF Z$="Q" OR Z$="q" OR Z$="C" OR Z$="c" THEN 1625 ELSE 1622
1625 IF Z$="C" OR Z$="c" THEN 1675
1626 LOCATE 24,1 :PRINT "
                  ";
1630 LOCATE 16,1 :LPRINT CHR$(27)+"A"+CHR$(8) :BEEP
1640 Z$=INKEY$
1650 IF LEN(Z$)=0 THEN 1640
1660 LPRINT CHR$(27)+"2"+CHR$(12)
1675 VIEW :CLS
1680 RETURN
1690 'ACCESS TEST DATA FOR ENTRY, STORAGE, RETRIEVAL, OR MODIFICATION *********
1700 SCREEN 2 :CLS :PRINT "CURRENTLY, ONLY KEYBOARD ENTRY OF DATA IS AVAILABLE"
1710 CHDIR "\TESTS" :LOCATE 16,1 :FILES "*.*"
1720 LOCATE 3,1 :INPUT "ENTER TEST I.D. (8 CHARACTERS MAX.) :",TEST$
1730 CHDIR TEST$
1740 LOCATE 5,1 :INPUT "ENTER MATERIAL FRINGE CONSTANT (#/IN/FRINGE) :",F
1750 LOCATE 7,1 :INPUT "ENTER REMOTE NORMAL STRESS (#/(IN)^2) :",SIG
1760 LOCATE 9,1 :INPUT "ENTER CRACK SIZE (IN) :",A
1770 LOCATE 11,1 :INPUT "ENTER ELLIPTIC INTEGRAL VALUE (PHI) :",PHI
1780 LOCATE 13,1 :INPUT "ARE VALUES CORRECT (Y or N)  ";B$
1790 IF B$="N" THEN 1720 ELSE INPUT "STORE DATA (Y or N)";B$
1800 IF B$="N" THEN 1840
1810 OPEN "O",#1,"TESTDATA"
1820 PRINT #1,F,SIG,A,PHI
```

```
1830 CLOSE #1
1840 CLS :RETURN
1850 'ACCESS SLICE DATA FOR ENTRY, STORAGE, RETRIEVAL, OR MODIFICATION *********
1860 SCREEN 2 :CLS :INPUT "ENTER DATA FROM KYBD OR FILE (K or F):",F$
1870 IF F$="F" THEN 2150
1880 IF J0=1 THEN 1900
1890 CHDIR "SLICES" :J0=1
1900 LOCATE 3,1 :INPUT "ENTER SLICE I.D. (8 CHARACTERS MAX.) :",SLICE$
1910 LOCATE 5,1 :INPUT "ENTER SLICE THICKNESS (IN) :",TS
1920 LOCATE 7,1 :INPUT "ENTER FRINGE MULTIPLICATION FACTOR (1,3,5,...) :",MF
1930 LOCATE 9,1 :INPUT "ENTER NUMBER OF DATA SETS, (N,R1,R2) ( <40 ) :",M
1940 LOCATE 11,1 :INPUT "ARE THESE VALUES CORRECT (Y or N)  ";B$
1950 IF B$="N" THEN 1900 ELSE CLS
1960 LOCATE 1,1 :PRINT "ENTER DATA SETS WHEN PROMPTED (Ni,R1i,R2i)...."
1970 FOR I=1 TO M
1980 IF I>22 THEN J=I-22 :K=40 ELSE J=I :K=1
1990 LOCATE J+1,K :PRINT USING "\  \ ##";"SET";I :LOCATE J+1,K+9
2000 INPUT "",N(I),R1(I),R2(I)
2010 NEXT I
2020 LOCATE 24,1 :INPUT "ARE ALL VALUES CORRECT (Y or N)";B$
2030 IF B$="N" THEN CLS :GOTO 1960
2040 IF B$="N" THEN CLS :GOTO 1960
2050 LOCATE 24,1 :PRINT "
2060 LOCATE 24,1 :INPUT "STORE SLICE DATA (Y or N)";B$
2070 IF B$="N" THEN 2140
2080 OPEN "O",#1,SLICE$
2090 PRINT #1,TS,MF,M
2100 FOR I=1 TO M
2110 PRINT #1,N(I),R1(I),R2(I)
2120 NEXT I
2130 CLOSE #1
2140 CLS :RETURN
2150 'ENTER SLICE DATA FROM FILE ************************************************
2160 IF J0=1 THEN 2180
```

```
2170 CHDIR "SLICES" :J0=1
2180 CLS :LOCATE 15,1 :FILES
2190 LOCATE 1,1 :INPUT "ENTER SLICE I.D. FROM FILE LIST :",SLICE$
2200 OPEN "I",#1,SLICE$
2210 INPUT #1,TS,MF,M :CLS :PRINT TEST$,SLICE$
2220 LOCATE 2,1 :PRINT TS,MF,M
2230 FOR I=1 TO M
2240 IF I>20 THEN K=40 :J=I-17 ELSE K=1 :J=I+3
2250 INPUT #1,N(I),R1(I),R2(I)
2260 LOCATE J,K :PRINT N(I),R1(I),R2(I)
2270 NEXT I
2280 CLOSE #1 :GOTO 2020
```

```
5 '********************** PROGRAM "LOOPS.BAS" ****************************
10 SCREEN 2
20 LPRINT CHR$(27)+"A"+CHR$(8)
30 CLS
40 WINDOW (-.391,-.05)-(.391,.5)
50 PI=3.141593
60 DEF FND(A,L,R)=2!^L/(2!*A*L*SIN(R))
70 DEF FNT(L,R)=SIN((L+1!)*R)
80 DEF FNZ2(B,D,T,X,L)=1!/(4!*D^2*X^(2!*L))-B*T/(2!*D*X^L)+B^2
90 DEF FNX(B,D,T,Z,L)=EXP((-1!/L)*(LOG(D)+LOG(B*T+SQR((B*T)^2-(2!*B)^2+(2!*Z)^2)
)))
100 INPUT "ENTER A, B, LAMBDA, & m :",A,B,L,M
110 Z20=FNZ2(B,FND(A,L,PI/2!),FNT(L,PI/2!),.4,L)
120 Z2M=FNZ2(B,FND(A,L,PI/2!),FNT(L,PI/2!),.04,L)
130 DZ=(SQR(Z2M)-SQR(Z20))/(M-1)
140 CLS
150 H=&HFFFF :LINE (-.25,0)-(0,0)
160 LINE (-.25,.4)-(.25,.4),,,&HFF00
170 LINE (-.25,.05)-(.25,.05),,,&HFF00
180 F=0
190 Z0=SQR(Z20) :ZM=SQR(Z2M)
200 LOCATE 5,68 :PRINT USING "##.##";Z0
210 LOCATE 21,68 :PRINT USING "##.##";ZM
220 G$="\ \ ##.###"
230 LOCATE 18,1
240 PRINT USING G$;"A=",A
250 PRINT USING G$;"B=",B
260 PRINT USING G$;"L=",L
270 F=F+1 :N=M+1
280 FOR Z=Z0 TO ZM+DZ/8! STEP DZ
290 N=N-1
300 PSET (0,0)
310 DIVM=100!*(1!-1!/(N+1!))
320 DR=PI/DIVM
```

```
330 FOR R=DR TO PI-DR/2! STEP DR
340 D=FNX(B,FND(A,L,R),FNT(L,R),Z,L)
350 X=D*COS(R)
360 Y=D*SIN(R)
370 LINE -(X,Y),,,H
380 NEXT R
390 NEXT Z
400 LOCATE 1,1
410 INPUT "OVERLAY ";B$
420 C$="\                          \"
430 LOCATE 1,1 :PRINT USING C$;" "
440 IF B$="N" THEN 510
450 LOCATE 1,1 :INPUT "A,B,LAMBDA: ",A,B,L
460 LOCATE 1,1
470 PRINT USING C$;" "
480 IF F=1 THEN H=&HF000
490 IF F=2 THEN H=&H1000
500 GOTO 270
510 D$=INKEY$
520 IF D$<>"C" THEN 510
530 LPRINT CHR$(27)+"2"
540 END
```

The vita has been removed from the scanned document